Doctoral Dissertation

Studies on the folding mechanism of halophilic RNase H1 and role of type 1 RNase H in DNA repair

好塩菌 RNase H1 のフォールディング機構と DNA 修復における 1 型 RNase H の役割に関する研究

Elias Tannous

October 2014

Graduate School of Engineering

Osaka University

To my inspiring mother

Odette

TABLE OF CONTENTS

LIST OF ABBREVIATIONS

RNase H	ribonuclease H
rNMP	ribonucleotide monophosphate
rNTP	ribonucleotide triphosphate
PCNA	proliferating cell nuclear antigen
RFC	replication factor C
Pol	polymerase
Exo	exonuclease
dsDNA	double-strand DNA
dsRNA	double-strand RNA
Halo-RNases H1/H2	RNases H1/H2 from *Halobacterium* sp. NRC-1
Halo-NTD	N-terminal domain (residues 1-68) of Halo-RNase H1
Halo-CTD	C-terminal domain (residues 69-199) of Halo-RNase H1
2A-RNase H1	Halo-RNase H1 derivative with double mutations (Asp75→Ala and Asp139→Ala)
6A-RNase H1	Halo-RNase H1 derivative with sextuple mutations (Asp132→Ala, Asp133→Ala, Asp173→Ala, Asp174→Ala, Asp197→Ala, and Asp198→Ala)
8A-RNase H1	Halo-RNase H1 derivative with octuple mutations introduced into 2A- and 6A-RNases H1
JRNase	junction ribonuclease
$dsDNA^{R1}$	double-stranded DNA containing a single ribonucleotide
R9-D9/D18	18 base pair RNA_9-DNA_9/DNA_{18} duplex
Rn-D9/D18	RNA_n-DNA_9/DNA_{18} duplex
R(9-n):Rn-D9/D18	R9-D9/D18 duplex with a nick at the 5'-side of the n^{th} ribonucleotide from the RNA-DNA junction
D15-R1-D13/D29	29 base pair DNA_{15}-RNA_1-DNA_{13}/DNA_{29} duplex
CD	circular dichroism
GdnHCl	guanidine hydrochloride
EDTA	ethylenediaminetetraacetic acid
PDB	protein data bank

CHAPTER 1

GENERAL INTRODUCTION

1.1. RIBONUCLEASE H

Ribonuclease H (EC 3.1.26.4), usually shortened as RNase H, is an endoribonuclease that specifically cleaves the RNA strand of RNA/DNA hybrids [1]. That's where the “H” in RNase H comes from; i.e., “hybrids”. Not until RNase H from *Escherichia coli* (*E. coli*) was heterologously constructed and sequenced in 1983 by Kanaya and Crouch [2], were comprehensive investigations launched. Long before that, RNase H was described several times in the literature. It was first described in 1969 by Stein *et al.* [3] referring to the enzyme isolated from calf thymus extracts. It was later purified from *E. coli* cell extracts allowing its partial characterization in 1973 [4-6]. The DNA sequencing analysis that was done in 1983 limited the size of the protein in *E. coli* to 155 amino acids [2], allowing its easy production and high-throughput purification, thus yielding its three-dimensional structure determination in 1990 [7]. In the same year, 1990, another enzyme, which shares the same hydrolytic activity, was found in *E. coli* and designated as RNase HII [8] (II referring to the sequence of discovery) although it shares very low sequence similarity with the originally described enzyme designated as RNase HI, but it was later shown that they both share a similar fold and a similar active site. Since then, prokaryotic and eukaryotic RNases H, which show the amino acid sequence similarities to *E. coli* RNases HI/HII, have been designated as RNases HI/HII and RNases H1/H2 respectively [9,10]. However, prokaryotic RNases HI/HII have been recently designated as RNases H1/H2 for simplicity.

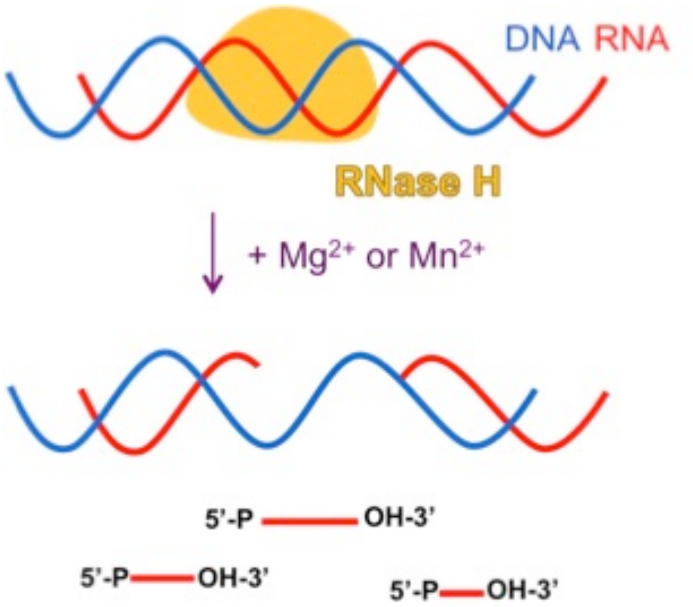

Figure 1.1. **Schematic drawing representing the enzymatic activity of RNase H**

RNase H specifically cleaves the RNA strand of RNA/DNA hybrids in the presence of divalent metal ion cofactor, mostly Mg^{2+} or Mn^{2+}, yielding oligoribonucleotides with 3'-hydroxyl and 5'-phosphate termini [1] (**Fig. 1.1**). RNase H is widely present in various organisms, including bacteria, archaea, and eukaryotes. It is also present in retroviruses as a C-terminal domain of reverse transcriptase. Based on the difference in their amino acid sequences, RNases H have been classified into two types: type 1 and type 2 [9,10]. Type 1 RNases H include prokaryotic RNase H1, eukaryotic RNase H1, and retroviral RNase H. Type 2 RNases H include prokaryotic RNase H2, eukaryotic RNase H2, and bacterial RNase H3. These RNases H, except for heterotrimeric eukaryotic RNases H2, are monomeric. Multiple *rnh* genes (gene encoding RNase H) are found in the genome of most organisms. For example, the *E. coli* genome contains two *rnh* genes: *rnh*A (encoding RNase H1) and *rnh*B (encoding RNase H2) (**Fig. 1.2**). Similarly, the *Saccharomyces cerevisiae* and human genomes contain two genes encoding RNase H1 and RNase H2 (rnh1 and rnh201/202/203 for *S. cerevisiae* and rnaseh1 and rnaseh2A/2B/2C for human) respectively. *Bacillus subtilis* contains three *rnh* genes, only two of them encoding functional enzymes, RNase H2 and RNase H3 [11]. *Shewanella* sp. SIB1 contains three functional *rnh*

genes encoding RNase H1, RBD-RNase H1 (type 1 RNase H with a double-stranded RNA binding domain at the N-terminus), and RNase H2 [12].

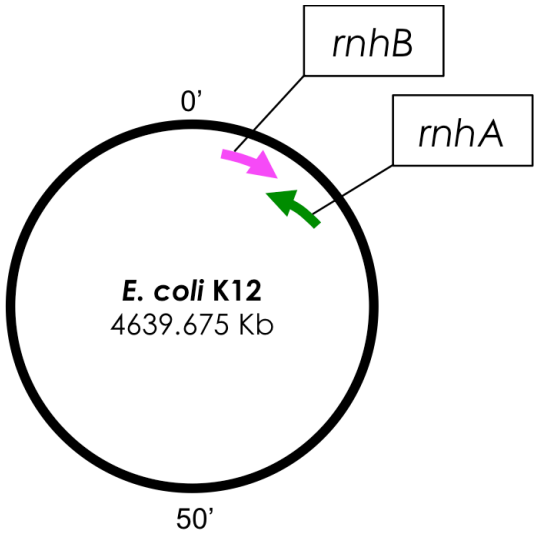

Figure 1.2. **Position of *rnh*A and *rnh*B genes on *E. coli* K12 map.**

1.2. PHYSIOLOGICAL ROLES OF RNASE H

In eukaryotes and prokaryotes, RNase H is believed to play several essential roles in cell growth and in maintaining the accuracy of the cell cycle [13]. Of these physiological roles, RNase H plays a role in DNA replication of the lagging strand, by removing the RNA primer of the Okazaki fragment (**Fig. 1.3.a**) [14-18]. It also plays a role in processing the R-loops, the byproducts of transcription, which can block the proceeding of the replication fork if not resolved (**Fig. 1.3.b**) [19-21]. Of the most confirmed physiological roles, RNase H (precisely RNase H2) initiates the ribonucleotide excision repair (RER) pathway, a repair pathway that sanitizes the

genomic DNA from ribonucleotides misincorporated into its sequence, otherwise causing genomic instability (**Fig. 1.3.c**) [13,18,22-26]. In retroviruses, RNase H, which exists as a C-terminal domain of the reverse transcriptase (**Fig. 1.3.d**), non-specifically degrades the RNA genome after it is reversely transcribed, specifically removes the tRNA primer used to synthesize the (-) strand of DNA, and specifically creates and removes the polypurine tract (PPT) primer used to synthesize the (+) strand DNA, which are all indispensable for the retrovirus proliferation [27].

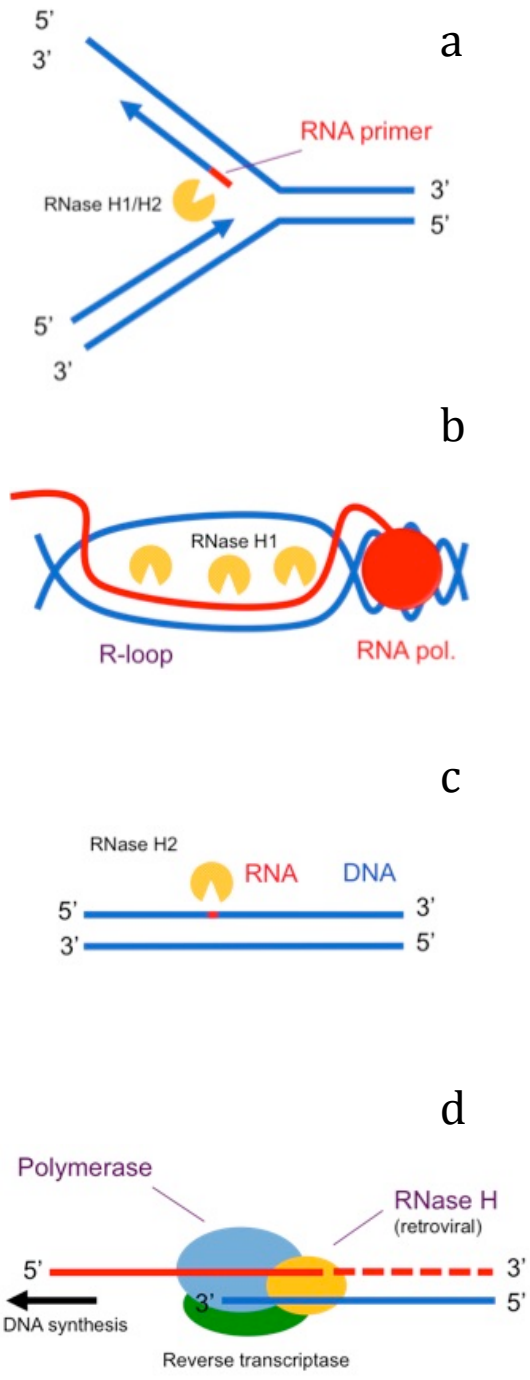

Figure 1.3. **Schematic drawing representing the involvement of RNase H in several physiological roles** (a) DNA replication on the lagging strand (b) R-loop processing (c) DNA repair (d) retroviral replication

The loss of these enzymes has had different effects on various organisms. While the loss of all functional RNases H renders *B. subtilis* unable to grow [28], it leads to temperature sensitivity [28] and the accumulation of untreated R loops, thus leading to DNA replication initiation at sites other than the oriC [29], in *E. coli*, and higher sensitivity to alkylating agents in *S. cerevsiae* [30]. In mouse, the loss of either

RNase H1 [17] or RNase H2 [25,26] causes embryonic lethality. In human, mutations in RNase H2 subunits cause Aicardi-Goutieres syndrome and mimic congenital viral brain infection [31]. In retroviruses, inactivation of the RNase H domain of reverse transcriptase abolishes virus infectivity [32,33] and therefore retroviral RNase H is regarded as a target for AIDS therapy [34,35].

1.3. MODE OF FUNCTION

The key to enzymatic function is the proper recognition of and binding to the substrate [36-38]. RNase H, which cleaves the phosphodiester bond between two ribonucleotides only when found in hybrid with DNA, accommodates the DNA strand in its phosphate-binding pocket and positions its active site on the RNA strand. The DNA strand of the hybrid is recognized by its ability to adopt a B form conformation; whereas, the RNA strand is recognized through direct contact with the 2'-OH groups of consecutive ribonucleotides. In addition to the main chain fold shared among all RNases H, some RNases H have an additional domain, such as a hybrid binding domain (HBD), TATA binding protein-like (TBP-like) domain, N- or C-terminal extension as a substrate binding domain, or simply a basic protrusion that aids the binding mechanism. The removal of these domains showed a severe decrease in the binding ability to the substrate. For example, while *E. coli* RNase H1 [39] and *Shewanella* sp. SIB1 RNase H1 [12] have a basic protrusion only, others like *Homo sapiens* RNase H1 [40] and *S. cerevisiae* RNase H1 [41] have both a basic protrusion and a hybrid binding domain. Some RNases H like *T. kodakaraensis* RNase H2 [42] and *T. maritima* RNase H2 [43] have a C-terminal extension as a small substrate

binding domain, *B. stearothermophilus* RNase H2 [43] have an N-terminal extension as a small substrate binding domain, and *B. stearothermophilus* RNase H3 [44] and *A. aeolicus* RNase H3 [45] have a TBP-like substrate binding domain.

Upon substrate binding, RNase H employs two metal ions in its active site. Whether it belongs to type 1 or type 2, and since both types share a similar acidic active site motif (DEDD or DEDE) [10] with the exception of LC9-RNase H1 [46] having an atypical active site motif (DEDN), and all having a conserved steric configuration, all RNases H are believed to hydrolyze the substrate with the same two-metal-ion catalysis mechanism [47]. According to this mechanism, the first metal ion, denoted as metal ion A, activates the nucleophilic attack; the second metal ion,

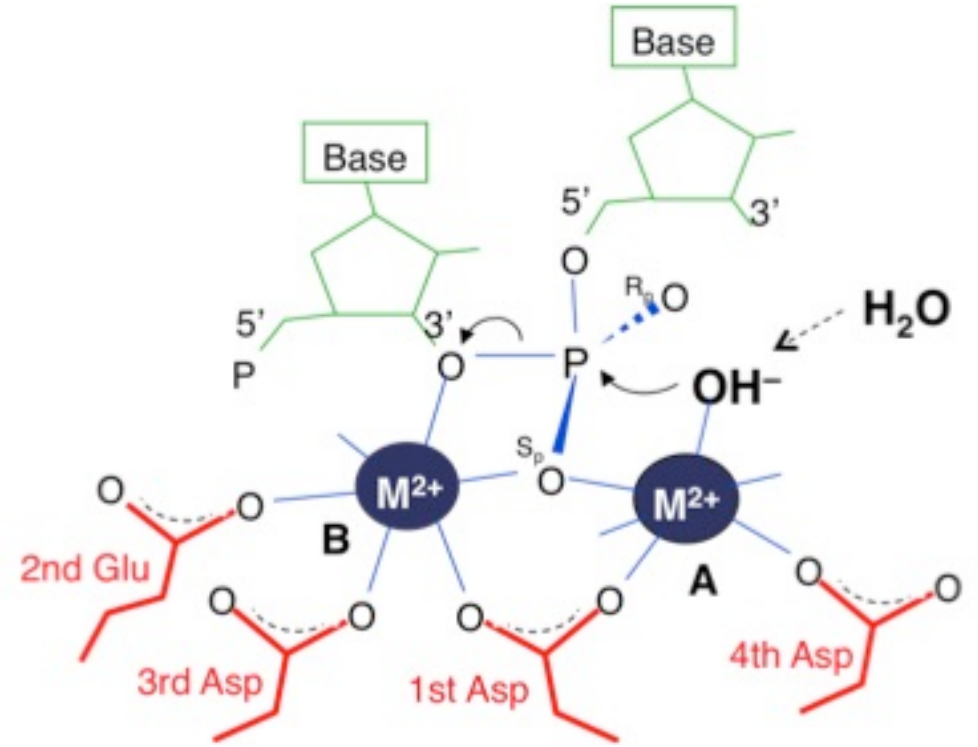

Figure 1.4. **Schematic representation of the two-metal-ion catalysis mechanism of RNase H.** The side chains of the four acidic active site residues (DEDD) are shown in red. The RNA bases are colored green. The attacking hydroxyl ion is highlighted in boldface.

denoted as metal ion B, is required to destabilize the enzyme substrate complex promoting the phosphoryl transfer reaction, and both metal ions A and B stabilize the transition state and aid the product release (**Fig. 1.4**). This was further clarified when the crystal structure of Bh-RNase HC (E188A) was reported in complex with the reaction intermediate and product [48] and in comparison with that in complex with the substrate [37], suggesting that the movement of metal ions A and B facilitates the cleavage process. First, the distance between the metal ions decreases as metal ion A brings the nucleophile closer to the scissile phosphate. Second, metal ion B changes from fully dehydrated and irregular coordination by five ligands in the substrate complex to the hydrated and octahedral coordination in the product complex making the distance between the two metal ions larger, destabilizing the enzyme-substrate complex and reducing the energy barrier to form the product along with the dissociation of metal ion A [48].

1.4. SUBSTRATE SPECIFICITY

Although the two types of RNase H share a lot of characteristics including structural arrangement of the main chain and the active site as well as their catalytic mechanism, they showed clear differences in the substrate preferences *in vitro*, which might reflect that on their *in vivo* function, thus making their physiological roles diverse.

While type 1 RNase H1 prefers and cleaves RNA/DNA hybrids efficiently when at least four interactions (hydrogen bonds) are formed between the enzyme and the 2'-OH groups of four ribonucleotides present in a consecutive [36,37] or non-

consecutive manner [38], type 2 RNase H2 shows a weak activity against this kind of substrate. Instead, type 2 RNase H2 exhibits efficient activity on double-strand DNA (dsDNA) containing a single ribonucleotide, specifically at the 5'-side of the ribonucleotide terming this activity as junction ribonuclease (JRNase) activity [22,43,49-52]. The specific contacts between the protein (conserved tyrosine and GRG residues) and the 2'-OH group of RNA, and distortion of the nucleic acid backbone at the 5'-side of the ribonucleotide are required for JRNase activity [52].The significance of this activity is in the important role it plays in initiating the ribonucleotide excision repair pathway (RER) which removes single ribonucleotides misincorporated into the genome by some DNA polymerases in eukaryotes [13,24-26] and prokaryotes [53]. As the cellular concentrations of rNTPs in yeast were estimated to be 10 to 100 times higher than those of dNTPs and consequently the frequency of ribonucleotides misincorporated by replicative polymerases was shown to be higher than thought [54], the need for the JRNase activity of RNase H2 becomes more essential as it is the only enzyme characterized up to now which is able to recognize and cleave at the 5'-side of a single ribonucleotide embedded in dsDNA. The RER pathway described in yeast suggests that this pathway is most efficient when the ribonucleotide is first incised by RNase H2 at the 5'-side and further excised by the flap endonuclease FEN1 with strand displacement synthesis carried out by DNA polymerase (Pol) δ, PCNA clamp, its loader RFC, and completed by DNA ligase [24]. Other enzymes like Exo1 and Pol ε were shown to have the ability to substitute for FEN1 and Pol δ respectively with less but reasonable efficiency.

Besides initiating the RER pathway, RNases H2 exhibit JRNase activity that catalyzes the cleavage of an Okazaki fragment-like substrate [50], a substrate

mimicking newly synthesized strands during replication of the lagging strand, at the 5'-side of the ribonucleotide, leaving a mono-ribonucleotide uncleaved.

RNase H1 does not exhibit JRNase activity on a dsDNA containing a single ribonucleotide [12,46,51,55,56] and RNase H3 showed both the ability [57,58] and inability [44,51] to cleave this same substrate. However, RNases H1 from *Halobacterium* sp. NRC-1 (Halo-RNase H1) [59], *Sulfolobus tokodaii* (Sto-RNase H1) [60], *Thermotoga maritima* (Tma-RNase H1) [55], and *Escherichia coli* (*E. coli* RNase H1) [50,55] exhibit an activity that catalyzes the cleavage of an Okazaki fragment-like substrate at the RNA-DNA junction (3'-side of the ribonucleotide of the RNA-DNA junction) suggesting a role for RNases H1 in the complete removal of the RNA primers from the Okazaki fragment during the lagging strand DNA synthesis.

As opposed to the normal function of RNase H to cleave the RNA strand of RNA/DNA hybrid, Sto-RNase H1 and retroviral RNases H exhibit double-stranded ribonuclease (dsRNase) activity which degrades the RNA strand of a double-stranded RNA (dsRNA) [60].

1.5. HALOPHILIC RNASE H

Despite the fact that the widely conserved RNase H in most organisms shares the main structural and functional characteristics, it shows several evolutionary diversifications that enable it to tolerate the variety of environments in which its host organism exists, conserving its main function of cleaving the RNA strand of an RNA/DNA hybrid.

Halo-RNase H1 is a type 1 RNase H from *Halobacterium* sp. NRC-1. The source organism is an extreme halophilic archaeon that lives in high saline environments including salt production facilities and salt mines, in addition to natural salt lakes and ponds and in the Dead Sea. Its optimal growth temperature is 42°C with an optimum of 4.3 M NaCl. In turn, it maintains an intracellular concentration of KCl of 4 M [61]. Therefore, its entire protein machinery is dependent on salt in terms of function and stability [62].

Halophilic proteins that have been studied so far are characterized by the abundance of acidic residues, a scarce amount of basic residues, and low hydrophobicity [63]. These acidic residues prevent the protein from aggregation in a high salt condition by competing with salt ions for free water, thus forming a solvation shell having a superior water binding capacity [64]. The majority of these acidic residues are localized on the surface of the protein and in close proximity to each other causing negative electrostatic repulsion when in a low salt condition and consequently destabilizing the folded state of the protein or preventing the protein from folding [63,65]. While in a high salt condition, these acidic residues help halophilic proteins maintain structural and functional integrity by promoting electrostatic interactions with salts in solution [66,67]. Structural studies of several halophilic proteins confirmed the presence of these electrostatic interactions and a few low affinity ions were found bound on the protein surface [68]. Thermodynamic theories suggest that halophilic proteins bind hundreds of salt molecules and thousands of water molecules by coordinating hydrated salt ions with their exposed carboxyl groups [69]. However, these suggested models were not yet visible by crystal structures probably because of the resolution limits.

Another stabilizing agent for halophilic proteins is the salt-bridges frequently found on the surface of halophilic proteins formed between the negatively charged residues (Asp, Glu) and the positively charged residues (Arg, Lys, His). The increased numbers of these salt-bridges found in halophilic proteins in contrast with their mesophilic counterparts suggest that they contribute to the overall stability of halophilic proteins.

In an unusual, yet interesting example, Halo-RNase H1 was shown to be active in low salt condition in the presence of moderate concentrations of divalent metal ions [59], an exception to all characterized enzymes from extreme halophilic organisms.

1.6. OBJECTIVE OF THE STUDY

Although all the characterized proteins from extreme halophilic organisms were shown to exist in a partially folded state in a low salt condition due to the negative charge repulsion caused by the abundance of acidic residues on the surface of these proteins thus rendering those classified as enzymes to become inactive, type 1 RNase H from extreme halophilic archaeon *Halobacterium* sp. NRC-1 (Halo-RNase H1) was shown to be active in the presence of moderate concentrations of Mg^{2+} or Mn^{2+} ions in a low salt condition with the ability to retain activity in the presence of 2.5 M NaCl [59]. This activity triggered me to examine whether the folding of Halo-RNase H1 is independent of salt and whether the substrate binding and stability of Halo-RNase H1 are affected by salt.

Moreover, Halo-RNase H1 has an ability to cleave the RNA-DNA junction of an Okazaki fragment-like substrate [59]. To distinguish this activity from the JRNase activity of RNase H2 that catalyzes the cleavage of an Okazaki fragment-like substrate at the 5'-side of the ribonucleotide of the RNA-DNA junction [50], this activity and JRNase activity of RNase H2 are designated as 3'- and 5'-JRNase activities respectively. In addition to Halo-RNase H1, several type 1 RNases H, including *E. coli* RNase H1, Sto-RNase H1, and Tma-RNase H1 exhibit 3'-JRNase activity. These results prompted me to investigate whether this 3'-JRNase activity can act on a dsDNA containing single ribonucleotides misincorporated into their sequence and hence play a role in DNA repair.

The objective of the present study is therefore divided into two main parts. The first is to clarify the folding mechanism of Halo-RNase H1; and the second is to clarify the role of type 1 RNase H in DNA repair.

This thesis is divided into six chapters.

Chapter 1 introduces RNase H and summarizes previous findings describing its structure and function.

Chapter 2 describes the effect of divalent metal ions on Halo-RNase H1. Analysis using CD spectroscopy showed that divalent metal ions were able to substitute for salt and induce folding of Halo-RNase H1 in a low salt condition thus playing a dual role in the catalysis and folding of Halo-RNase H1.

Chapter 3 presents the crystal structure of Halo-RNase H1 that was determined in the presence of 10 mM $MnCl_2$. Its main chain fold and the steric configuration of its active site highly resemble other RNases H except that it has one

bi-Asp site and one quad-Asp site on its surface and this surface is negatively charged.

Chapter 4 discusses the mechanism by which divalent metal ions induce folding of Halo-RNase H1 using structure-based mutational studies. Mutations at the active site and at the bi/quad-Asp site showed that divalent metal ions initiate folding by first suppressing the negative charge repulsion at the bi/quad-Asp site and then stabilize the folded state by binding to the active site.

Chapter 5 shows that the 3'-JRNase activity exhibited by type 1 RNases H on Okazaki fragment-like substrates is also exhibited on dsDNA containing a single ribonucleotide, by using *E. coli* RNase H1 as a representative member of type 1 RNases H. The ability of type 1 RNase H and type 2 RNase H from the same organism (*Escherichia coli*) to completely remove a single ribonucleotide incorporated into dsDNA was demonstrated, thus playing a possible role in DNA repair mechanism.

Chapter 6 summarizes the novel findings and the significance of this study. The chapter ends with a general conclusion.

CHAPTER 2

ROLE OF DIVALENT METAL IONS IN CATALYSIS AND FOLDING OF HALO-RNASE H1

2.1. INTRODUCTION

Halophilic proteins, isolated from organisms living in environments with elevated salt concentrations, are usually characterized by the abundance of acidic residues on their surface, low content of basic residues, and low hydrophobicity [63]. The negative charge repulsion caused by these acidic residues on the protein surface renders the protein unable to fold in a low salt condition thus yielding inactive enzymes. In a low salt condition, these proteins exist in a partially folded state and can only fold when the negative charge repulsion are suppressed with high salt concentrations.

Halo-RNase H1, a type 1 RNase H from *Halobacterium* sp. NRC-1, is an acidic protein with isoelectric point (p*I*) of 4.2. It shows 33 % amino acid sequence identity with a representative member of non-halophilic RNases H1, *E. coli* RNase H1, a basic protein with p*I* value of 9.0. Halo-RNase H1 lacks the basic protrusion found in *E. coli* RNase H1 and some other RNases H, which plays an important role in substrate binding [39]. Halo-RNase H1 has been shown to exhibit activity in a low salt condition, in the presence of moderate concentrations of Mg^{2+} or Mn^{2+}. It has also been shown to retain this activity in the presence of up to 2.5 M NaCl. Halo-RNase H1 complements the temperature-sensitive growth phenotype of the mutant *E. coli* strain MIC2067 lacking all functional RNases H (RNase H1 and RNase H2) [59]. Therefore, it would be of great interest to determine whether, in contrast to other

halophilic proteins, folding of Halo-RNase H1 is independent of salt and whether substrate binding and stability of Halo-RNase H1 are affected by salt.

In this chapter, I showed that Halo-RNase H1 requires either salt or divalent metal ions for folding and it assumes a partially folded state (I) in the absence of both. Halo-RNase H1 assumes a native folded state (N) in the presence of ≥2 M NaCl, ≥5 mM $MnCl_2$, or ≥300 mM $MgCl_2$. Determination of the enzymatic activity showed that the optimum concentration of divalent metal ions for activity is several-fold lower in a high salt condition than in a low salt condition. These results suggest that in a low salt condition, Halo-RNase H1 requires divalent metal ions not only for activity but also for folding, while in a high salt condition, Halo-RNase H1 requires them only for activity. Hence, I conclude that divalent metal ions play a dual role in the catalysis and folding of Halo-RNase H1.

2.2. MATERIALS AND METHODS

2.2.1 PLASMID CONSTRUCTION

The pET25b derivative for over-expression of the Halo-RNH1 gene (pET-Halo1) was constructed by PCR. The genomic DNA of *Halobacterium* sp. NRC-1, which was kindly donated by Dr. M. Tokunaga, was used as a template. The sequences of the PCR primers used to amplify Halo-RNH1 are 5'-TGCAGCATATGCCAGTCGTCGAGTGCGACATCCAGACCGC-3' for primer 1, and 5'-GCCGCGTCGAATTCCTTATCAGGCATCGTCGAGGGCC-3' for primer 2, where the *Nde*I (primer 1) and *Eco*RI (primer 2) sites are underlined. The resultant

DNA fragment was digested with *Nde*I and *Eco*RI, and ligated into the *Nde*I-*Eco*RI sites of pET25b (Novagen).

All DNA oligomers for PCR were synthesized by Hokkaido System Science. PCR was performed with a GeneAmp PCR system 2400 (Applied Biosystems). The DNA sequences were confirmed by a Prism 310 DNA sequencer (Applied Biosystems).

2.2.2. OVERPRODUCTION AND PURIFICATION

E. coli BL21-CodonPlus(DE3) (Stratagene) was used as a host strain to over-express the gene encoding Halo-RNase H1. The transformant of this strain with the pET25b derivative was grown at 37°C in LB medium containing 50 $\mu g \cdot ml^{-1}$ ampicillin and 30 $\mu g \cdot ml^{-1}$ chloramphenicol. When the absorbance at 600 nm reached approximately 0.5, 1 mM isopropyl thio-β-D-galactoside (IPTG) was added to the culture medium and cultivation was continued at 37°C for an additional 4 h. The subsequent purification procedures of the recombinant protein, which were different from those previously reported for Halo-RNase H1 [59], were carried out at 4°C. Cells were harvested by centrifugation at 8000 *g* for 10 min, suspended in 10 mM Tris-HCl (pH 8.0) containing 1 mM EDTA (buffer A), lysed by sonication, and centrifuged at 30,000 *g* for 30 min. The supernatant was collected, dialyzed against buffer A, and loaded onto a HiTrap Q HP column (5 ml) (GE Healthcare) equilibrated with the same buffer. The protein was eluted from the column with a linear gradient of NaCl from 0 to 1 M. The fractions containing the protein were collected, dialyzed against 5 mM sodium phosphate (pH 6.8), and applied to a hydroxyapatite column (5 ml) (BIO-RAD) equilibrated with the same buffer. The flow-through fraction was collected, dialyzed against 20 mM sodium acetate (pH 5.5) containing 1 mM EDTA and applied to a Mono Q column (1 ml) (GE Healthcare) equilibrated with the same

buffer. The protein was eluted from the column with a linear gradient of NaCl from 0 to 1 M. The fractions containing the protein were collected and loaded to a HiLoad 16/60 Superdex 200pg column (GE Healthcare) equilibrated with buffer A. The fractions containing the protein were collected, dialyzed against 10 mM Tris-HCl (pH 8.0), and used for biochemical characterization.

E. coli MIC3009 was used as a host strain to over-express the gene encoding *E. coli* RNase H1. The transformant of this strain with the pJAL600 plasmid, which was previously constructed [70], was grown at 32°C in LB medium containing 0.1 $mg{\cdot}ml^{-1}$ ampicillin. When the absorbance at 600 nm reached approximately 0.5, the temperature of the growth medium was raised to 42°C and cultivation was continued at 42°C for additional 4 h. Cells were harvested by centrifugation at 8000 *g* for 10 min, suspended in 20 mM Tris-HCl (pH 7.5) containing 1 mM EDTA (buffer A), lysed by sonication, and centrifuged at 30,000 *g* for 30 min and applied to a phosphocellulose P-11 (1 ml) column equilibrated with the same buffer. The protein was eluted from the column with a linear gradient of NaCl from 0 to 0.5 M. The fractions containing the protein were collected and loaded to a HiLoad 16/60 Superdex 200pg column (GE Healthcare) equilibrated with buffer A. The fractions containing the protein were collected, dialyzed against 10 mM Tris-HCl (pH 7.5), and used for biochemical characterization.

The purity of the proteins was analyzed by Tricine SDS-PAGE (SDS-PAGE using the tricine buffer) using a 15% polyacrylamide gel [71], followed by staining with Coomassie Brilliant Blue (CBB). The protein concentration was determined from UV absorption using a cell with an optical path length of 1 cm and an A_{280} value for 0.1% (1.0 $mg{\cdot}ml^{-1}$) solution of 1.26 for Halo-RNase H1 and 2.02 for *E. coli* RNase H1. These values, except for that of *E. coli* RNase H1 experimentally determined

[72], were calculated by using absorption coefficients of 1576 $M^{-1}\cdot cm^{-1}$ for Tyr and 5225 $M^{-1}\cdot cm^{-1}$ for Trp at 280 nm [73].

2.2.3. CD SPECTRA

The CD spectra were measured on a J-725 spectropolarimeter (Japan Spectroscopic) at 25°C. The protein was dissolved in 10 mM Tris-HCl (pH 8.0) containing various concentrations of NaCl, KCl, $MnCl_2$, $MgCl_2$, or $CaCl_2$. For measurement of the far-UV CD spectra (200–260 nm), the protein concentration was approximately 0.1 $mg\cdot ml^{-1}$ and a cell with an optical path length of 2 mm was used. For measurement of the near-UV CD spectra (250–320 nm), the protein concentration was approximately 1.0 $mg\cdot ml^{-1}$ and a cell with an optical path length of 10 mm was used. The mean residue ellipticity, θ, which has the units of $deg\cdot cm^{-2}\cdot dmol^{-1}$, was calculated by using an average amino acid molecular mass of 110 Da.

2.2.4. THERMAL DENATURATION

Thermal denaturation of the protein was analyzed by monitoring the change in CD values at 222 nm as the temperature was increased. The protein was dissolved in 10 mM Tris-HCl (pH 8.0) containing 50 mM or 3 M NaCl, 20 mM $MnCl_2$, 300 mM $MgCl_2$, 3 M NaCl and 20 mM $MnCl_2$, or 3 M NaCl and 300 mM $MgCl_2$. The protein concentration and optical path length were 0.1 $mg\cdot ml^{-1}$ and 2 mm, respectively. The temperature of the protein solution was linearly increased by approximately 1.0°C/min. Thermal denaturation of the proteins was reversible at the conditions examined. The temperature of the midpoint of the transition, T_m, was calculated from curve fitting of the resultant CD values versus temperature data on the basis of a least squares analysis.

2.2.5. ANS FLUORESCENCE SPECTROSCOPY

Binding of 1-anilino-8-naphthalenesulfonic acid (ANS) (Wako) to the protein was analyzed by measuring the fluorescence of ANS at 20°C. The protein (1 μM) and ANS (50 μM) were dissolved in 10 mM Tris-HCl (pH 8.0) in the presence or absence of 20 mM $MnCl_2$, 3 M NaCl, or 6 M GdnHCl. The fluorescence emission was monitored from 400 to 600 nm at an excitation wavelength of 380 nm using spectrofluorophotometer RF-5300PC (Shimadzu). The spectrum obtained in the absence of the protein was used as a blank.

2.2.6. ENZYMATIC ACTIVITY

The RNase H activity was determined by using 12 bp RNA/DNA hybrid (R12/D12) as a substrate. This oligomeric substrate was prepared by hybridizing 1 μM of the 5'-(6-carboxyfluorescein)-labeled 12 base RNA (5'-cggagaugacgg-3') with a 1.5 molar equivalent of the complementary DNA as described previously [11]. Hydrolysis of the substrate at 37°C for 15 min and separation of the products on a 20% polyacrylamide gel containing 7 M urea were carried out as described previously [11]. The reaction buffer was 10 mM Tris-HCl (pH 8.5) containing 1 mM DTT, 0.01% BSA, 50 mM or 3 M NaCl, and various concentrations of $MgCl_2$ or $MnCl_2$ for Halo-RNase H1, and 10 mM Tris-HCl (pH 8.0) containing 1 mM DTT, 0.01% BSA, 50 mM or 3 M NaCl, and 10 mM $MgCl_2$ for *E. coli* RNase H1. The substrate concentration was 1 μM for Halo-RNase H1, and 0.5 μM for *E. coli* RNase H1. The products were detected by Typhoon 9240 Imager (GE Healthcare) and quantified using Image Quant 5.2 analysis software. One unit is defined as the amount of enzyme degrading 1 μmol of the substrate per min at 37°C. The specific activity was defined as the enzymatic activity per milligram of protein.

2.2.7. BINDING ANALYSIS TO SUBSTRATE

Binding of the proteins to the substrate was analyzed in the absence of divalent metal ions using a Biacore X instrument (Biacore) as described previously [55]. The proteins were dissolved in 10 mM Tris-HCl (pH 8.0) containing 50 mM or 3 M NaCl, 1 mM EDTA, 1 mM β-Me, and 0.005 % Tween P20 at various concentrations. The proteins were injected at 25°C at a flow rate of 10 μl·min^{-1} onto the sensor chip on which the 29 bp RNA/DNA hybrid was immobilized. To determine the association constant, K_A, the concentration of the protein injected onto the sensor chip was varied for Halo-RNase H1 and *E. coli* RNase H1. From the plot of the equilibrium binding responses as a function of the concentrations of the proteins, the K_A value was determined using the steady-state affinity software available in BIAEVALUATION (Biacore).

2.2.8. HOMOLOGY MODELING

A model for the three-dimensional structure of Halo-RNase H1 without the N-terminal domain was built by SWISS-MODEL - automated protein homology-modeling server - (Swiss Institute of Bioinfomatics) [74], using the structure of the RNase H domain of the bifunctional protein Rv2228c from *Mycobacterium tuberculosis* (PDB ID: 3HST) [75] as a template. These proteins share the amino acid sequence identity of 45%. The model was viewed and edited with PyMOL (www.pymol.org). Calculations of the electrostatic surface potentials were performed by solving the Poisson-Boltzmann equation with PyMOL Adaptive Poisson-Boltzmann Solver (APBS) tools [76].

2.3. RESULTS AND DISCUSSION

2.3.1. TERTIARY MODEL OF HALO-RNASE H1

Halobacterium sp. NRC-1 RNase H1 (Halo-RNase H1) is characterized by the high content (17.5%) of acidic amino acid residues. A tertiary model of the RNase H domain of this protein shows the abundance of acidic residues on the surface, with some aspartate residues forming clusters (**Fig. 2.1**). As a result, the surface of the RNase H domain of Halo-RNase H1 is negatively charged (**Fig. 2.2**). The overall structure of the RNase H domain of Halo-RNase H1 is similar to that of *E. coli* RNase H1, except that it lacks a basic protrusion. The steric configurations of the four acidic active site residues (Asp75, Glu115, Asp139, and Asp189) are similar to those of *E. coli* RNase H1. Because at least a single divalent metal ion binds to the active site of *E. coli* RNase H1 even in the absence of the substrate [77-79], this divalent metal ion may also bind to the active site of Halo-RNase H1 even in the absence of the substrate.

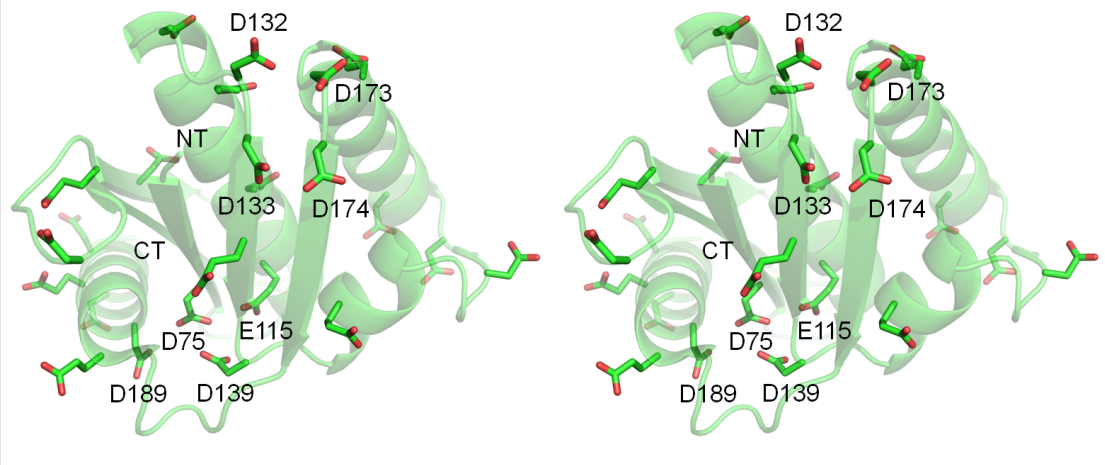

***Figure 2.1*. A tertiary model of Halo-CTD**. Stereoview of the tertiary model of Halo-CTD. The side chains of the acidic residues on the surface, including the four acidic active site residues (D75, E115, D139, D189) and four residues appearing as a cluster (D132, D133, D173, D174), are shown as deep green stick models, in which the oxygen atoms are colored red. NT and CT represent N and C-termini.

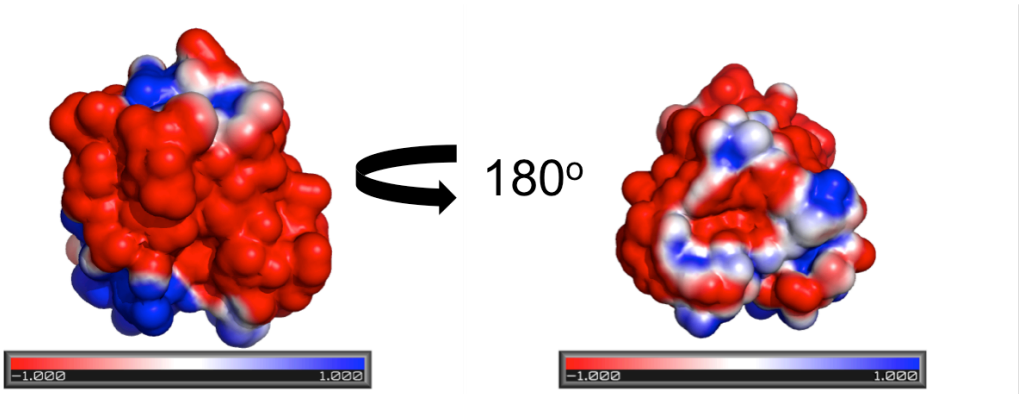

Figure 2.2. **Electrostatic surface potentials of Halo-CTD.** A tertiary model of Halo-CTD shows the electrostatic surface potentials. The negative and positive potentials are in red and blue respectively. The electrostatic potential value ranges from -1 to +1 kT/e. The view direction of the structure in the left panel, which is rotated by 180° in the right panel, is the same as in Fig. 2.1.

2.3.2. REQUIREMENT OF SALT OR DIVALENT METAL IONS FOR FOLDING OF HALO-RNASE H1

To examine whether Halo-RNase H1 requires salt or divalent metal ions for folding, the far-UV CD spectrum of Halo-RNase H1 was measured in the presence or absence of various concentrations of NaCl (**Fig. 2.3**), $MnCl_2$ (**Fig. 2.4.a**), or $MgCl_2$ (**Fig. 2.4.b**). In the absence of salt and divalent metal ions, the far-UV CD spectrum of Halo-RNase H1 gives a trough with a minimum [θ] value of -13,000 at 205 nm, which is accompanied by a shoulder with a [θ] value of -8,000 at 222 nm. However, this spectrum is considerably changed in the presence of salt or divalent metal ions so that the helical content of the protein increases. As a result, the far-UV CD spectrum of Halo-RNase H1 gives a broad trough with a minimum [θ] value of approximately -13,000 at 222 nm in the presence of ≥2 M NaCl (**Fig. 2.3**), ≥5 mM $MnCl_2$ (**Fig. 2.4.a**), or ≥300 mM $MgCl_2$ (**Fig. 2.4.b**). This spectrum was not significantly changed in the presence of both 2 M NaCl and 10 mM $MnCl_2$ or 300 mM $MgCl_2$. A similar spectrum was obtained in the presence of 2 M KCl or 200 mM $CaCl_2$. These results indicate

that Halo-RNase H1 requires either high concentration of salt or moderate concentrations of divalent metal ions for folding. In contrast, *E. coli* RNase H1 requires neither salt nor divalent metal ions for folding [80]. Its spectrum is not significantly changed even in the presence of 2.5 M NaCl [81], suggesting that its structure is not significantly changed in a high salt condition.

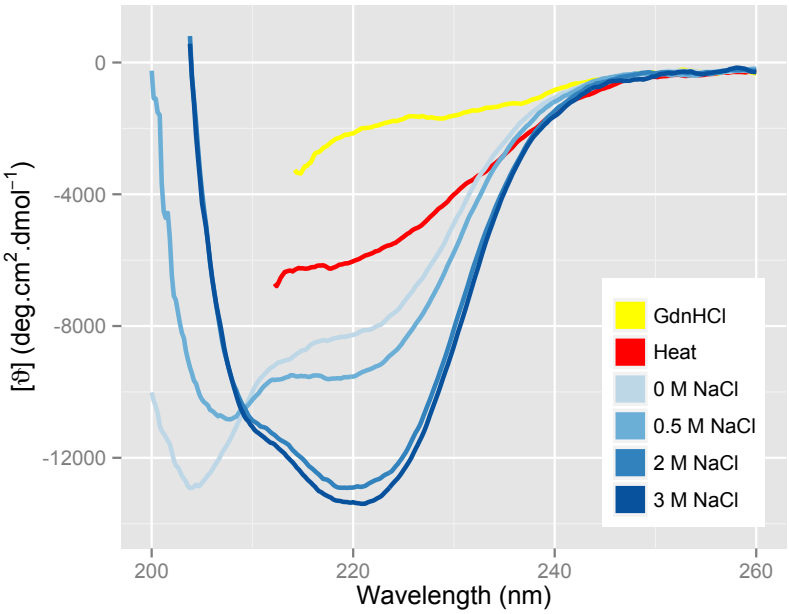

Figure 2.3. **Far-UV CD spectra of Halo-RNase H1.** The far-UV CD spectra measured in the presence of 0 M, 0.5 M, 2 M, or 3 M NaCl (gradient of blue colored lines ranging from light to dark respectively) shown in comparison with those of Halo-RNase H1 in GdnHCl-denatured state (yellow line) and in a heat-denatured state (red line).

To examine whether Halo-RNase H1 is partially folded or almost fully unfolded in the absence of salt and divalent metal ions, the far- and near-UV CD spectra of Halo-RNase H1 were measured in the presence of 3 M NaCl at 100°C (for heat-denatured state) or in the absence of salt and divalent metal ions and presence of 6 M GdnHCl at 25°C (for GdnHCl-denatured state). The far-UV CD spectra of Halo-RNase H1 were not measured at ≤ 210 nm in these conditions due to striking spectral fluctuation. As shown in **Figure 2.3**, the far-UV CD spectrum of Halo-RNase H1 without salt and divalent metal ions was different from those of Halo-RNase H1 in a

heat-denatured and GdnHCl-denatured state. The depth of the trough (or shoulder) in the former spectrum was deeper than those in the latter spectra. Likewise, the near-UV CD spectrum of Halo-RNase H1 without salt and divalent metal ions, which reflects the environment of the tryptophan and tyrosine residues, was different from those of Halo-RNase H1 in a heat-denatured and GdnHCl-denatured state, as shown in **Figure 2.5**. The near-UV CD spectrum of Halo-RNase H1 in a native state gave three peaks with [θ] values of 30 at 275 nm, 50 at 285 nm, and 55 at 295 nm. The spectrum of Halo-RNase H1 without salt and divalent metal ions also gave these peaks but with much lower [θ] values. These peaks almost fully disappeared in the spectra of Halo-RNase H1 in a heat-denatured and GdnHCl-denatured state. These results suggest that Halo-RNase H1 is partially folded in the absence of salt and divalent metal ions. Therefore, we define the structure of Halo-RNase H1 in the absence of salt and divalent metal ions as a partially folded state (intermediate state) and that in the presence of salt or divalent metal ions as a folded state (native state), and designate Halo-RNase H1s in an intermediate and native state as Halo-RNase $H1^I$ and Halo-RNase $H1^N$, respectively. Halo-RNase $H1^I$ and Halo-RNase $H1^N$ change their conformations in a reversible manner. The far-UV CD spectra of Halo-RNase H1 in the presence of 0.5 M NaCl (**Fig. 2.3**), 1 mM $MnCl_2$ (**Fig. 2.4.a**), and 10-50 mM $MgCl_2$ (**Fig. 2.4.b**) suggest that these concentrations of salt and divalent metal ions are not sufficient to shift an equilibrium between Halo-RNase $H1^I$ and Halo-RNase $H1^N$ so that the fraction of Halo-RNase $H1^N$ increases to nearly 100%.

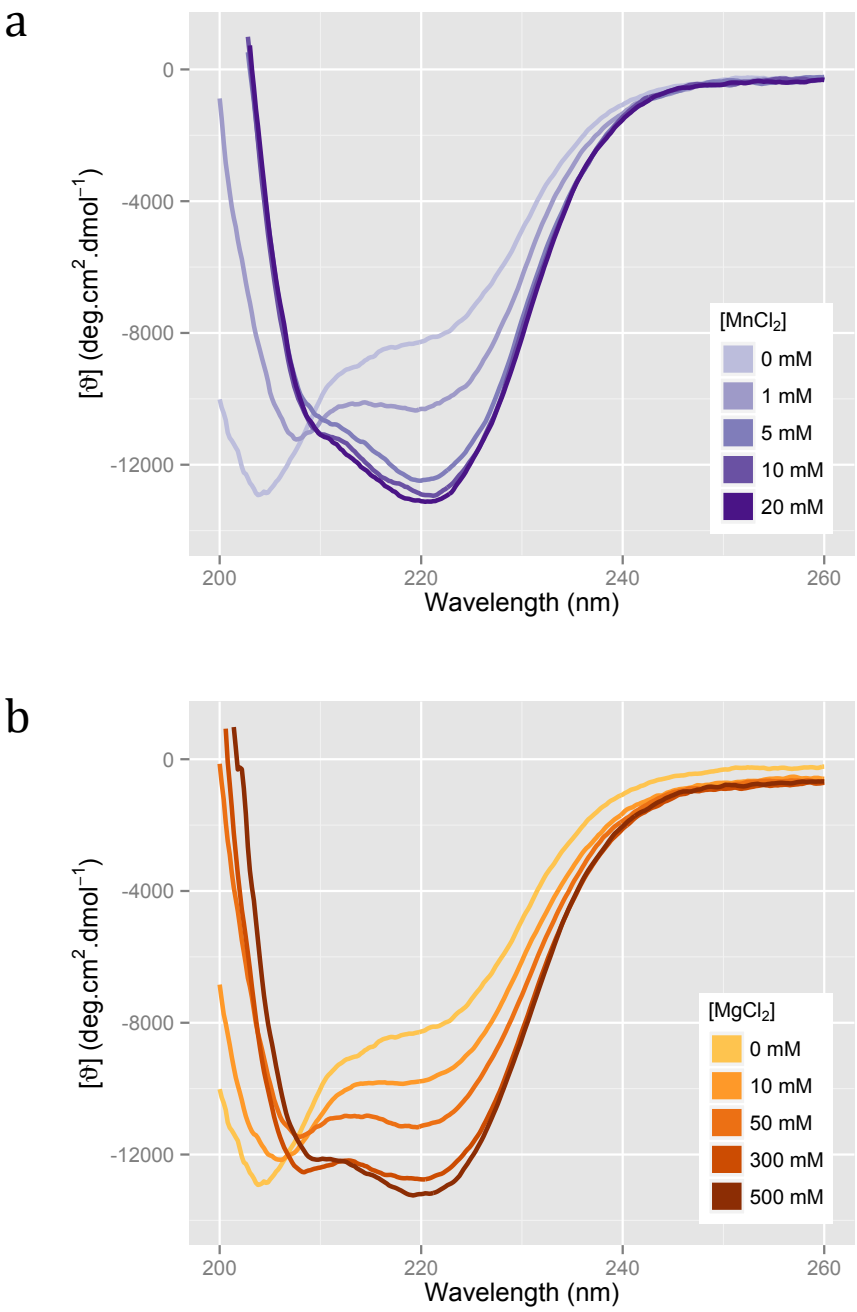

Figure 2.4. **Far-UV CD spectra of Halo-RNase H1.** (a) The far-UV CD spectra measured in the absence of salt and the presence of 0 mM, 1 mM, 5 mM, 10 mM, or 20 mM $MnCl_2$ (gradient of purple colored lines ranging from light to dark respectively) are shown. (b) The far-UV CD spectra measured in the absence of salt and the presence of 0 mM, 10 mM, 50 mM, 300 mM, or 500 mM $MgCl_2$ (gradient of orange colored lines ranging from light to dark respectively) are shown.

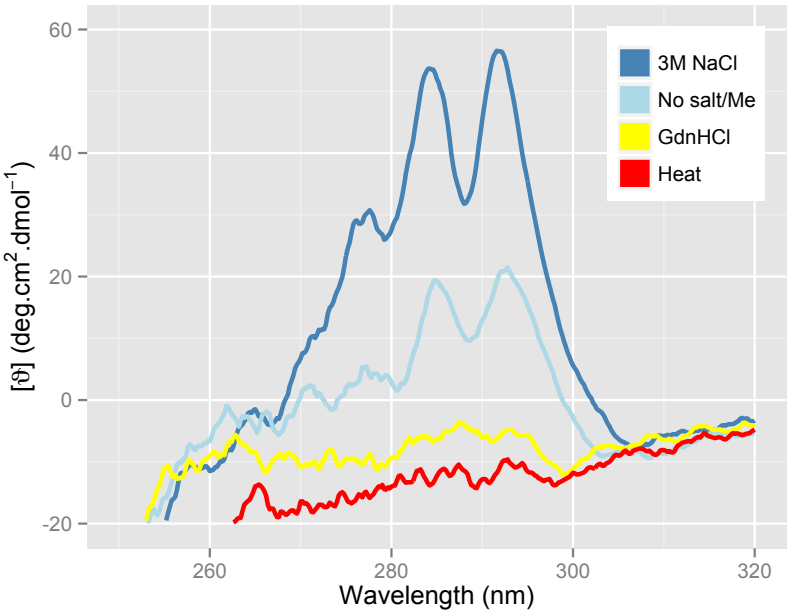

Figure 2.5. **Near-UV CD spectra of Halo-RNase H1.** The near UV-CD spectrum shown in the absence of salt and divalent metal ions (light blue) is shown in comparison with those of Halo-RNase H1 in a native state (blue), GdnHCl-denatured state (yellow), and heat-denatured state (red).

2.3.3. PROTEIN STABILITY

To examine whether salt and divalent metal ions affect the stability of Halo-RNase $H1^N$, thermal denaturation of Halo-RNase H1 was analyzed in the presence of divalent metal ions (20 mM $MnCl_2$ or 300 mM $MgCl_2$), salt (3 M NaCl), or both of them (20 mM $MnCl_2$ or 300 mM $MgCl_2$ and 3 M NaCl) by CD spectroscopy. Thermal denaturation of Halo-RNase H1 was reversible and followed a two-state mechanism in these conditions. The results are shown in **Figure 2.6**. The T_m values of Halo-RNase H1 determined in these conditions are summarized in **Table 2.1**. The thermal denaturation curves in the presence of the Mn^{2+} ions are not shown in **Figure 2.6**, because they were nearly identical to those in the presence of the Mg^{2+} ions. The T_m value of Halo-RNase H1 determined in the presence of both divalent metal ions and salt is higher than those determined in the presence of divalent metal ions alone and salt alone by 26-30°C and 9-10°C respectively, suggesting that salt and divalent

metal ions independently contribute to the stabilization of Halo-RNase $H1^N$ by 26-30°C and 9-10°C, respectively.

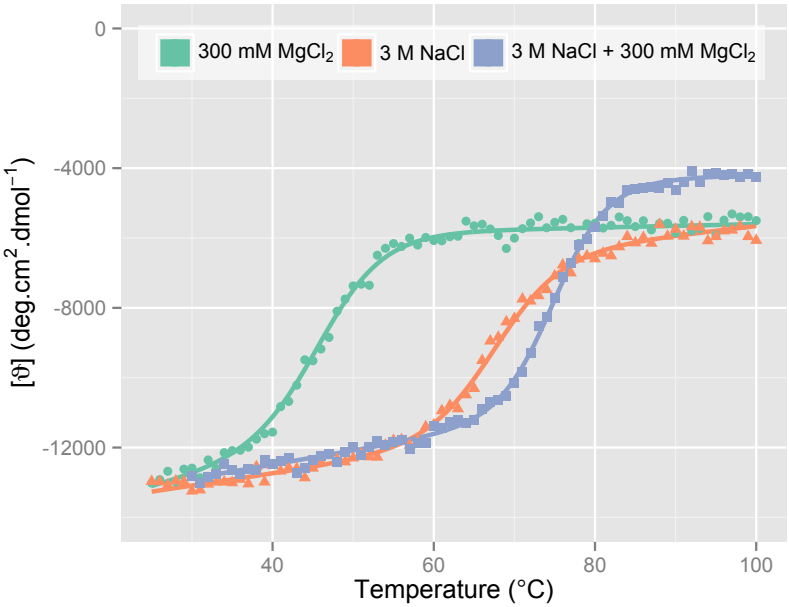

Figure 2.6. **Thermal denaturation curves of Halo-RNase H1.** The thermal denaturation curves of Halo-RNase H1 measured in the presence of 300 mM $MgCl_2$ (green), 3 M NaCl (orange), or 300 mM $MgCl_2$ and 3 M NaCl (slate) are shown. These curves were obtained at pH 8.0 by monitoring the change in CD value at 222 nm at a scan rate of 1°C/min. The theoretical curves are drawn on the assumption that the proteins are denatured via a two-state mechanism.

It has been reported that *E. coli* RNase H1 is stabilized by approximately 10°C in the presence of 2 mM $MnCl_2$, 50 mM $CaCl_2$, or 100 mM $MgCl_2$, and 17°C in the presence of 2.5 M NaCl [81]. The stabilization effects of the divalent metal ions and NaCl are roughly additive. Divalent metal ions stabilize the protein by binding to the active site and suppressing negative charge repulsion at this site. Salt stabilizes the protein by increasing hydrophobic interactions at the protein core. Thus, the stabilization mechanisms of Halo-RNase H1 with salt and divalent metal ions are similar to those of *E. coli* RNase H1, except that salt stabilizes Halo-RNase H1 not only by increasing hydrophobic interactions at the protein core but also by decreasing negative charge repulsion on the protein surface. Halo-RNase H1 seems to be more

significantly stabilized by salt than is *E. coli* RNase H1, probably because electrostatic repulsion on the protein surface of Halo-RNase H1 are stronger than those of *E. coli* RNase H1.

Halo-RNase H1^{I} is incompletely folded probably because it is too unstable to be folded in the absence of salt and divalent metal ions. The finding that Halo-RNase H1 is folded in the presence of 20 mM $MnCl_2$ and absence of salt suggests that negative charge repulsion at the active site are major forces that prevent folding of Halo-RNase H1 in the absence of divalent metal ions and salt. Suppression of negative charge repulsion at the active site by binding of divalent metal ion(s) may be sufficient to facilitate folding of Halo-RNase H1.

Protein	Metal	Salt	T_m (°C)	ΔT_m[a] (°C)
Halo-RNH1	300 mM $MgCl_2$		46.2 ± 0.1	-
	20 mM $MnCl_2$		50.0 ± 0.1	+3.8
		3 M NaCl	66.9 ± 0.1	+20.7
	300 mM $MgCl_2$	3 M NaCl	76.5 ± 0.1	+30.3
	20 mM $MnCl_2$	3 M NaCl	76.0 ± 0.1	+29.8

***Table 2.1.* T_m values of Halo-RNase H1 and its derivatives** The melting temperature (T_m), which is the temperature of the midpoint of the thermal denaturation transition, was determined from the thermal denaturation curve. The thermal denaturation curves of Halo-RNase H1 in the presence of 300 mM $MgCl_2$, 3 M NaCl, or 300 mM $MgCl_2$ and 3 M NaCl are shown in Fig. 2.6. as representatives.

[a] ΔT_m is calculated as T_m of Halo-RNase H1 determined – T_m of Halo-RNase H1 determined in the presence of 300 mM $MgCl_2$.

2.3.4. ANS FLUORESCENCE SPECTROSCOPY

To examine whether 1-anilino-8-naphthalenesulfonic acid (ANS) binds more effectively to Halo-RNase H1 in a partially folded state than to that in a fully folded or unfolded state, as reported for non-halophilic proteins [82], ANS binding to Halo-RNase H1 was analyzed in the presence or absence of salt (3 M NaCl), divalent metal ions (20 mM $MnCl_2$), or 6 M GdnHCl, by measuring the fluorescence spectrum of ANS. ANS is an organic compound usually used as a fluorescent molecular probe. It contains both a sulfonic acid and an amine group. It becomes highly-fluorescent when it binds to a hydrophobic pocket of proteins [82]. As shown in **Figure 2.7**, Halo-RNase H1 exhibits ANS fluorescence in the presence of salt. However, it exhibits little ANS fluorescence in the presence of divalent metal ions, suggesting that ANS does not bind to Halo-RNase $H1^N$. It binds to Halo-RNase $H1^N$ in the presence of salt, probably due to an increase in hydrophobicity on the protein surface. Halo-RNase H1 exhibits little ANS fluorescence either in the absence of salt and divalent metal ions or in the presence of 6 M GdnHCl, suggesting that ANS binds to neither Halo-RNase

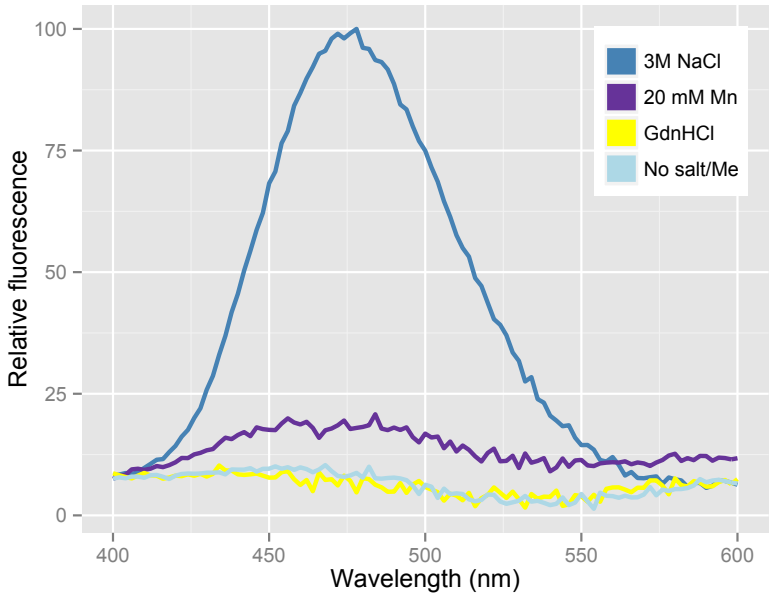

Figure 2.7. **ANS fluorescence spectra.** The ANS fluorescence spectra of Halo-RNase H1 was measured at 20°C and pH 8.0 in the absence (light blue) or the presence of 20 mM $MnCl_2$ (purple), 3 M NaCl (blue), or 6 M GdnHCl (yellow).

$H1^I$ nor Halo-RNase H1 in an unfolded state. The high content of acidic residues on the protein surface may prevent the exposure of hydrophobic pockets in a partially folded state. It is also possible that hydrophobic pockets do not exist in a partially folded state of halophilic proteins.

2.3.5. ENZYMATIC ACTIVITY

The enzymatic activity of Halo-RNase H1 was determined in the presence of 50 mM or 3 M NaCl at 37°C using the R12/D12 substrate. The concentration of $MnCl_2$ or $MgCl_2$ varied from 1 to 100 mM. *E. coli* RNase H1 did not exhibit activity in the presence of 3 M NaCl. The separation of oligoribonucleotides produced upon hydrolysis of the substrate in the presence of 50 mM or 3 M NaCl on a urea gel is shown in **Figure 2.8**. Halo-RNase H1 cleaved the substrate at all sites between a4 and g11 with

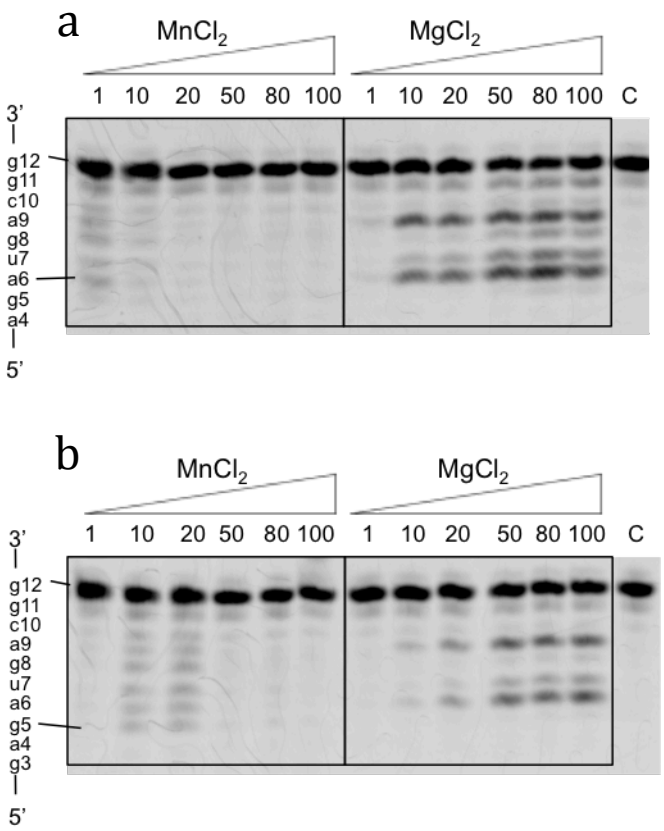

Figure 2.8. **Cleavage of R12/D12 substrate with Halo-RNase H1.** The 5'-end labeled R12/D12substrate was hydrolyzed by Halo-RNase H1 at 37°C for 15 min in the presence of various concentrations of $MnCl_2$ or $MgCl_2$ and 3 M (a) or 50 mM (b) NaCl. The hydrolysates were separated on a 20% polyacrylamide gel containing 7 M urea. The concentration of the substrate was 1 µM. The amount of enzyme added to the reaction mixture (10 µl) was 1 ng. The enzyme and divalent metal ions used to hydrolyze the substrate are shown above the gel together with the concentrations of the divalent metal ions. The sequence of R12 is indicated along the gel.

similar efficiencies in the presence of the Mn^{2+} ions regardless of the presence of 50 mM or 3 M NaCl. Likewise, it cleaved the substrate at four sites between a6 and c10, preferably at a6-u7 and a9-c10, in the presence of the Mg^{2+} ions regardless of the presence of 50 mM or 3 M NaCl. These results indicate that the cleavage-site specificity of Halo-RNase H1, which varies for different divalent metal ions, is not seriously changed regardless of the presence of 50 mM or 3 M NaCl. However, the optimum concentration of divalent metal ions for activity in the presence of 3 M NaCl (1 mM for $MnCl_2$ or 20 mM for $MgCl_2$) was lower than that in the presence of 50 mM NaCl (20 mM for $MnCl_2$ or 100 mM for $MgCl_2$). The latter concentration is similar to that reported previously [59]. In a high salt condition, in which Halo-RNase H1 is folded, a physiological concentration of divalent metal ions seems to be sufficient to permit their binding to the active site and thereby to activate the enzyme. In contrast, in a low salt condition, in which Halo-RNase H1 is incompletely folded, higher concentrations of divalent metal ions are necessary to permit their binding to the active site and thereby to facilitate folding of the enzyme prior to the activation. Thus, divalent metal ions play a dual role in catalysis and folding of Halo-RNase H1.

2.3.6. BINDING TO SUBSTRATE

Binding of Halo-RNase H1 to 29 bp RNA/DNA hybrid (R29/D29) was analyzed at 25°C and pH 8.0 in the absence of divalent metal ions and presence of 50 mM or 3 M NaCl using surface plasmon resonance. Binding of *E. coli* RNase H1 to this substrate was also analyzed for comparative purposes. The protein was injected onto a sensor chip on which the R29/D29 substrate was immobilized. Halo-RNase H1 did not bind to the substrate in the presence of 50 mM NaCl because it is not folded in a low salt condition, but bound to it in the presence of 3 M NaCl (**Fig. 2.9**).

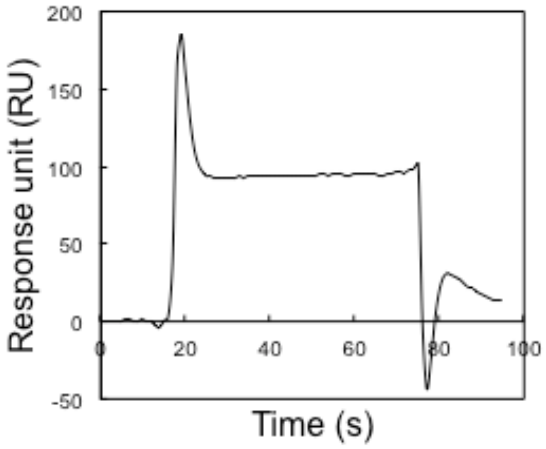

Figure 2.9. **Binding of Halo-RNase H1 to 29 bp RNA/DNA hybrid.** Sensogram from Biacore showing the binding of Halo-RNase H1 (800 nM) to immobilized 29bp RNA/DNA hybdrid in the presence of 3 M NaCl.

In contrast, *E. coli* RNase H1 bound to the substrate in the presence of 50 mM NaCl, but did not bind to it in the presence of 3 M NaCl. This is the reason why *E. coli* RNase H1 does not exhibit activity in the presence of 3 M NaCl. The association constant, K_A, of Halo-RNase H1 was estimated to be 4.0 x 10^6 M^{-1} from the equilibrium binding level to the substrate in the presence of 3 M NaCl, while that of *E. coli* RNase H1 was estimated to be 2.7 x 10^7 M^{-1} in the presence of 50 mM NaCl, which is comparable to that previously determined using the R36/D36 substrate (4.7 x 10^7 M^{-1}) [39]. Thus, the K_A value of Halo-RNase H1 is lower than that of *E. coli* RNase H1 by 8 fold, but is comparable to that of *Thermotoga maritima* RNase H1, which has been determined to be 6.3 x 10^6 M^{-1} at pH 8.0 in the presence of 50 mM NaCl using the same substrate [55]. Like *E. coli* RNase H1, *T. maritima* RNase H1 loses the ability to bind to the substrate at high (≥0.5 M) NaCl concentrations [55].

According to the co-crystal structures of *Bacillus halodurans* RNase H1 [37] and human RNase H1 [36] with the substrate, the RNA/DNA hybrid binds to the protein, in such a way that the RNA backbone fits in one groove containing the active site and the DNA backbone fits in the other groove. At the RNA-binding groove, the 2'-OH

groups of four or five consecutive ribonucleotides form hydrogen bonds with the backbone atoms of the protein. At the DNA-binding groove, several polar residues form a phosphate-binding pocket, which is responsible for anchoring of the B-form DNA. High similarity of a tertiary model of Halo-RNase H1 to that of *T. maritima* RNase H1 and the crystal structures of *E. coli* RNase H1, *B. halodurans* RNase H1, and human RNase H1 strongly suggests that the RNA/DNA hybrid binds to Halo-RNase H1 in a similar manner. The binding affinity of Halo-RNase H1 is lower than that of *E. coli* RNase H1 but is comparable to that of *T. maritima* RNase H1, probably because *E. coli* RNase H1 contains a basic protrusion whereas Halo-RNase H1 and *T. maritima* RNase H1 do not. Electrostatic interactions between the basic protrusion and substrate have been reported to be important for substrate binding [39,83], more precisely for initial contact with the substrate [36]. In a high salt condition, these electrostatic interactions may be suppressed and therefore the binding affinity of *E. coli* RNase H1 is greatly reduced. The reason why *E. coli* RNase H1 and *T. maritima* RNase H1 almost fully lose their binding ability to the substrate in a high salt condition remains to be clarified. However, the strengthened binding ability of Halo-RNase H1 at high salt concentration can be due to the ion uptake theory proposed by S. Bergqvist *et al*. [84]. While non-halophilic enzymes release ions (mainly cations) upon binding to the negatively charged DNA, binding of halophilic enzymes is characterized by the uptake of cations abundant in the medium as they are approaching the DNA, where these cations form a bridge between the DNA phosphate backbone and the negatively charged regions on the protein surface [85]. Alternatively, the conformation of the substrate may be changed in a high salt condition, in such a way that the RNA and DNA backbones of the substrate do not fit

in two grooves on the protein surface of non-halophilic enzymes but fit in those of halophilic enzymes.

2.4. CONCLUSION

In this chapter, I showed that divalent metal ions play a dual role in the catalysis and folding of *Halobacterium* sp. NRC-1 RNase H1 (Halo-RNase H1). In a low salt condition, Halo-RNase H1 requires divalent metal ions not only for activity but also for folding. In a high salt condition, Halo-RNase H1 requires them only for activity. Divalent metal ions stabilize a native structure of Halo-RNase H1 by binding to the active site and suppressing negative charge repulsion at this site. Salt stabilizes a native state of Halo-RNase H1 by increasing hydrophobic interactions at the protein core and decreasing negative charge repulsion on the protein surface. Halo-RNase H1 is incompletely folded in the absence of salt and divalent metal ions due to its great instability. In contrast, *E. coli* RNase H1 is fully folded in this condition. However, *E. coli* RNase H1 loses the binding ability to the substrate in a high salt condition, probably due to a slight conformational change of the substrate binding site of the protein and/or the substrate. Halo-RNase H1 may acquire the binding ability to the substrate in a high salt condition by increasing the content of the acidic residues on the protein surface. Thus, Halo-RNase H1 may lose the ability to fold in a low salt condition at the cost of its functional adaptation to high salt environment. ANS does not bind to Halo-RNase H1 in a partially folded state suggesting that hydrophobic pockets may not be exposed in a partially folded state of halophilic proteins as compared to molten globules of mesophilic proteins.

CHAPTER 3

CRYSTAL STRUCTURE OF HALO-RNASE H1

3.1. INTRODUCTION

As shown in the previous chapter, Halo-RNase H1 exists in a partially folded state (I) in a low salt condition. Uniquely, not only high concentration of salt but also moderate concentrations of divalent metal ions are able to shift the equilibrium from a partially folded state (I) to a native state (N). Primary structure analysis of Halo-RNase H1 shows that it consists of an N-terminal domain (NTD) in addition to its C-terminal RNase H domain (CTD). Blast analysis detected no significant homology for the NTD with amino acid sequences of other studied proteins. It also shows the presence of several bi-aspartate (bi-Asp) sites in its sequence. Therefore, it is of great interest to know how the NTD is folded and how these bi-Asp sites are localized in the tertiary structure of the protein. It is also interesting to analyze the role of the NTD and if it contributes to the activity of this enzyme.

In this chapter, the crystal structure of Halo-RNase H1 was determined in a low salt condition in the presence of 10 mM $MnCl_2$ and refined to 1.4 Å. The refined model consists of two molecules both lacking the N-terminal domain (NTD). The main chain fold of Halo-RNase H1 and the steric configuration of its four active site residues show high similarity with other RNases H1. The surface of the protein is negatively charged due to the abundance of acidic residues. Three bi-Asp sites are found to be present on the surface, two of which are located close to each other forming a quad-Asp site. Molecule A in the crystal lattice containing two molecules

(A and B) contacts the active site of molecule B through its bi-Asp site, the active site of molecule A" from another lattice through its quad-Asp site, and the quad-Asp site of molecule A' through its active site. All these contacts are mediated with manganese ions.

Biochemical characterization of Halo-RNase H1 derivatives without an N- or C-terminal domain indicates that the NTD is dispensable for stability, activity, folding, and substrate binding.

3.2. MATERIALS AND METHODS

3.2.1. PLASMID CONSTRUCTION

The plasmid pET25b derivative construction, pET-Halo1, for overproduction of Halo-RNase H1 was previously described in Section 2.2.1. The pET25b derivatives for over-expression of the Halo-CTD and Halo-NTD genes were constructed by PCR. Plasmid pET-haloRNH1 was used as a template. The sequences of the PCR primers are 5'-TGCAGCATATGCCAGTCGTCGAGTGCGACATCCAGACCGC-3' for primer 1, 5'-GCCGCGTCGAATTCCTTATCAGGCATCGTCGAGGGCC-3' for primer 2, 5'-TGCAGCATATGCGCGTGCACGCCTACTTCG-3' for primer 3, and 5'-GCCGCGTCGAATTCCTTATCAGCCGCCGCGGTCGGGTTG-3' for primer 4, where the *Nde*I (primers 1 and 3) and *Eco*RI (primers 2 and 4) sites are underlined. Primers 2 and 3 and primers 1 and 4 were used to amplify the Halo-CTD, and Halo-NTD genes respectively. The resultant DNA fragments were digested with *Nde*I and *Eco*RI, and ligated into the *Nde*I-*Eco*RI sites of pET25b (Novagen).

All DNA oligomers for PCR were synthesized by Hokkaido System Science. PCR was performed with a GeneAmp PCR system 2400 (Applied Biosystems). The DNA sequences were confirmed by a Prism 310 DNA sequencer (Applied Biosystems).

3.2.2. OVERPRODUCTION AND PURIFICATION

Overproduction of Halo-RNase H1, Halo-CTD, and Halo-NTD using *E. coli* BL21-CodonPlus(DE3) (Stratagene) transformants with pET25b derivatives were performed as described in Section 2.2.2. The purification procedures of Halo-NTD were slightly modified, such that the hydroxyapatite column chromatography step was eliminated. All purification procedures were carried out at 4°C.

The purity of the proteins was analyzed by Tricine SDS-PAGE (SDS-PAGE using the tricine buffer) using a 15% polyacrylamide gel [71], followed by staining with Coomassie Brilliant Blue (CBB). The protein concentration was determined from UV absorption using an A_{280} value of 1.26 for Halo-RNase H1, 1.39 for Halo-CTD, and 0.99 for Halo-NTD for a 0.1% (1.0 mg ml^{-1}) solution. These values were calculated by using e of 1576 M^{-1} cm^{-1} for Tyr and 5225 M^{-1} cm^{-1} for Trp at 280 nm [73].

3.2.3. CRYSTALLIZATION

For crystallization, Halo-RNase H1 was dialyzed against 10 mM Tris-HCl (pH 8.0) containing 20 mM $MnCl_2$ at 4°C for folding, and loaded onto a Heparin HP column (5 ml) (GE Healthcare) equilibrated with the same buffer. The protein was eluted from the column with a linear gradient of NaCl from 0 to 0.5 M. The fractions containing the protein were collected, dialyzed against the same buffer containing 0.4 M NaCl, and used for crystallization.

The crystallization conditions were initially screened using crystallization kits from Hampton Research (CA, USA) (Crystal Screens I and II) and Emerald Biostructures (WA, USA) (Wizard I, II, III and IV). The conditions were surveyed using sitting-drop vapor-diffusion method at 4°C and 20°C. Drops were prepared by mixing the protein solution at the concentration of 6 mg ml^{-1} with the reservoir solution at equal volume (1 µl), and were vapor-equilibrated against 100 µl reservoir solution. Cube-shaped single crystals appeared after two months at 4°C in Wizard III No. 39 [100 mM imidazole (pH 6.8), 20% polyethylene glycol (PEG) 8000, and 3% 2-methyl-2,4-pentanediol (MPD)]. Since the crystal was obtained in the reservoir solution containing 20% PEG 8000, it was used directly for diffraction data collection without further cryoprotection.

3.2.4. X-RAY DIFFRACTION DATA COLLECTION AND STRUCTURE DETERMINATION

X-ray diffraction data set of Halo-RNase H1 was collected at a wavelength of 0.9 Å at -173°C using synchrotron radiation on the BL44XU station at SPring-8 (Hyogo, Japan). The data set was indexed, integrated and scaled using the program HKL2000. The structure was solved by the molecular replacement method using MOLREP [86] in the CCP4 program suite. The crystal structure of Sto-RNase H1 (PDB code 2EHG) was used as a starting model. Automatic model building was done using ARP/wARP [87]. Structural refinement was carried out using REFMAC5 of the CCP4 program and the model was corrected using COOT [88]. The statistics for data collection and refinement are summarized in **Table 3.1**. The figures were prepared using PyMOL (http://www.pymol.org). Calculations of the electrostatic surface potentials were performed by solving the Poisson–Boltzmann equation with PyMOL Adaptive Poisson–Boltzmann Solver (APBS) tools [76].

3.2.5. PROTEIN DATA BANK ACCESSION NUMBER

The coordinates and structure factors for Halo-RNase H1 have been deposited in the Protein Data Bank under accession code 4NYN.

3.2.6. GEL FILTRATION CHROMATOGRAPHY

For estimation of the molecular mass of Halo-RNase H1 in the presence of Mn^{2+} ion, the protein was applied to a HiLoad 16/60 Superdex 200pg column (GE Healthcare) equilibrated with 10 mM Tris-HCl (pH 7.5) containing 10 mM $MnCl_2$. Thyroglobulin (670 kDa), bovine gamma globulin (158 kDa), chicken ovalbumin (44 kDa), horse myoglobin (17 kDa), and vitamin B_{12} (1.35 kDa) were used as markers.

3.2.7. CD SPECTRA

The far-UV (200-260 nm) CD spectra were measured on a J-725 spectropolarimeter (Japan Spectroscopic) at 25°C as described in Section 2.2.3.

3.2.8. THERMAL DENATURATION

Thermal denaturation of the protein was analyzed by monitoring the change in CD values at 222 nm as the temperature was increased as described in Section 2.2.4.

3.2.9. ENZYMATIC ACTIVITY

The RNase H activity was determined by using 12 bp RNA/DNA hybrid (R12/D12) as a substrate as described in Section 2.2.6. One unit is defined as the amount of enzyme degrading 1 μmol of the substrate per min at 37°C. The specific activity was defined as the enzymatic activity per milligram of protein.

3.2.10. BINDING ANALYSIS TO SUBSTRATE

Binding of the proteins to the substrate was analyzed in the absence of divalent metal ions using a Biacore X instrument (Biacore) as described in Section 2.2.7.

3.3. RESULTS AND DISCUSSION

3.3.1. CRYSTALLIZATION AND STRUCTURE DETERMINATION

Halo-RNase H1 was crystallized in the presence of 10 mM $MnCl_2$. Attempts to crystallize the protein in the presence of high concentrations (≥2 M) of NaCl have so far been unsuccessful. The crystal structure of Halo-RNase H1 was determined at 1.4Å resolution. The refined model consists of two Halo-RNase H1 molecules (A and B) in an asymmetric unit. Molecule A consists of residues 67 to 199 with two manganese ions, while molecule B consists of residues 68-199 with three manganese ions. The N-terminal domain (NTD) (residues 1-66) is not visible in the electron density map probably due to structural disorder. The structures of these two molecules are nearly identical with each other with the root-mean-square deviation (RMSD) value of 0.81Å for 132 Cα atoms. We used the structure of molecule A in this study. Details of the data-collection statistics and refinement are summarized in **Table 3.1**.

Crystal	**Halo-RNase H1**
Wavelength (Å)	0.9
Space group	I41
Cell parameters	
a, b, c (Å)	115.8, 115.8, 38.28
$\alpha=\beta=\gamma$ (^{o})	90.0
Resolution range (Å)	50.0-1.41
Highest-resolution shell (Å)	1.43-1.41
Reflections measured	362,644
Unique reflections	48,997
Completeness (%)	99.9 (98.9) [a]
R_{merge} (%)[b]	7.4 (38.1) [a]
Average I/σ (I)	31.6 (3.6) [a]
Refinement statistics	
Resolution limits (Å)	40.9-1.41
No. of atoms	
Protein/water/Mn^{2+}	1994/303/5
R_{work} (%) / R_{free} (%)[c]	17.5/20.5
RMS deviations from ideal values	
Bond lengths (Å)	0.008
Bond angles (^{o})	1.02
Average B-factors (Å^2)	
Protein A/B	16.3/18.1
Water/ Mn^{2+}	25.8/12.3

Ramanchandran plot (%)	
Most favored regions	98.0
Additional allowed regions	2.0

Table 3.1. **Data collection and refinement statistics.** [a] Values in parentheses are for the highest resolution cell. [b] R_{merge} = S $|I_{hkl}-\langle I_{hkl}\rangle|$ / SI_{hkl}, where I_{hkl} is an intensity measurement for reflection with indices *hkl* and $\langle I_{hkl}\rangle$ is the mean intensity for multiply recorded reflections. [c] R_{free} was calculated using 5% of the total reflections chosen randomly and omitted from refinement.

3.3.2. OVERALL STRUCTURE

The crystal structure of Halo-RNase H1 is shown in **Figure 3.1**. The overall structure of Halo-RNase H1 consists of a five-stranded mixed β-sheet with three antiparallel (β1-β3) and two parallel (β4 and β5) strands and five α-helices (αA, αB, αC, αD and αE). It lacks the basic protrusion, which consists of αC-helix and a following loop and is important for substrate binding of *E. coli* RNase H1 [39].

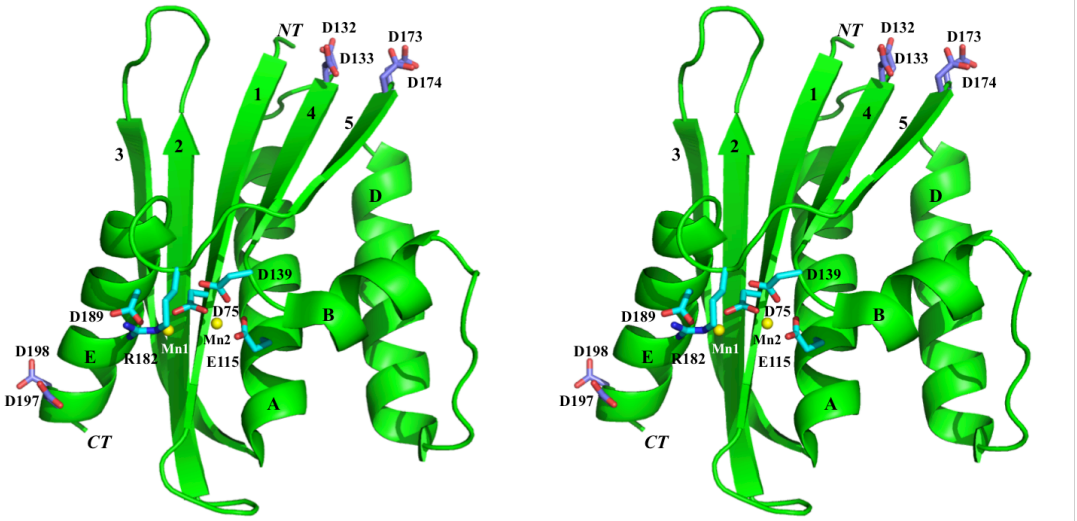

Figure 3.1. **Crystal structure of Halo-RNase H1.** Stereoview of the crystal structure of Halo-RNase H1. Four acidic active site residues (Asp75, Glu115, Asp139, and Asp189), Arg182, and six bi-aspartate residues (Asp132, Asp133, Asp173, Asp174, Asp197 and Asp198) are shown by cyan and slate stick models, respectively, in which the oxygen and

nitrogen atoms are colored red and blue, respectively. Two Mn^{2+} ions (Mn1 and Mn2) are shown as yellow spheres. NT and CT represent N- and C-termini respectively.

The Halo-RNase H1 structure is highly similar to those of metagenome-derived LC11-RNase H1 [38,56] and Sto-RNase H1 [89] with the RMSD values of 1.38 and 1.49 Å for 132 and 128 Cα atoms respectively (**Fig. 3.2**). The amino acid sequence of Halo-RNase H1 is compared with those of LC11-RNase H1, Sto-RNase H1 and *Bacillus halodurans* RNase H1 (Bh-RNase H1) on the bases of their crystal structures in **Figure 3.3**. The sequence of Halo-RNase H1 shows 34.3, 21.5, and 12.7% identities to those of LC11-RNase H1, Sto-RNase H1, and Bh-RNase H1 respectively.

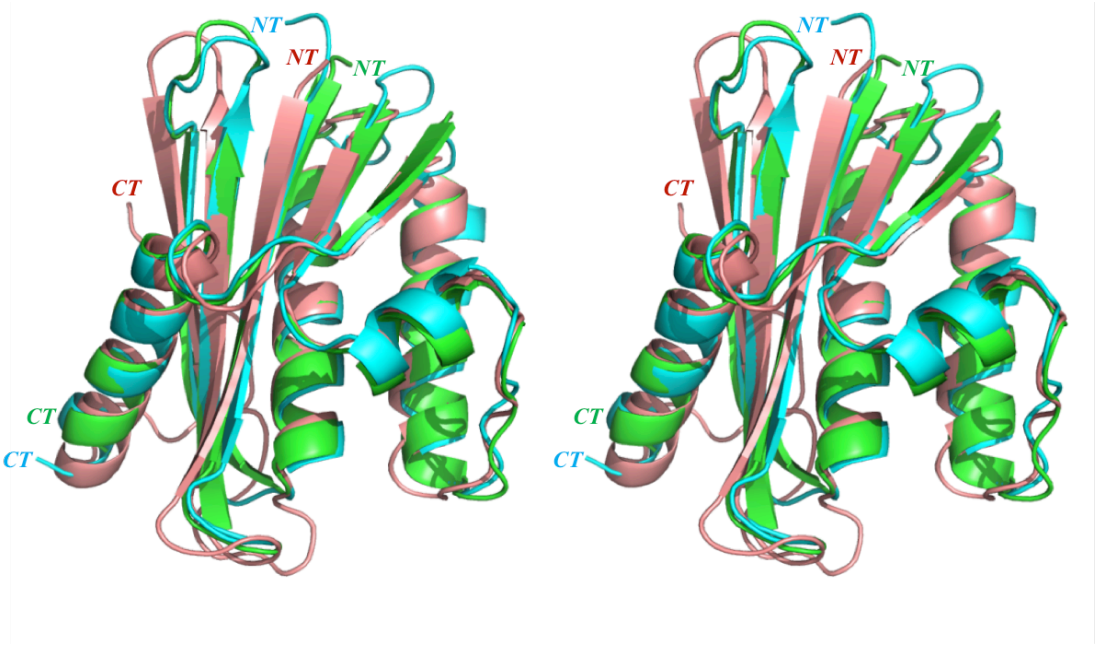

***Figure 3.2*. Crystal structure of Halo-RNase H1.** Stereoview of the structure of Halo-RNase H1 (green) superimposed on those of LC11-RNase H1 (cyan, PDB code 3U3G) and Sto-RNase H1 (salmon, PDB code 2EHG).

3.3.3. ACTIVE SITE

The four acidic residues, Asp75, Glu115, Asp139, and Asp189, form the active site of Halo-RNase H1, in which two Mn^{2+} ions (Mn1 and Mn2) bind (**Fig. 3.1**). The corresponding residues are Asp9, Glu49, Asp77, and Asp128 for LC11-RNaseH1, Asp7, Glu52, Asp77, and Asp125 for Sto-RNaseH1, and Asp71, Glu109, Asp132, and Asp192 for Bh-RNaseH1 (**Fig. 3.3**). In addition, Arg182 form the active site of Halo-RNase H1 (**Fig. 3.1**). This residue probably promotes a product release by perturbing the coordination of metal ion A, as proposed for the corresponding residues of Bh-RNase H1 [37], Sto-RNase H1 [89], and LC11-RNase H1 [56], which are Glu188, Arg118, and Arg121 respectively (**Fig. 3.3**). Superimposition of the structure of Halo-RNase H1 around the active site onto those of LC11-RNaseH1 and Sto-RNaseH1, and that of Bh-RNaseH1 in complex with the substrate and Mg^{2+} ions indicates that the steric configurations of the five active site residues of Halo-RNase H1 are very similar to those of LC11-RNaseH1, Sto-RNaseH1, and Bh-RNaseH1 (**Fig. 3.4**). The positions of the two Mn^{2+} ions in the Halo-RNase H1 structure are also similar to those of the Mg^{2+} ions in the co-crystal structure of Bh-RNase H1.

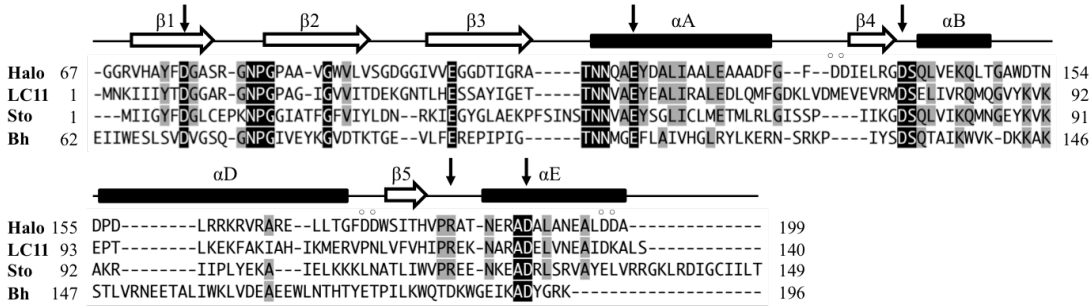

Figure 3.3. **Alignment of the amino acid sequences.** The amino acid sequences of Halo-RNase H1 (Halo), LC11-RNase H1 (LC11), Sto-RNase H1 (Sto) and Bh-RNase H1 (Bh) are compared with one another on the basis of their crystal structures. The ranges of the secondary structures of Halo-RNase H1 are shown above the sequences. The amino acid residues that are conserved in at least three and four different proteins are highlighted in grey and black respectively. The four acidic active-site residues and Arg182 are indicated

by arrows. The six bi-aspartate residues are indicated by the open circles above the sequences. Gaps are denoted by dashes. The numbers represent the positions of the amino acid residues relative to the initiator methionine for each protein.

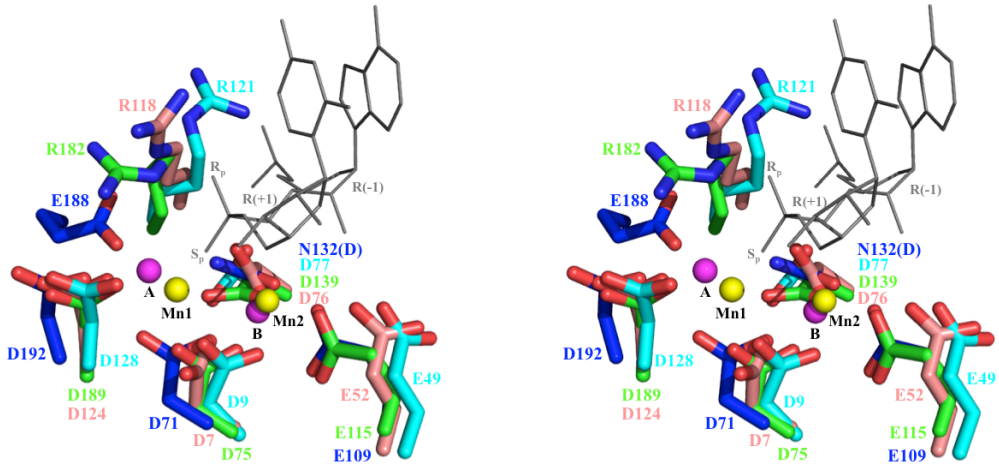

Figure 3.4. **Crystal structure of Halo-RNase H1.** Stereoview of the active-site structures of RNases H1. The side chains of the active-site residues of Halo-RNase H1 (green), LC11-RNase H1 (cyan), and Sto-RNase H1 (salmon) are superimposed onto those of Bh-RNase H1 in complex with the substrate and metal ions (blue, PDB code 1ZBI). In the cocrystal structure of Bh-RNase H1, two Mg^{2+} ions A and B are shown as magenta spheres and the position of the RNA strand of the substrate with the scissile phosphate group between R(-1) and R(+1) is shown. Two Mn^{2+} ions, Mn1 and Mn2, in the Halo-RNase H1 structure are also shown as yellow spheres.

3.3.4. CRYSTAL PACKING

The packing of the Halo-RNase H1 molecules within the crystal lattice is shown in **Figure 3.5**. Two molecules (molecules A and B) contact with each other, such that two Mn^{2+} ions (Mn1 and Mn2) are coordinated with the active site residues of molecule B and Asp198 of molecule A (**Fig. 3.6.a**). Mn1 is hexacoordinated with D75 Oδ1, D189 Oδ1, D198 Oδ1, and three water molecules, and Mn2 is hexacoordinated with D75 Oδ2, E115 Oε1, D139 Oε1, and three water molecules. One additional Mn^{2+} ion, which is located 2.2 Å away from Gly103 of molecule B, is not shown, because this Mn^{2+} ion probably binds to the protein non-specifically. The packing of the Halo-RNase H1 molecules between three crystal lattices is also shown in **Figure 3.5**. Molecule A in one crystal lattice and molecule A' in another crystal lattice contact with each other, such that two Mn^{2+} ions (Mn1 and Mn2) are coordinated with the active site residues of molecule A and Asp173/Asp174 of molecule A' (**Fig. 3.6.b**). Mn1 is hexacoordinated with D75 Oδ1, D189 Oδ1, D173 Oδ1, and three water molecules, and Mn2 is hexacoordinated with D75 δ2, E115 Oε1, D139 Oδ1, D174 Oδ1, and two water molecules. The contact between Asp173/Asp174 of molecule A and the active site of the fourth Halo-RNase H1 molecule, molecule A'', which is similar to that between molecules A and A' is shown in **Figure 3.5**. Thus, the active site of Halo-RNase H1 always contacts with Asp173/Asp174 or Asp198 of another molecule through Mn^{2+} ions. According to the co-crystal structures of Bh-RNase H1 [37] and human RNase H1 [36] in complex with the substrate and metal cofactors, two metal ions are coordinated with the four acidic active site residues and the scissile phosphate group of the substrate. Therefore, Asp173/Asp174 or Asp198 probably stabilizes the Mn^{2+} ions bound to the active site as a substitute of the substrate.

To examine whether Halo-RNase H1 folded in the presence of Mn^{2+} ions exists as a monomer in solution, the protein was subjected to gel filtration column chromatography in the presence of 10 mM $MnCl_2$. The protein was eluted from the column as a single peak with the estimated molecular mass of 18 kDa, which is lower than, but comparable to that calculated from the amino acid sequence of Halo-RNase H1 (20980 Da). This result indicates that Halo-RNase H1 exists as a monomer in solution in the presence of 10 mM $MnCl_2$ and the intermolecular interactions observed in the crystals are artifact of the crystal packing.

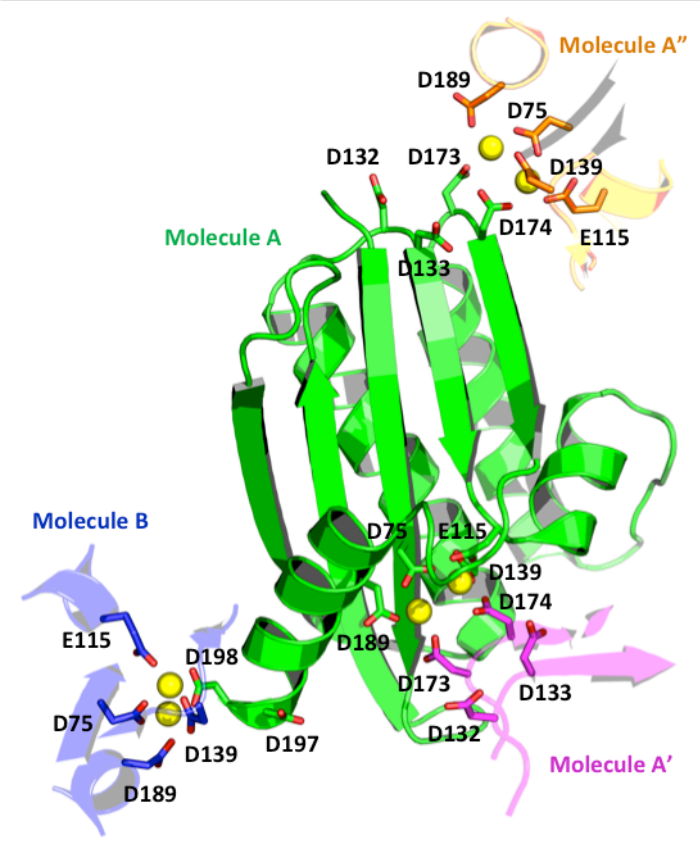

Figure 3.5. **The crystal packing of Halo-RNase H1.** Two molecules, molecules A and B, in the asymmetric unit are colored green and blue respectively. Another two molecules (molecule A' and A") that contacts molecule A are colored magenta and orange respectively. Four active site residues, Asp197, Asp198, Asp132, Asp133, Asp173, and Asp174 of molecule A are shown by green stick models. Four active site residues of molecule B are shown by blue stick models. Asp 132, Asp133, Asp173, and Asp174 of molecule A' are shown by magenta stick models. Four acidic active site residues of

molecule A" are shown by orange stick models. In these stick models, the oxygen atoms are colored red. Two Mn^{2+} ions (Mn1 and Mn2) bound to the active sites of molecules A and B and A" are shown as yellow spheres.

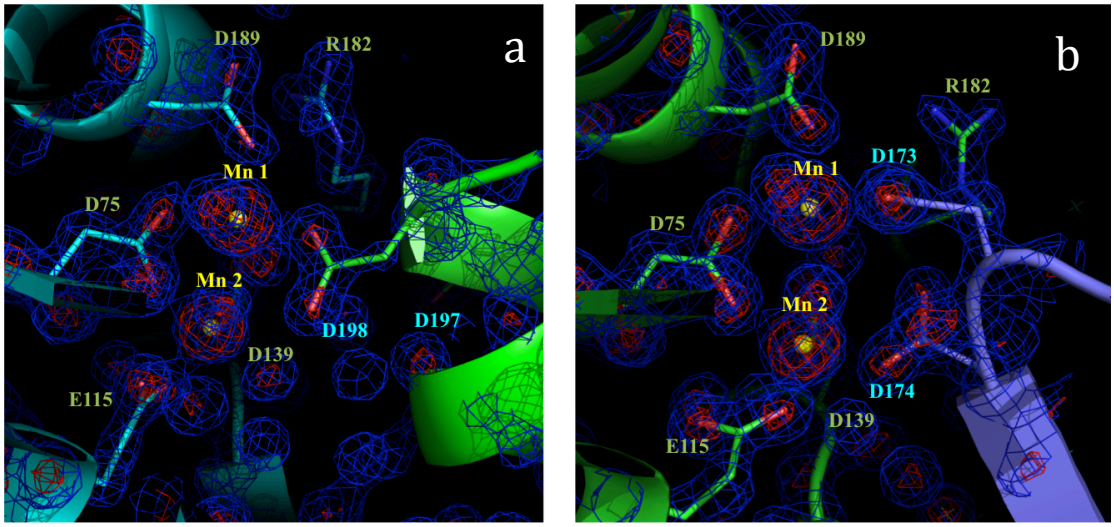

Figure 3.6. **Electron density around the active-site.** The structures around the active sites of molecule B (panel a) and molecule A (panel b) are shown. The structures around the active site of molecule A" are not shown as they resemble those of molecule A. Four active site residues and R182, which are labeled in yellow, two of the six bi-aspartate residues, which are labeled in cyan, and two Mn^{2+} ions, which are labeled in yellow, are shown. The $2F_o$-F_c maps contoured at the 2.0σ and 5.0σ levels are shown in blue and red respectively.

3.3.5. SURFACE PROPERTIES

The Halo-RNase H1 structure shows the abundance of acidic residues on the surface, with some aspartate residues forming clusters (**Fig. 3.7**), as do the structures of other halophilic proteins [64,65,68,90-94]. As a result, the surface of Halo-RNase H1 is negatively charged (**Fig. 3.8**).

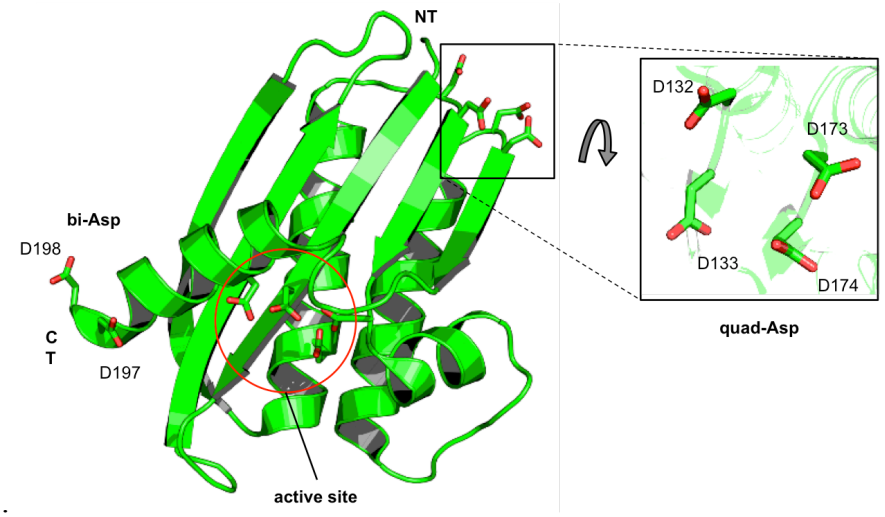

Figure 3.7. **Crystal structure of Halo-RNase H1.** The side chains of the acidic residues of the active site (Asp75, Glu115, Asp139, Asp189), the bi-Asp site (Asp197, Asp198), and quad-Asp site (Asp132, Asp133, Asp173, Asp174) are shown as green stick models in which the oxygen atoms are colored red.

Three bi-aspartate sites are present on the surface of Halo-RNase H1. They are Asp132-Asp133, Asp173-Asp174, and Asp197-Asp198 sites, which are located at the loop between αA-helix and β4-strand, the loop between αD-helix and β5-strand, and the C-terminal region, respectively (**Fig. 3.1**). The Asp132-Asp133 and Asp173-Asp174 sites are located close to each other. The bi-aspartate sites are also present on the surface of various halophilic proteins, such as nucleoside diphosphate kinase from *Halobacterium salinarum* (PDB code 2AZ1), malate dehydrogenase from *Haloarcula marismortui* (PDB code 4JCO), and malate synthase from *Haloferax volcanii* (PDB code 3OYX). These sites probably greatly contribute to an increase in the negative surface charge density of proteins.

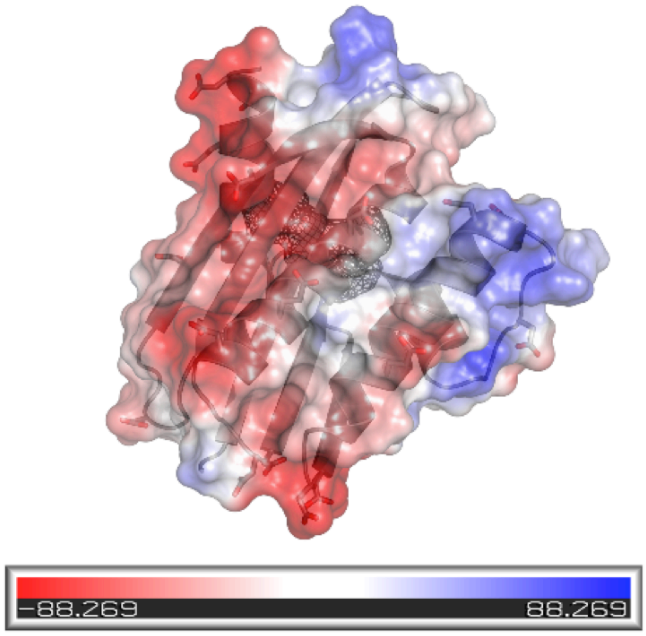

Figure 3.8. **Electrostatic surface potentials of Halo-RNase H1.** The negative and positive potentials are in red and blue respectively.

3.3.6. PREPARATION OF HALO-NTD AND HALO-CTD

To analyze the role of an N-terminal domain of Halo-RNase H1, Halo-NTD (residues 1-68) and Halo-CTD (residues 69-199) were constructed. Halo-NTD and Halo-CTD with the calculated molecular masses of 6,975 and 14,023 Da, respectively, were overproduced in *E. coli* in a soluble form and purified to give a single band on SDS-PAGE (**Fig. 3.9**). The amount of the protein purified from 1 liter of culture was typically 15 mg for both Halo-NTD and Halo-CTD. It has previously been reported that it is not possible to overproduce the Halo-RNase H1 derivative without the N-terminal 60 residues in *E. coli* [59]. An eight-residue extension at the N-terminus of Halo-CTD may somehow prevent the production of the protein in *E. coli* cells.

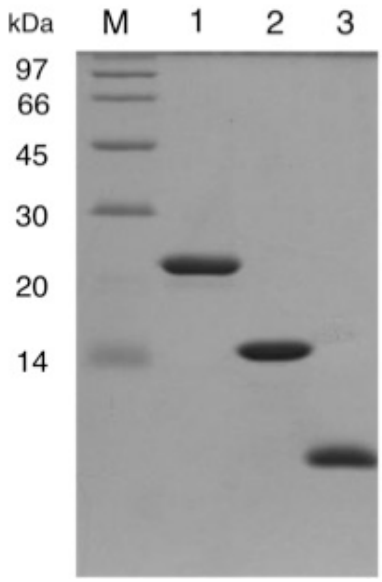

Figure 3.9. **Tricine SDS-PAGE of Halo-RNase H1 and its derivatives.** The purified proteins of Halo-RNase H1 (lane 1), Halo-CTD (lane 2), and Halo-NTD (lane 3) were subjected to electrophoresis on a 15% polyacrylamide gel in the presence of SDS. After electrophoresis, the gel was stained with Coomassie Brilliant Blue. Lane M, a low-molecular-weight marker kit (GE Healthcare).

3.3.7. BIOCHEMICAL PROPERTIES OF HALO-NTD AND HALO-CTD

The far-UV CD spectra of Halo-NTD and Halo-CTD indicate that Halo-NTD is folded regardless of the presence or absence of salt, whereas Halo-CTD is folded in a salt-dependent manner (**Fig. 3.10**). Halo-CTD is partially folded into an intermediate state (I) in the absence of salt, but is folded into a native state (N) in the presence of ≥2 M NaCl, as is the intact protein. Likewise, in the absence of salt, Halo-NTD is folded regardless of the presence or absence of divalent metal ions, whereas Halo-CTD is folded in a divalent metal ion-dependent manner. Halo-CTD is fully folded in the presence of ≥5 mM $MnCl_2$ or ≥300 mM $MgCl_2$, as is the intact protein. Therefore, there is no significant difference in the folding behavior between Halo-CTD and the intact protein.

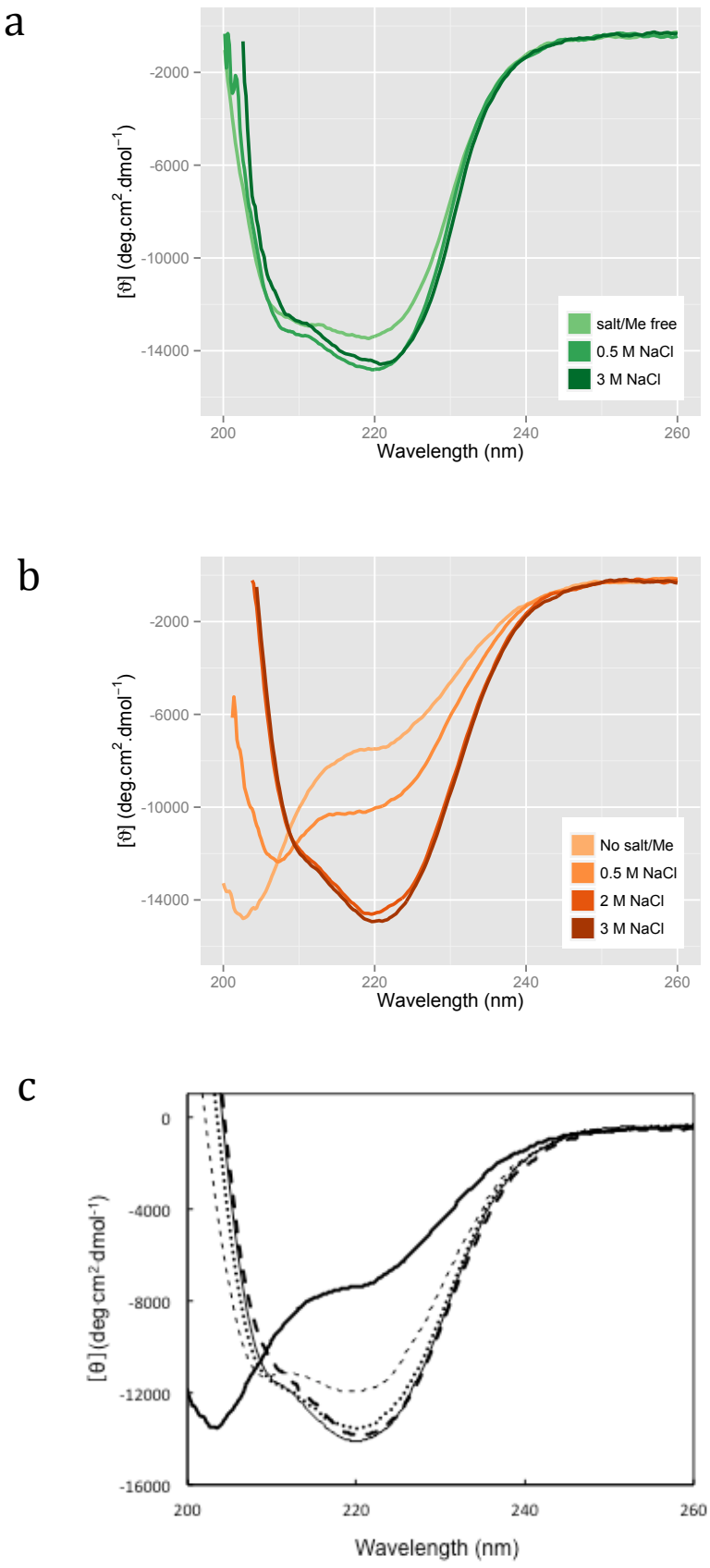

Figure 3.10. **Far-UV CD spectra of Halo-NTD and Halo-CTD.** The spectra of Halo-NTD (a) measured in the presence of 0 M, 0.5 M, or 3 M NaCl (gradient of green colored lines

ranging from light to dark respectively) are shown. The spectra of Halo-CTD (b) measured in the presence of 0 M, 0.5 M, 2 M or 3 M NaCl (gradient of orange colored lines ranging from light to dark respectively) are shown. The spectra of Halo-CTD (c) measured in the presence of 0 mM (solid thick line), 1 mM (dashed thin line), 2 mM (dotted thick line), 5 mM (solid thin line), or 10 mM (dashed thick line) $MnCl_2$ are shown.

Halo-NTD and Halo-CTD are thermally denatured with a single transition in a reversible manner at the same conditions examined and described in **Section 2.2.4** for the intact protein, as revealed by CD spectroscopy. The T_m values of Halo-NTD determined in the presence of 50 mM or 3 M NaCl and those of Halo-CTD determined in the presence of divalent metal ions (20 mM $MnCl_2$ or 300 mM $MgCl_2$) and/or salt (3 M NaCl) are summarized in **Table 3.2**. Comparison of the T_m values of Halo-CTD suggests that salt and divalent metal ions independently contribute to the stabilization of Halo-CTD, but more significantly than to the stabilization of the intact protein, by 30-34°C and 12-17°C respectively. The reason why salt and divalent metal ions more significantly contribute to the stabilization of Halo-CTD than to that of the intact protein remains to be clarified. Like Halo-CTD and the intact protein, Halo-NTD is greatly stabilized by 3M NaCl by 35°C, probably due to an increase in hydrophobic interactions at the protein core and a decrease in negative charge repulsion on the protein surface.

Protein	Metal	Salt	T_m (°C)	ΔT_m [a] (°C)
Halo-CTD	300 mM $MgCl_2$		45.7 ± 0.1	-0.5
	20 mM $MnCl_2$		53.8 ± 0.1	+7.6
		3 M NaCl	66.6 ± 0.1	+20.4
	300 mM $MgCl_2$	3 M NaCl	79.5 ± 0.1	+33.3
	20 mM $MnCl_2$	3 M NaCl	83.8 ± 0.1	+37.6
Halo-NTD		50 mM NaCl	44.6 ± 0.2	-1.6
		3 M NaCl	81.8 ± 0.1	+35.6

***Table 3.2.* T_m values of Halo-CTD and Halo-NTD** The melting temperature (T_m), which is the temperature of the midpoint of the thermal denaturation transition, was determined from the thermal denaturation curve. [a] ΔT_m is calculated as T_m of Halo-CTD or Halo-NTD determined – T_m of Halo-RNase H1 (46.2°C) determined in the presence of 300 mM $MgCl_2$.

Halo-CTD cleaved the R12/D12 substrate with similar cleavage site specificity to that of the intact protein either in the presence of $MnCl_2$ or $MgCl_2$ (**Fig. 3.11**). The optimum concentrations of $MnCl_2$ and $MgCl_2$ for activity of Halo-CTD are similar to those of the intact protein. The specific activities of Halo-CTD determined in the presence of 10 mM $MnCl_2$, 100 mM $MgCl_2$, and 50 mM or 3 M NaCl, which are nearly identical with one another, highly resemble those of the intact proteins. The K_A value of Halo-CTD (1.0 x 10^6 M^{-1}) determined in the presence of 3 M NaCl and absence of divalent metal ions by surface plasmon resonance using the R29/D29 substrate is lower than that of the intact protein, but only by 4-fold. In contrast, the K_A value of Halo-NTD (0.022 x 10^6 M^{-1}) is lower than that of the intact protein by 180-fold. The results mentioned above thus indicate that an N-terminal domain of Halo-

RNase H1 is dispensable for stability, activity, folding, and substrate binding. It may possess an *in vivo* function that cannot be detected otherwise.

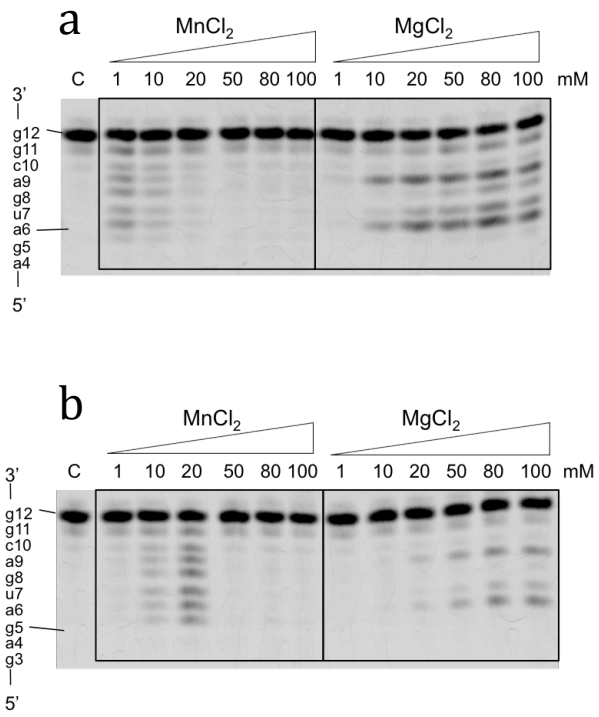

Figure 3.11. **Cleavage of R12/D12 substrate with Halo-CTD.** The 5'-end labeled R12/D12 substrate was hydrolyzed by Halo-CTD at 37°C for 15 min in the presence of various concentrations of $MnCl_2$ or $MgCl_2$ and 3 M (a) or 50 mM (b) NaCl. The hydrolysates were separated on a 20% polyacrylamide gel containing 7 M urea. The concentration of the substrate was 1 μM. The amount of enzyme added to the reaction mixture (10 μl) was 1 ng. The enzyme and divalent metal ions used to hydrolyze the substrate are shown above the gel together with the concentrations of the divalent metal ions. The sequence of R12 is indicated along the gel.

3.4. CONCLUSION

Halo-RNase H1 is partially and fully folded in the absence and presence of high concentrations (≥2 M) of salt respectively. It is also fully folded in the presence of ≥5 mM $MnCl_2$ or ≥300 mM $MgCl_2$. Determination of the crystal structure of Halo-RNase H1 in the presence of 10 mM $MnCl_2$ indicates that the structure of Halo-RNase H1 highly resembles those of other RNases H1, except that it has three bi-aspartate sites on the surface and its surface is negatively charged. Two Halo-RNase H1 molecules contact each other through the coordination of two Mn^{2+} ions with the active site residues of one molecule and one or two bi-Asp site residues of another molecule, suggesting that cancellation of negative charge repulsion at both active and bi-aspartate sites is necessary to yield a folded protein. Contribution of a bi-glutamate site on halophilic characteristics of protein has also been reported for nucleoside diphosphate kinase from *Halomonas* sp. 593 [95]. However, it still remains to be determined whether folding of Halo-RNase H1 is initiated by cancellation of negative charge repulsion at the active site or bi-aspartate sites.

Biochemical characterizations of the Halo-RNase H1 derivatives without an N- or C-terminal domain indicate that the N-terminal domain is dispensable for stability, activity, folding, and substrate binding.

CHAPTER 4

DIVALENT METAL ION-INDUCED FOLDING MECHANISM OF HALO-RNASE H1

4.1. INTRODUCTION

Although the main purpose of determining the crystal structure of Halo-RNase H1, described in Chapter 3, is to understand where divalent metal ion(s) bind to the protein and induce folding in a low salt condition, this metal binding site(s) is not clear. The reason behind this goes back to the fact that Halo-RNase H1 exists as a monomer in the solution in the presence of 10 mM $MnCl_2$ and the intermolecular interactions observed in the crystals are only an artifact of the crystal packing.

However, the crystal structure identified three positions in which manganese ions mediated the contacts between two molecules of the same or different crystal lattice. To understand whether these sites also play a role in inducing and stabilizing the folded state of Halo-RNase H1 in monomeric form, mutations that suppress the negative charge repulsion at these sites were done.

In this chapter, a series of mutant proteins of Halo-RNase H1 was constructed to suppress the negative charge repulsion at the active site (2A-RNase H1), at the bi/quad-Asp site (6A-RNase H1), or at both sites (8A-RNase H1). The far-UV CD spectra of these mutants suggest that 2A-RNase H1 mainly exists in a partially folded (I) state, 6A-RNase H1 exists in both the I and native (N) states, and 8A-RNase H1 exists in the N state in a low salt condition. Another RNase H from the same organism (Halo-RNase H2) was analyzed for a comparative reason. Halo-RNase H2 also exists

in the I and N states in low and high salt conditions respectively, but does not exist in the N state in the absence of salt and presence of divalent metal ions. Halo-RNase H1 contains a quad-Asp site, whereas Halo-RNase H2 does not contain it, suggesting that binding of divalent metal ions(s) to the quad-Asp site induces folding of Halo-RNase H1.

4.2. MATERIALS AND METHODS

4.2.1. PLASMID CONSTRUCTION

The pET25b derivatives for overproduction of the Halo-RNase H1 mutants, 2A, 6A-, and 8A-RNases H1, were constructed by PCR using the KOD-Plus Mutagenesis kit (Toyobo, Kyoto, Japan) according to the manufacturer's instructions. The pET25b derivative for overproduction of Halo-RNase H1, which was previously constructed and described in Section 2.2.1, was used as a template. The mutagenic primers were designed in such a way that the GAC and GAT codons for Asp are changed to GCC and GCT for Ala respectively, except for the GAC codon for Asp197, which is changed to the GCA codon for Ala.

Plasmid pGEX-Halo2 for overproduction of the glutathione S-transferase (GST)-Halo-RNase H2 fusion protein, in which Halo-RNase H2 is attached to the C-terminus of GST through a linker containing the thrombin cleavage site, was constructed by ligating the DNA fragment amplified by PCR into the *Bam*HI-*Eco*RI sites of the pGEX-2T vector (GE Healthcare, Little Chalfont, Buckinghamshire, England). The genomic DNA of *Halobacterium* sp. NRC-1, which was kindly donated by Dr. M. Tokunaga, was used as a template. The sequences of the PCR primers are 5'-CGCGGATCCATGGCGCGGTTCGG-3' for the 5'-primer and 5'-

CCGGAATTCCGGTTATCAAAACTCGTCCAG-3' for the 3'-primer, where the *Bam*HI (5'-primer) and *Eco*RI (3'-primer) sites are underlined.

All DNA oligomers for PCR were synthesized by Hokkaido System Science. PCR was performed with a GeneAmp PCR system 2400 (Applied Biosystems). The DNA sequences were confirmed by a Prism 310 DNA sequencer (Applied Biosystems).

4.2.2. OVERPRODUCTION AND PURIFICATION

E. coli BL21-CodonPlus(DE3) (Stratagene) was used as a host strain for overproduction of the Halo-RNase H1 mutants and GST-Halo-RNase H2 fusion protein. The transformants of this strain with the pET-Halo1 derivatives and pGEX-Halo2 were grown at 37°C in LB medium containing 50 $\mu g \cdot ml^{-1}$ ampicillin and 30 $\mu g \cdot ml^{-1}$ chloramphenicol. When the absorbance at 600 nm reached approximately 0.5, 1 mM isopropyl thio-β-D-galactoside (IPTG) was added to the culture medium and cultivation was continued at 37°C for an additional 4 h. The subsequent purification procedures of the Halo-RNase H1 mutants and Halo-RNase H2 were carried out at 4°C.

Halo-RNase H1 and its mutants (2A-, 6A-, and 8A-RNases H1) were purified as previously described for Halo-RNase H1 in Section 2.2.2, except that the buffer for the Mono Q column step is changed from 20 mM sodium acetate (pH 5.5) to 10 mM Tris-HCl (pH 7.0).

For purification of Halo-RNase H2, cells were harvested by centrifugation at 8000 *g* for 10 min, suspended in 10 mM sodium phosphate (pH 7.3) containing 140 mM NaCl, 2.7 mM KCl, and 2 mM DTT (buffer A), lysed by sonication, and centrifuged at 30,000 *g* for 30 min. The supernatant was collected, dialyzed against buffer A, and loaded onto a GSTrap HP column (5 ml) (GE Healthcare) equilibrated

with the same buffer. On-column thrombin cleavage of the GST-Halo-RNase H2 fusion protein was performed by loading thrombin dissolved in 5 mL of buffer A onto the column and incubating the column at 15°C for 20 min. The amount of thrombin loaded onto the column was 8% (w/w) of that of the fusion protein loaded onto the column. The Halo-RNase H2 molecules released from the fusion protein upon thrombin cleavage were eluted from the column by buffer A. GST was afterward eluted by 50 mM Tris-HCl (pH 8.0) containing 10 mM reduced glutathione (Wako). The fractions containing Halo-RNase H2 were collected, dialyzed against 10 mM Tris-HCl (pH 7.0) containing 1 mM EDTA, and applied to a Mono Q column (1 ml) (GE Healthcare) equilibrated with the same buffer. The protein was eluted from the column with a linear gradient of NaCl from 0 to 1 M. The fractions containing the protein were collected and loaded to a HiLoad 16/600 Superdex 200pg column (GE Healthcare) equilibrated with 10 mM Tris-HCl (pH 8.0). The fractions containing the protein were collected and used for biochemical characterization.

The purity of the protein was analyzed by SDS-PAGE [96] using a 15% (w/v) polyacrylamide gel, followed by staining with Coomassie Brilliant Blue (CBB). The protein concentration was determined from UV absorption using a cell with an optical path length of 1 cm and an A_{280} value for 0.1% (1.0 mg·ml^{-1}) solution of 1.26 for Halo-RNase H1 and its derivatives and 0.49 for Halo-RNase H2. These values were calculated by using absorption coefficients of 1576 M^{-1}·cm^{-1} for Tyr and 5225 M^{-1}·cm^{-1} for Trp at 280 nm [73].

4.2.3. CD SPECTRA

The far-UV CD spectra (200-260 nm) were measured on a J-725 spectropolarimeter (Japan Spectroscopic) at 25°C as described in Section 2.2.3.

4.2.4. THERMAL DENATURATION

Thermal denaturation of the protein was analyzed by monitoring the change in CD values at 222 nm as the temperature was increased. The protein was dissolved in 10 mM Tris-HCl (pH 8.0) containing 2 M NaCl or the same buffer containing 2 M NaCl and 1 mM $MnCl_2$. The protein concentration and optical path length were 0.1 $mg{\cdot}ml^{-1}$ and 2 mm respectively. The temperature of the protein solution was linearly increased by approximately 1.0°C/min. Thermal denaturation of the protein was reversible at the conditions examined. The temperature of the midpoint of the transition, T_m, was calculated from curve fitting of the resultant CD values versus temperature data on the basis of a least squares analysis.

4.2.5. ENZYMATIC ACTIVITY

The RNase H and JRNase activities were determined by using 5'-fluorescein-labeled RNA/DNA hybrid (R12/D12) and 29 bp DNA15-RNA1-DNA13/DNA29 (D15-R1-D13/D29) as substrates respectively, as described previously [43], except that the hydrolytic reaction was performed at 37°C instead of 30°C. The reaction buffer was 10 mM Tris-HCl (pH 8.5) containing 1 mM DTT, 0.01% BSA, 50 mM or 3 M NaCl, and various concentrations of $MgCl_2$ or $MnCl_2$. The substrate concentration was 1 μM. The products were detected by Typhoon 9240 Imager (GE Healthcare) and quantified using Image Quant 5.2 analysis software. One unit is defined as the amount of enzyme degrading 1 μmol of the substrate per min at 37°C. The specific activity was defined as the enzymatic activity per milligram of protein.

4.2.6. HOMOLOGY MODELING

A model for the three-dimensional structure of Halo-RNase H2 was built by SWISS-MODEL – an automated protein homology-modeling server - (Swiss Institute

of Bioinfomatics) [74], using the structure of Tk-RNase H2 (PDB ID: 2dfh) as a template. These proteins share the amino acid sequence identity of 38.8%. The model was viewed and edited with PyMOL (www.pymol.org).

4.3. RESULTS AND DISCUSSION

4.3.1. CONSTRUCTION OF HALO-RNASE H1 MUTANTS

According to the crystal structure of Halo-RNase H1 folded in the presence of manganese ions (PDB code 4NYN) and described in Chapter 3 of this thesis, molecule A of Halo-RNase H1 contacts three other molecules (molecules B, A', and A") at the active, bi-aspartate, and quad-aspartate sites through two manganese ions (**Fig. 3.5**). This is due to an artifact of the crystal packing, because size exclusion chromatography of Halo-RNase H1 in the presence of manganese ions suggests that the protein is monomeric in solution. Molecules A and B contact each other within the crystal lattice. Molecules A and A' or A" contact each other at the interface between two different crystal lattices. At the interface between molecules A and B, two manganese ions are coordinated with the active site residues of molecule B and one bi-aspartate site residue (Asp198) of molecule A. At the interface between molecules A and A' or A", two manganese ions are coordinated with the active site residues of molecule A and two quad-aspartate site residues (Asp173 and Asp174) of molecule A' or two quad-aspartate site residues of molecule A and the active site residues of molecule A". This result suggests that folding of Halo-RNase H1 is induced by binding of manganese ions to the active, bi-aspartate, and/or quad-aspartate sites. Binding of manganese ions to those sites probably suppresses negative charge

repulsion at those sites, which prevents folding of Halo-RNase H1 in a low salt condition. To examine whether suppression of negative charge repulsion at all of these sites is necessary to induce folding of Halo-RNase H1, Halo-RNase H1 mutants, 2A-, 6A- and 8A-RNases H1, in which two of the four acidic active site residues (Asp75 and Asp139), six bi/quad-aspartate site residues (Asp132, Asp133, Asp173, Asp174, Asp197, and Asp198), and all of these aspartate residues are replaced by Ala respectively, were constructed. These mutants were purified to give a single band on SDS-PAGE.

4.3.2. FOLDING OF HALO-RNASE H1 MUTANTS

Folding of 2A-, 6A- and 8A-RNases H1 was analyzed by CD spectroscopy. The far-UV CD spectra of 2A-RNase H1 (**Fig. 4.1**), 6A-RNase H1 (**Fig. 4.2**) and 8A-RNase H1 (**Fig. 4.3**) measured in the presence of various concentrations of $MnCl_2$ are compared with those of Halo-RNase H1 measured in the absence and presence of 20 mM $MnCl_2$. All spectra were measured in the absence of salt. The spectra of Halo-RNase H1 measured in the absence and presence of 20 mM $MnCl_2$ represent those of the Halo-RNase H1 proteins in the I and N states respectively. In both conditions, Halo-RNase H1 exists in equilibrium between the I and N states. However, the fraction of the N state is 0 and 100% in the absence and presence of 20 mM $MnCl_2$ respectively.

The spectrum of 2A-RNase H1 measured in the absence of $MnCl_2$ is similar to that of Halo-RNase H1, whereas those of 6A- and 8A-RNases H1 are different, which suggest that the mutations at the active site of Halo-RNase H1 do not significantly affect the structure of Halo-RNase H1, while those at the bi/quad-aspartate sites significantly change it in such a way that the fraction of the N state increases in the absence of $MnCl_2$. These spectra are changed in the presence of $MnCl_2$, in such a way

that the [θ] values at 205 and 220 nm increase and decrease respectively, as the $MnCl_2$ concentration increases. The [θ] value of 2A-RNase H1 at 220 nm decreases from approximately -8000 to -12000 when the $MnCl_2$ concentration increases to ≥1 mM, suggesting that the fraction of this protein in the N state is nearly 100% in the presence of ≥1 mM $MnCl_2$. In Chapter 1, I showed that higher concentrations (≥5 mM) of $MnCl_2$ are required to increase the fraction of the Halo-RNase H1 protein in the N state to 100%. This result suggests that suppression of negative charge repulsion at the active site increases the binding affinity of manganese ion(s) to the bi/quad-aspartate sites of Halo-RNase H1, because manganese ion(s) apparently binds/bind to the bi/quad-aspartate sites of 2A-RNase H1 more strongly than to those sites of Halo-RNase H1. Likewise, the [θ] value of 6A-RNase H1 at 220 nm decreases from approximately -11000 to -12500 when the $MnCl_2$ concentration increases to ≥5 mM, suggesting that the fraction of this protein in the N state is nearly 100% in the presence of ≥5 mM $MnCl_2$. The [θ] value of 8A-RNase H1 at 220 nm also decreases, but only slightly, in the presence of ≥1 mM $MnCl_2$, suggesting that the fraction of the N state is nearly 100% in the presence of ≥1 mM $MnCl_2$.

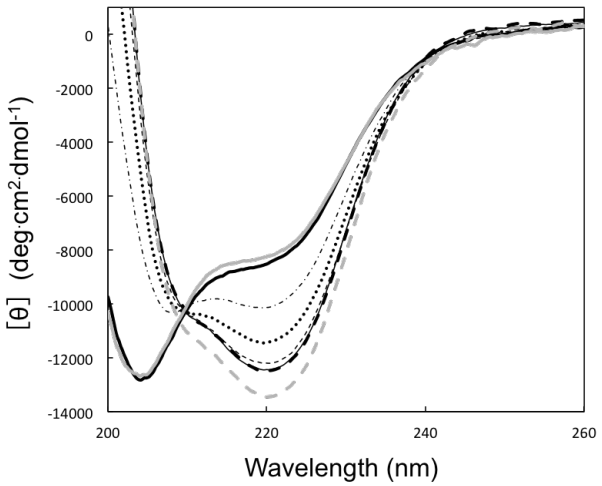

Figure 4.1. **CD spectra of 2A-RNase H1.** The far-UV CD spectra of 2A-RNase H1 measured at 25°C and pH 8.0 in the absence of salt and presence of various concentrations of $MnCl_2$ are shown in comparison with those of Halo-RNase H1 measured in the absence of salt and divalent metal ions (*grey solid thick line*) and in the absence of salt and the presence of 20 mM $MnCl_2$ (*grey dashed thick line*). $MnCl_2$ concentrations: 0 mM (*solid thick line*); 0.2 mM (*dashed-dotted thin line*); 0.4 mM (*dotted thick line*); 1 mM (*dashed thin line*); 5 mM (*solid thin line*); 20 mM (*dashed thick line*).

On the assumption that the [θ] values of 6A- and 8A-RNases H1 at 220 nm in the N state are -12500 and -12000 respectively, the fraction of these proteins in the N state in the absence of $MnCl_2$ is calculated to be 60% for 6A-RNase H1 and 95% for 8A-RNase H1. It is noted that the [θ] values of the mutants in the presence of 20 mM $MnCl_2$ are higher than those of Halo-RNase H1 by 1000-1500. It is unlikely that this difference is caused by the difference in the protein concentration, because the protein concentration was confirmed by the method of Bradford [97] as well. It is also unlikely that the fraction of these mutant proteins in the N state does not reach 100% even in the presence of 20 mM $MnCl_2$, because the spectra of these proteins in the presence of 20 mM $MnCl_2$ are nearly identical to that of Halo-RNase H1 in shape.

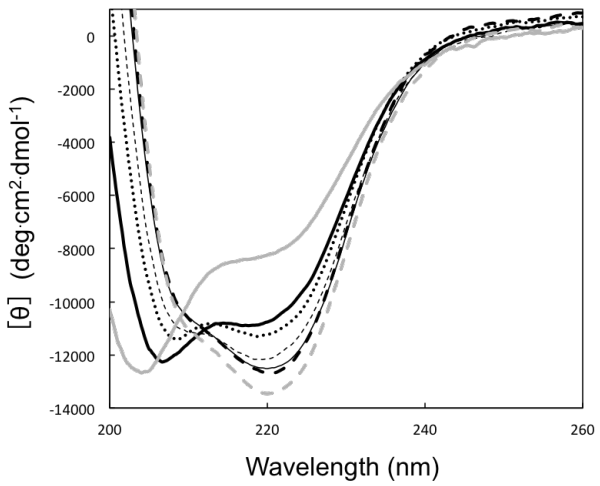

Figure 4.2. **CD spectra of 6A-RNase H1.** The far-UV CD spectra of 6A-RNase H1 measured at 25°C and pH 8.0 in the absence of salt and presence of various concentrations of $MnCl_2$ are shown in comparison with those of Halo-RNase H1 measured in the absence of salt and divalent metal ions (*grey solid thick line*) and in the absence of salt and the presence of 20 mM $MnCl_2$ (*grey dashed thick line*). $MnCl_2$ concentrations: 0 mM (*solid thick line*); 0.4 mM (*dotted thick line*); 1 mM (*dashed thin line*); 5 mM (*solid thin line*); 20 mM (*dashed thick line*).

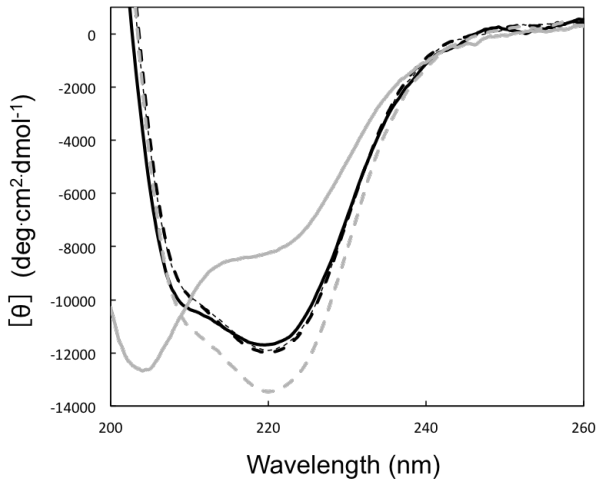

Figure 4.3. **CD spectra of 8A-RNase H1.** The far-UV CD spectra of 8A-RNase H1 measured at 25°C and pH 8.0 in the absence of salt and presence of various concentrations of $MnCl_2$ are shown in comparison with those of Halo-RNase H1 measured in the absence of salt and divalent metal ions (*grey solid thick line*) and in the absence of salt and the presence of 20 mM $MnCl_2$ (*grey dashed thick line*). $MnCl_2$ concentrations: 0 mM (*solid thick line*); 1 mM (*dashed thin line*); 20 mM (*dashed thick line*).

4.3.3. STABILITY OF 2A-RNASE H1

2A-RNase H1 is constructed to suppress negative charge repulsion at the active site of Halo-RNase H1 and to remove the metal-binding ability of Halo-RNase H1 at the active site. This negative charge repulsion is partially and fully suppressed by salt and divalent metal ions respectively, because Halo-RNase H1 folded in a high-salt condition is still stabilized by binding of divalent metal ion(s) to the active site in the same condition. However, only two of the four acidic active site residues are replaced by Ala in this mutant. To examine whether the metal-binding ability of Halo-RNase H1 at the active site is lost and negative charge repulsion at the active site is almost fully suppressed by these mutations, thermal denaturation of 2A-RNase H1 was analyzed in the presence of 2 M NaCl and in the presence and absence of 1 mM $MnCl_2$ by CD spectroscopy. Thermal denaturation of Halo-RNase H1 was analyzed in those conditions for comparative purposes. Thermal denaturation of those proteins was reversible and followed a two-state mechanism in those conditions. The T_m

values of Halo-RNase H1 and 2A-RNase H1 determined in those conditions are summarized in **Table 4.1**. The T_m value of Halo-RNase H1 determined in the presence of both salt and divalent metal ions is higher than that determined in the presence of salt alone by 4.5°C; whereas, the T_m value of 2A-RNase H1 determined in the presence of both salt and divalent metal ions is comparable to that determined in the presence of salt alone. These results suggest that the metal-binding ability of Halo-RNase H1 at the active site is lost by the double mutations of Asp75 and Asp139 to Ala.

Protein	$MnCl_2$ (mM)	T_m (°C)	ΔT_m [b] (°C)
Halo-RNase H1	0	58.6 ± 0.1	-
	1	63.1 ± 0.1	+4.5
2A-RNase H1	0	69.8 ± 0.1	+11.2
	1	68.9 ± 0.1	+10.3
6A-RNase H1	0	57.2 ± 0.2	-1.4
	1	ND	-

***Table 4.1.* T_m values of Halo-RNase H1 and its mutants[a]**

[a] The melting temperature (T_m), which is the temperature of the midpoint of the thermal denaturation transition, was determined from the thermal denaturation curve obtained by monitoring the change in CD values at 222 nm at pH 8.0 in the presence of 2 M NaCl and either in the presence or absence of 1 mM $MnCl_2$ as the temperature was increased. Errors represent those for the fitting of the curves.

[b] DT_m is calculated as T_m of Halo-RNase H1 or its mutants determined – T_m of Halo-RNase H1 determined in the absence of $MnCl_2$.

ND: not determined.

2A-RNase H1 is more stable than Halo-RNase H1 by 11.2°C in T_m in the presence of 2 M NaCl and absence of metal ions (**Table 4.1**). This value is higher than but comparable to the difference between the T_m values of Halo-RNase H1 determined in the presence of 3 M NaCl and in the presence and absence of 20 mM $MnCl_2$. The T_m value of Halo-RNase H1 determined in the presence of 3 M NaCl and 20 mM $MnCl_2$ is higher than that determined in the presence of 3 M NaCl and absence of $MnCl_2$ by 9.1°C. These results suggest that negative charge repulsion at the active site of Halo-RNase H1 is almost fully suppressed by the double mutations at the active site. Halo-RNase H1 is stabilized by only 4.5°C in T_m in the presence of 1 mM $MnCl_2$ in a high-salt condition, probably because the active site of Halo-RNase H1 is not fully occupied by manganese ion(s) due to its relatively low binding affinity. The stability of Halo-RNase H1 and 2A-RNase H1 was not analyzed in the presence of 3 M NaCl and 20 mM $MnCl_2$ in this study, because thermal denaturation of 2A-RNase H1 was not reversible in this condition.

It is no doubt that negative charge repulsion at the bi/quad-aspartate sites of Halo-RNase H1 is fully suppressed and the metal-binding ability of Halo-RNase H1 at these sites is lost by the mutations at these sites, because all six aspartate residues forming them are replaced by Ala. However, it remains to be determined whether suppression of negative charge repulsion at those same sites contributes to the stabilization of the protein, because the protein is folded only when negative charge repulsion, also at those same sites, is suppressed. The T_m value of 6A-RNase H1 determined in the presence of 2 M NaCl and absence of metal ions (57.2°C) is slightly lower than but comparable to that of Halo-RNase H1 (58.6°C) (**Table 4.1**). Likewise, the T_m value 2A-RNase H1 determined in the presence of 2 M NaCl and 1 mM $MnCl_2$ is comparable to that determined in the presence of 2 M NaCl and absence of $MnCl_2$

(**Table 4.1**). These results suggest that negative charge repulsion at the bi/quad-aspartate sites is fully suppressed and the metal-binding ability of Halo-RNase H1 at those sites is lost in a high-salt condition.

4.3.4. ENZYMATIC ACTIVITY OF 6A-RNASE H1

To examine whether the mutations at the bi/quad-aspartate sites affect the enzymatic activity of Halo-RNase H1, the activities of Halo-RNase H1 and 6A-RNase H1 were determined in the presence of 50 mM or 3 M NaCl using the R12/D12 substrate. The concentration of $MnCl_2$ or $MgCl_2$ varied from 0.1 to 50 or 1 to 100 mM respectively. The separation of oligoribonucleotides produced upon hydrolysis of the substrate in the presence of 50 mM or 3 M NaCl on a urea gel is shown in **Figure 4.4**. Both Halo-RNase H1 and 6A-RNase H1 similarly cleaved the substrate at all sites between a4 and g11 in the presence of manganese ions and at four sites between a6 and c10, preferably at a6-u7 and a9-c10, in the presence of magnesium ions. The specific activities of these proteins in the presence of various concentrations of $MnCl_2$ were estimated by comparing the intensity of the band of the substrate shown in **Figure 4.4**, which remains uncleaved, and were plotted as a function of $MnCl_2$ concentration in **Figure 4.5**. Both proteins exhibit the highest activities in the presence of 50 mM NaCl and 10 mM $MnCl_2$. In the presence of 3 M NaCl, both proteins exhibit the highest activities in the presence of 1 mM $MnCl_2$. The specific activity of 6A-RNase H1 is lower than that of Halo-RNase H1 by 50% in the presence of 50 mM NaCl and 10 mM $MnCl_2$ and 30% in the presence of 3 M NaCl and 1 mM $MnCl_2$. This result suggests that the sextuple mutations at the bi/quad-aspartate sites reduce the activity of Halo-RNase H1 by 30-50%.

Halo-RNase H1 exhibits little activity in the presence of 1 mM $MnCl_2$ in a low-salt condition (50 mM NaCl), because the fraction of the protein in the N state is low

(~20%) in this condition. In contrast, 6A-RNase H1 exhibits comparable activity to that determined in the presence of 3 M NaCl and 1 mM $MnCl_2$, even in the presence of 50 mM NaCl and 1 mM $MnCl_2$, probably because the fraction of this protein in the N state increases to nearly 90% in this condition (**Fig. 4.2**).

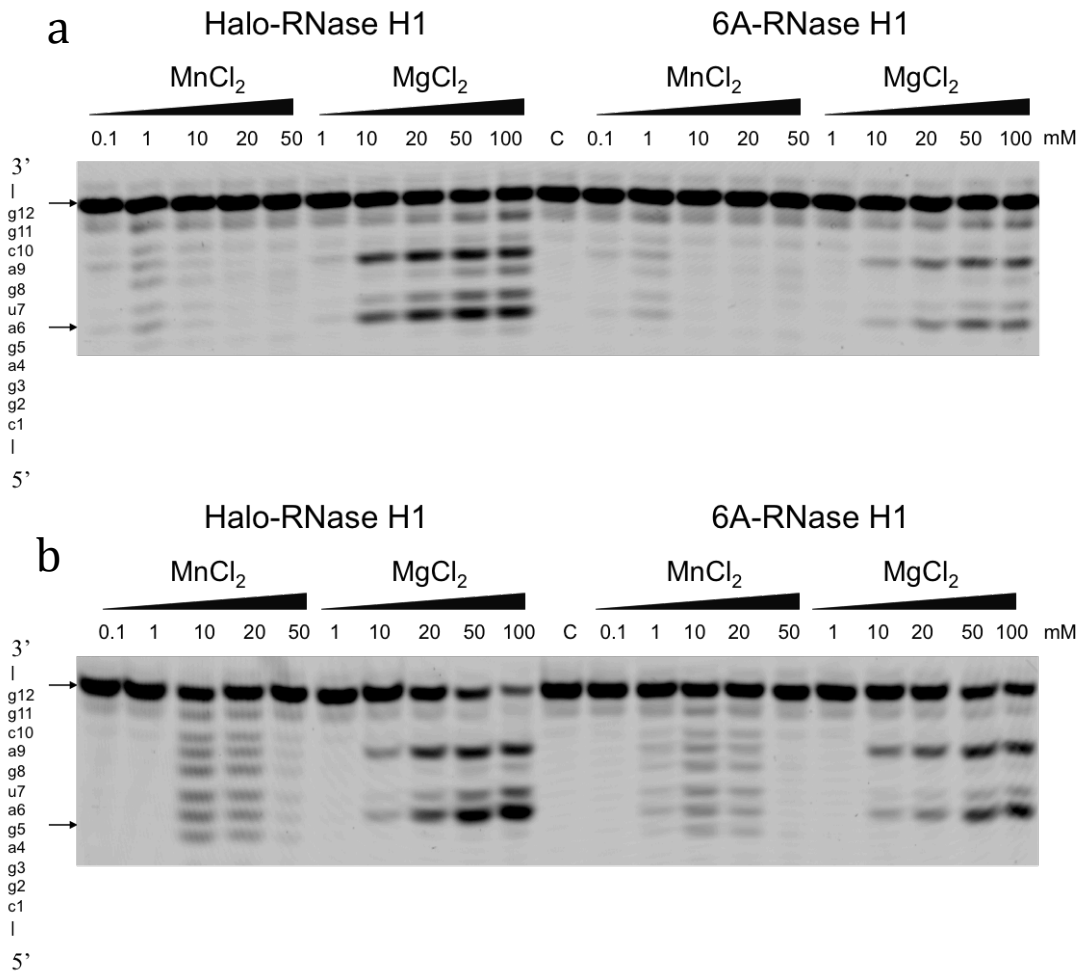

Figure 4.4. **Cleavage of R12/D12 substrate with Halo-RNase H1 and 6A-RNase H1.** The 5'-end labeled R12/D12 substrate was hydrolyzed by Halo-RNase H1 or 6A-RNase H1 at 37°C for 15 min in the presence of various concentrations of $MnCl_2$ or $MgCl_2$ and in the presence of 50 mM (b) or 3 M (a) NaCl. The hydrolysates were separated on a 20% polyacrylamide gel containing 7 M urea. The concentration of the substrate was 1 μM. The amount of the enzyme added to the reaction mixture (10 μl) was 1 ng. The enzyme and divalent metal ions used to hydrolyze the substrate are shown above the gel together with the concentrations of the divalent metal ions. The sequence of R12 is indicated along the gel.

The activities of Halo-RNase H1 and 6A-RNase H1 determined in the presence of 3 M NaCl and 1 mM $MnCl_2$ are approximately 30% of those determined in the presence of 50 mM NaCl and 10 mM $MnCl_2$. These activities greatly decrease when the $MnCl_2$ concentration increases to 10 mM (**Fig. 4.5**). In contrast, the activities of Halo-RNase H1 and 6A-RNase H1 determined in the presence of 3 M NaCl and 10 mM $MgCl_2$ do not significantly change or rather increase when the $MgCl_2$ concentration increases to 100 mM (**Fig. 4.4**). This discrepancy is probably caused by the difference in the binding affinities of the manganese and magnesium ions to the active site of Halo-RNase H1. Optimum concentration of the manganese ions for the activity of Halo-RNase H1 is apparently significantly lower than that of the magnesium ions (**Fig. 4.4**), suggesting that the binding affinity of the manganese ions to the active site of Halo-RNase H1 is higher than that of the magnesium ions. If the $MnCl_2$ concentration exceeds the optimum one for activity, additional manganese ion(s) may bind to the active site and may inhibit the activity of Halo-RNase H1.

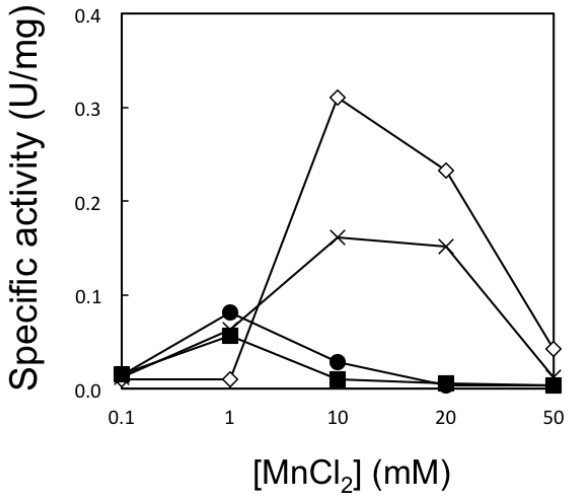

Figure 4.5. **Manganese dependencies of Halo-RNase H1 and 6A-RNase H1 activities.** The specific activities of Halo-RNase H1 in the presence of 50 mM (open diamond) and 3M (closed circle) NaCl and those of 6A-RNase H1 in the presence of 50 mM (cross) and 3 M (closed square) NaCl, which are estimated from the gels shown in Figure 4.4, are plotted as a function of the $MnCl_2$ concentration.

4.3.5. AMINO ACID SEQUENCE OF HALO-RNASE H2

Halo-RNase H2 is composed of 212 amino acid residues with a calculated molecular mass of 22,109 Da and an isoelectric point (p*I*) of 4.6. The amino acid sequence of Halo-RNase H2 is compared with those of the representative members of prokaryotic RNases H2, such as RNases H2 from *Thermococcus kodakarensis* (Tk-RNase H2), *Thermotoga maritima* (Tma-RNase H2), *Bacillus stearothermophilus* (Bst-RNase H2), and *Aquifex aeolicus* (Aae-RNase H2) in **Figure 4.6**.

```
                         β1                β2    αA
                                  **
Halo  1 ------------MARFGVDEAGKGPVLGSMFAAAVAGDPAAVP----DGVADSKRLSADRRA 46
Tk    1 ------------MKIAGIDEAGRGPVIGPMVIAAVVVDENSLPKLEELKVRDSKKLTPKRRE 50
Bst  60 MRYERELYAAGIERIAGIDEAGRGPLAGPVVAASVILPPDAYLP----GLDDSKRLTAAKRE 117
Tma   1 MGID-ELYKKEFGIVAGVDEAGRGCLAGPVVAAAVVLEKEIEG------INDSKQLSPAKRE 55
Aae   1 MLNYELELWEKGLLVAGVDEAGRGPLAGPVVAAAVILPPFTEPF----IKGDSKKLTKKERE 58

          αB       β3     αC          αD               β4
                                                        *
Halo    ELDDRVR-ASMRVGVAEVPVDRIDDPETDMNTLTVAAQADALGRVVADGMAGYVDAGDVNEQRF 109
Tk      KLFNEILGVLDDYVILELPPDVIGSREGTLNEFEVENFAKALNSLKVKPDVIYADAADVDEERF 114
Bst     ALFAQIEACAVAVGIGIVSAAEID--ERNIYEATKQAMAKAVSALSPPPDYLLVDAMAVPCALP 179
Tma     RLLDEIMEKA-AVGIGIASPEEID--LYNIFNATKLAMNRALENLSVKPSFVLVDGKGIELSVP 116
Aae     EAYEEIKNKALAVGTAVVDSAVID--RVNILRATKLAMKRALKDLKYHYDIVITDYVKLEGEN- 119

          αE       β5     αF              αG
                          *
Halo    GRRVANRVAADVAVTAEHGADDEYDLVAAASIVAKVARDAHVDALAAAFDADIGS----GYPSD 169
Tk      ARELGERLNFEAEVVAKHKADDIFPVVSAASILAKVTRDRAVEKLKEEYGE-IGS----GYPSD 173
Bst     QRRLMK-------------GDANSASIAAASIMAKVTRDRLMKELDRRYP-QYGFARHMGYGTP 229
Tma     GTCLVK-------------GDQKSKLIGAASIVAKVFRDRLMSEFHRMYP-QFSFHKHKGYATK 166
Aae     CMPLVK-------------GDEKSLNCACASIIAKVIRDKIMEIYHKIYP-DFNFASNKGYPSK 169

             αH                   αI

Halo    STTREFLAAYVREHGELPECARASWQTSRDALGAAEQSALDEF-------------------- 212
Tk      PRTRAFLENYYREHGEFPPIVRKGWKTLKKIAEKVESEKKAEERQATLDRYFRKV--------- 228
Bst     EHLEAIRRYG--ITPEHRRSFAPVKEAAGVEN-------------------------------- 259
Tma     EHLNEIRKNG--VLPIHRLSFEPVLELL------------------------------------ 192
Aae     THLEKVEKGE--YTEIHRKSFSPLKKKLF----------------------------------- 196
```

Figure 4.6. **Alignment of the amino acid sequences.** The amino acid sequences of Halo-RNase H2 (Halo), Tk-RNase H2 (Tk), Bst-RNase H2 (Bst), Tma-RNase H2 (Tma), and Aae-RNase H2 (Aae) are compared with one another. The accession numbers are AE004437 for Halo-RNase H2, AB012613 for Tk-RNase H2, BAB91155 for Bst-RNase H2, AAD35996 for Tma-RNase H2, and AAC07736 for Aae-RNase H2. The ranges of the secondary structures of Halo-RNase H2 deduced from its tertiary model are shown above the sequences. The four acidic active site residues are shaded and marked with asterisks. A GRG or GKG motif and a tyrosine residue that are responsible for recognition of a single ribonucleotide misincorporated into dsDNA are shaded. The dashes stand for the gaps. The

numbers represent the positions of the amino acid residues relative to the initiator methionine for each protein. PCNA interacting peptide (PIP) motif is boxed.

Halo-RNase H2 shows the amino acid sequence identities of 39% to Tk-RNase H2, 22% to Tma-RNase H2, 25 % to Bst-RNase H2 (without N-terminal extension), and 25% to Aae-RNase H2. Unlike Halo-RNase H1 and Bst-RNase H2, Halo-RNase H2 possesses neither N- nor C-terminal extension. Four acidic active site residues that form the metal binding site are conserved as Asp7, Glu8, Asp100, and Asp130 in Halo-RNase H2. A GRG motif and a tyrosine residue that are responsible for recognition of a single ribonucleotide misincorporated into double-stranded DNA (dsDNA) [26] are not fully conserved but are conserved as a GKG motif (Gly10, Lys11, and Gly12) and Tyr166 in Halo-RNase H2. This GKG motif is conserved in *Archaeoglobus fulgidus* RNase H2 and *Chlamydophila pneumoniae* RNase H3, both of which exhibit an ability to cleave dsDNA containing a single ribonucleotide [58]. Furthermore, Halo-RNase H2 contains a proliferating cell nuclear antigen (PCNA) interacting peptide (PIP) box motif at the C-terminus, suggesting that Halo-RNase H2 interacts with PCNA at this region.

4.3.6. TERTIARY MODEL OF HALO-RNASE H2

Halo-RNase H2 is characterized by the high content (18.4%) of acidic amino acid residues. A tertiary model of this protein shows the abundance of acidic residues on the surface as does the crystal structure of Halo-RNase H1 (**Fig. 4.7**). These acidic residues include those of the two bi-aspartate sites (Asp49-Asp50 and Asp69-Asp70). As a result, the surface of Halo-RNase H2 is negatively charged, as is that of Halo-RNase H1. The overall structure of Halo-RNase H2 is similar to that of Tk-RNase H2 (PDB code 2dfh). The steric configurations of the four acidic active site residues are similar to those of Tk-RNase H2.

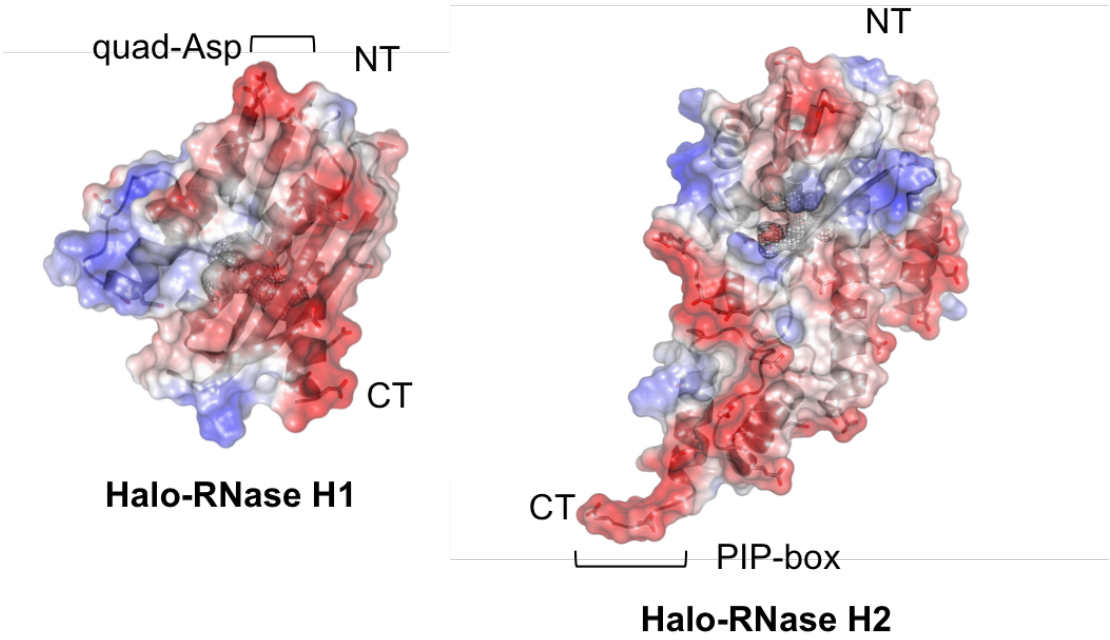

Figure 4.7. **A tertiary model of Halo-RNase H2.** Ribbon diagram with electrostatic surface potential of Halo-RNase H2 is shown in comparison with that of Halo-RNase H1. NT and CT represent N and C-termini. The negative and positive potentials are in red and blue respectively. The electrostatic potential value ranges from -100 to +100 kT e^{-1}. The positions of quad-aspartate site (Quad-Asp) of Halo-RNase H1 and PIP-box of Halo-RNase H2 are shown.

4.3.7. PREPARATION OF HALO-RNASE H2

To examine whether Halo-RNase H2 also requires salt or divalent metal ions for folding, Halo-RNase H2 was overproduced in *E. coli* as a glutathione S-transferase (GST)-Halo-RNase H2 fusion protein. Upon overproduction, this fusion protein accumulated in the cells in a soluble form. Halo-RNase H2 was released from the fusion protein by on-column cleavage with thrombin and was purified to give a single band on SDS-PAGE. The amount of the protein purified from 1 L culture was typically 2 mg. Attempts to overproduce Halo-RNase H2 alone have so far been unsuccessful, because the production level of this protein is too low to purify it in an amount sufficient for biochemical characterization.

4.3.8. FOLDING OF HALO-RNASE H2

Folding of Halo-RNase H2 was analyzed by CD spectroscopy. The far-UV CD spectra of Halo-RNase H2 measured at 25°C and pH 8.0 in the absence or presence of various concentrations of NaCl or divalent metal ions are shown in **Figure 4.8**. In the absence of salt and divalent metal ions, the far-UV CD spectrum of Halo-RNase H2 gives a trough with a minimum [θ] value of -14,000 at 202 nm, which is accompanied by a shoulder with a [θ] value of -6000 at 220 nm. This spectrum is greatly changed in the presence of 3 M NaCl, in such a way that it gives a trough with a minimum [θ] value of -12000 at 208 nm and the [θ] value at 220 nm decreases to -9500. This spectrum is changed when the NaCl concentration increases from 3 to 4 M, but only slightly, suggesting that Halo-RNase H2 is almost fully folded in the presence of 3 M NaCl. In contrast, the spectrum of Halo-RNase H2 measured in the absence of salt and divalent metal ions does not significantly change even in the presence of 20 mM $MnCl_2$ or 500 mM $MgCl_2$. These results suggest that Halo-RNase H2 is folded in a high salt condition, but is not folded in a low salt condition regardless of the presence

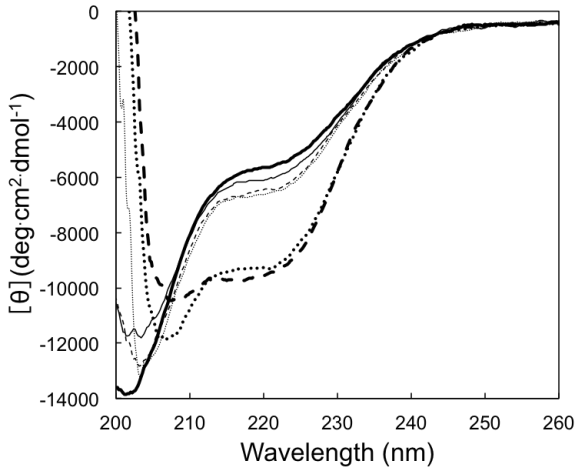

Figure 4.8. **CD spectra of Halo-RNase H2.** The far-UV CD spectra of Halo-RNase H2 measured at 25°C and pH 8.0 in the absence of salt and divalent metal ions (*solid thick line*), in the absence of salt and the presence of 10 mM $MnCl_2$ (*solid thin line*), 20 mM $MnCl_2$ (*dashed thin line*), and 500 mM $MgCl_2$ (*dotted thin line*), and in the presence 3 M NaCl (*dotted thick line*) and 4 M NaCl (*dashed thick line*) and the absence of divalent metal ions are shown.

of divalent metal ions. Thus, we conclude that requirement of divalent metal ions for protein folding as a substitute of salt is unique to Halo-RNase H1.

4.3.9. ENZYMATIC ACTIVITY OF HALO-RNASE H2

To examine whether Halo-RNase H2 exhibits JRNase activity, the enzymatic activity of Halo-RNase H2 was determined in the presence of 50 mM or 3 M NaCl and in the presence of various concentrations of $MnCl_2$ or $MgCl_2$ at 37°C using the 5'-fluorescein-labeled D15-R1-D13/D29 substrate. The concentration of $MnCl_2$ or $MgCl_2$ varied from 1 to 100 mM. The separation of the oligonucleotide (5'-fluorescein-labeled 15-mer DNA) produced upon hydrolysis of the substrate in the presence of 3 M NaCl on a urea gel is shown in **Figure 4.9**. Halo-RNase H2 was able to cleave the substrate at the (5')DNA-RNA(3') junction in the presence of 3 M NaCl and 10-100 mM $MgCl_2$ or 1-10 mM $MnCl_2$. Halo-RNase H2 was unable to cleave the substrate in a low salt condition at any concentration of $MnCl_2$ or $MgCl_2$ that was examined. These results are consistent with those obtained by CD spectroscopy that Halo-RNase H2 is partially folded in a low salt-condition even in the presence of 20 mM $MnCl_2$ or 500 mM $MgCl_2$, but is almost fully folded in the presence of 3 M NaCl.

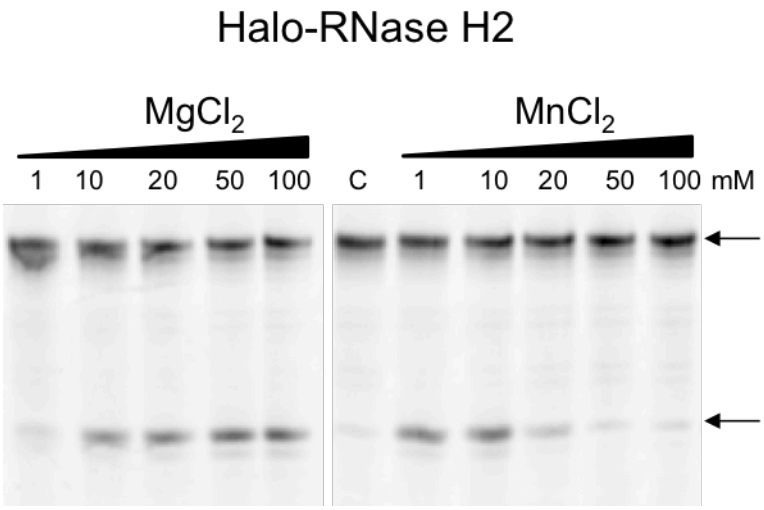

Figure 4.9. **Cleavage of DNA15-RNA1-DNA13/DNA29 substrate with Halo-RNase H2.** The 5'-end labeled DNA15-RNA1-DNA13/DNA29 substrate was hydrolyzed by Halo-

RNase H2 at 37°C for 15 min in the presence of 3 M NaCl and various concentrations of $MnCl_2$ or $MgCl_2$. The hydrolysates were separated on a 20% polyacrylamide gel containing 7 M urea. The concentration of the substrate was 1 μM. The amount of the enzyme added to the reaction mixture (10 μl) was 500 ng. Divalent metal ions used to hydrolyze the substrate and the concentrations of these divalent metal ions are shown above the gel. The arrows indicate the 5'-end labeled substrate (top) and 5'-end labeled 15-mer DNA (bottom).

4.3.10. DIVALENT METAL ION-INDUCED FOLDING MECHANISM OF HALO-RNASE H1

Comparison of the crystal structure of Halo-RNase H1 and a tertiary model of Halo-RNase H2 indicates that both proteins are characterized by the high content of acidic residues on the surface and share the similar configurations of the four acidic active site residues. The configurations of these active site residues are conserved in all RNases H so far examined [10]. The findings that one or two divalent metal ions bind to the active sites of *E. coli* RNase H1 [77,79,98], HIV-1 RNase H [99], and *B. stearothermophilus* RNase H3 [44] in a substrate-free form and two divalent metal ions bind to the active sites of *B. halodurans* RNase H1 [37], human RNase H1 [36], and *T. maritima* RNase H2 [52] in a substrate-bound form suggest that at least one divalent metal ion binds to the active sites of Halo-RNase H1 and Halo-RNase H2 in a substrate-free form when they are folded. However, Halo-RNase H2 is not folded in the presence of divalent metal ions in a low-salt condition. As mentioned above, 2A-RNase H1, in which negative charge repulsion at the active site is almost fully suppressed by the mutations, is also not folded in a low-salt condition. These results suggest that suppression of negative charge repulsion at the active site by binding of divalent metal ion(s) is not sufficient to induce folding of Halo-RNase H1 and Halo-RNase H2. When the localization of the aspartate residues on the surface of Halo-RNase H1 is compared with that of Halo-RNase H2, a quad-aspartate site is only present on the surface of Halo-RNase H1.

The structure of the quad-aspartate site of Halo-RNase H1 is shown in **Figure 4.10**. According to the crystal structure of Halo-RNase H1 folded in the presence of 10 mM $MnCl_2$, two molecules (molecules A and B) contact each other within the crystal lattice. Molecule A of one crystal lattice also contacts molecules A' and A" of other crystal lattices. Two quad-aspartate site residues (Asp173 and Asp174) of molecule A provide ligands for coordination of two manganese ions (Mn1 and Mn2), which are also coordinated with the four acidic active site residues of molecule A". In contrast, any quad-aspartate residue of molecule B does not provide any ligand for coordination of manganese ions. Comparison of the structures of the quad-aspartate sites, to which manganese ions bind and do not bind, indicates that the side chains of the quad-aspartate site residues, especially Asp173, greatly change their positions upon binding of manganese ions (**Fig. 4.10**).

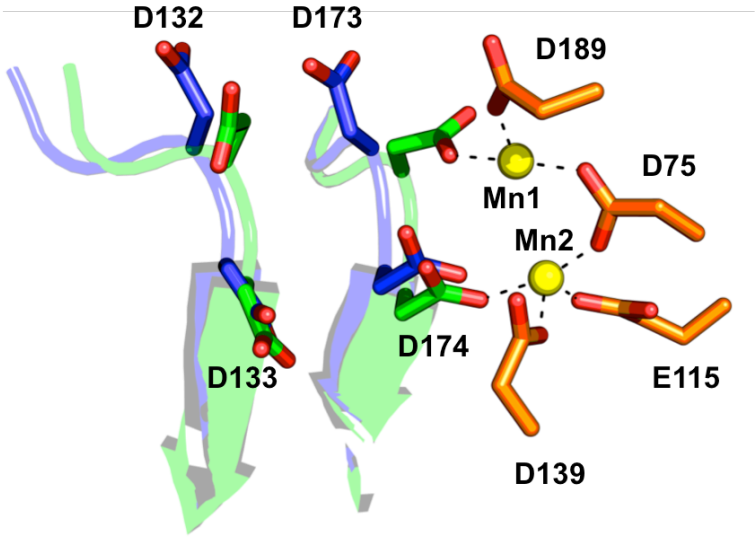

Figure 4.10. **The crystal structure of Halo-RNase H1 (PDB code 4NYN).** The structure of the quad-aspartate site of molecule A (green), which contacts the active site of molecule A" (orange) through two manganese ions (Mn1 and Mn2), is superimposed onto that of molecule B (blue), which does not contact another molecule. The side chains of the four quad-aspartate site residues and four acidic active site residues, and two manganese ions are shown as in (Fig. 3.5).

This result suggests that these residues are highly flexible and greatly change the positions of their side chains, in such a way that a manganese ion binds to the middle of this site in solution.

4.4. CONCLUSION

In this chapter, a series of the mutant proteins of Halo-RNase H1 was prepared in which the negative charge repulsion at the active site (2A-RNase H1), at the bi/quad-Asp site (6A-RNase H1), and at both these sites was suppressed by replacing the aspartate residues to alanine.

Using CD spectroscopy, I showed that 2A-RNase H1 mainly exists in a partially folded (I) state, 6A-RNase H1 exists in both the I and native (N) states, and 8A-RNase H1 exists in the N state in a low salt condition. I also showed that Halo-RNase H2, another RNase H from the same organism, exists in the I and N states in low and high salt conditions respectively, but does not exist in the N state in the absence of salt and presence of divalent metal ions. Comparing the structure of Halo-RNase H1 with the tertiary model of Halo-RNase H2 and the localization of the bi-Asp sites on the surface of these two proteins along with the results observed using CD spectroscopy have led me to propose that the suppression of negative charge repulsion at the quad-Asp site, uniquely found on the surface of Halo-RNase H1, by binding of divalent metal ion is required to initiate folding of Halo-RNase H1 and that at the active site is required to stabilize the folded state of this protein. The results that 6A-RNase H1 exists both in the I and N states, whereas 8A-RNase H1 mainly exists in the N state, and that the concentration of $MnCl_2$ required to induce folding of 2A-RNase H1 is significantly lower than that required to induce folding of Halo-RNase H1 support this proposal.

CHAPTER 5

ROLE OF TYPE 1 RNASE H IN DNA REPAIR

5.1. INTRODUCTION

Halo-RNase H1 has been identified as the first type 1 enzyme that can cleave an Okazaki fragment-like RNA-DNA/DNA substrate at the 3'-side of the ribonucleotide of the RNA-DNA junction [59]. To distinguish this activity from JRNase activity of RNase H2, that catalyzes the cleavage of an RNA-DNA/DNA substrate at the 5'-side of the ribonucleotide of the RNA-DNA junction [50], the two activities are designated as 3'- and 5'-JRNase activities respectively in this Chapter (**Fig. 5.1**). Since then, Sto-RNase H1 [60], Tma-RNase H1 [55], and *E. coli* RNase H1 [50,55] have been shown to exhibit 3'-JRNase activity for an Okazaki fragment-like substrate. The RNA-DNA junction of the RNA1-DNA9/DNA18 substrate, that represents an Okazaki fragment-like substrate containing a single ribonucleotide, is not cleaved by Halo-RNase H1 [59] and Sto-RNase H1 [60], suggesting that an upstream duplex structure is necessary for recognition of this junction by those RNase H1. However, it remains to be determined whether the RNA-DNA junction of the RNA1-DNA9/DNA18 substrate is cleaved by RNase H1 by supplying a short RNA fragment that facilitates the formation of an upstream duplex structure. It also remains to be determined whether the 3'-JRNase activity of RNases H1 catalyzes the cleavage of dsDNA containing a single ribonucleotide ($dsDNA^{R1}$) at the (5')RNA-DNA(3') junction.

E. coli RNase H1 has often been used as a representative member of type 1 RNases H, because its structure and function have been extensively studied [80]. In this Chapter, I showed that the RNA-DNA junction of the RNA1-DNA9/DNA18 substrate is not cleaved by *E. coli* RNase H1 but is cleaved by it when a short RNA fragment is supplied to facilitate the formation of an upstream duplex structure. I also showed that *E. coli* RNase H1 exhibits 3'-JRNase activity for dsDNA^{R1} in the presence of Mn^{2+} ions, regardless of whether this substrate is cleaved by 5'-JRNase activity of *E. coli* RNase H2 in advance or not. From these results, I propose that single ribonucleotides misincorporated into the genomes can be completely removed by a cooperative action of both RNases H1 and H2 in prokaryotic cells.

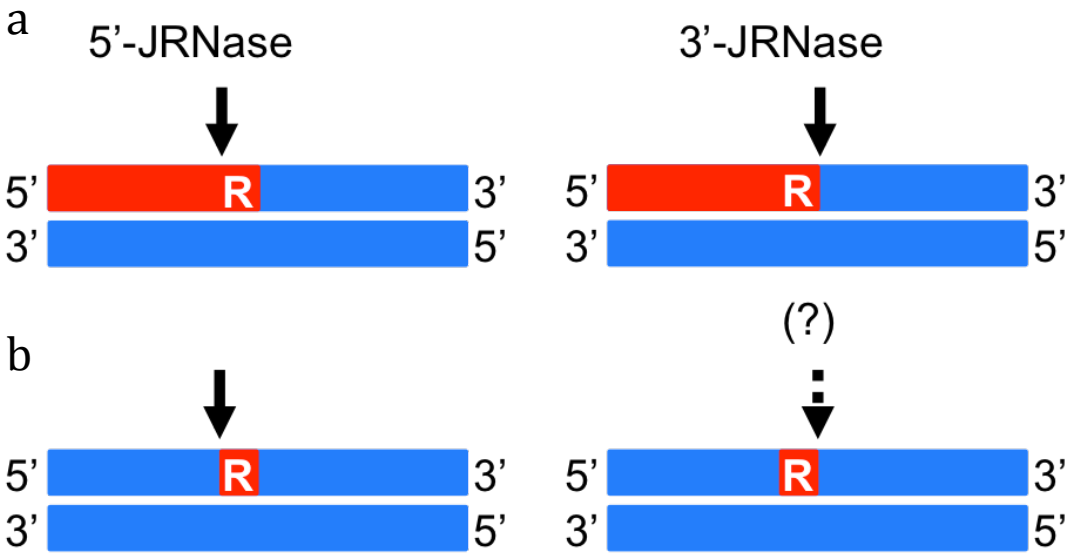

Figure 5.1. **Sites of cleavage by 5'- and 3'-JRNase activities of RNases H.** Cleavage sites of an Okazaki fragment-like RNA-DNA/DNA substrate (a) and dsDNA containing a single ribonucleotide (dsDNA^{R1}) (b) by 5'- and 3'-JRNase activities of RNases H are shown. RNA and DNA strands are shown by red and blue boxes respectively. The ribonucleotide of the (5')RNA-DNA(3') junction is indicated by R. The cleavage sites are indicated by arrows.

5.2. MATERIALS AND METHODS

5.2.1. PROTEIN PREPARATION

Overproduction and purification of *E. coli* RNase H1 using *E. coli* MIC3009 transformants with pJAL600 [70] (described in Section 2.2.2) and *E. coli* RNase H2 using *E. coli* MIC2067(DE3) transformants with pTYB600E [100] were performed as described previously. The purity of each protein was analyzed by SDS-PAGE [96] using 15% (w/v) polyacrylamide gel, followed by staining with Coomassie Brilliant Blue (CBB). The protein concentration was determined from UV absorption using a cell with an optical path length of 1 cm and an A_{280} value for 0.1% solution of 2.02 for *E. coli* RNase H1 and 0.56 for *E. coli* RNase H2. The value of *E. coli* RNase H1 was experimentally determined [72]. The value of *E. coli* RNase H2 was calculated by using absorption coefficients of 1576 M^{-1} cm^{-1} for Tyr and 5225 M^{-1} cm^{-1} for Trp at 280 nm [73].

5.2.2. OLIGONUCLEOTIDES

3’-FAM-labeled 18 b RNA_9-DNA_9 (R9-D9*), 11 b RNA_2-DNA_9 (R2-D9*), and 10 b RNA_1-DNA_9 (R1-D9*), 5’- and 3’-FAM-labeled 29 b DNA_{15}-RNA_1-DNA_{13} (*D15-R1-D13 and D15-R1-D13* respectively), 5’-FAM-labeled 29 b DNA (*D29), 7 b RNA (R7), 8 b RNA (R8), 18 b DNA (D18), and 29 b DNA (D29) were synthesized by Hokkaido System Science (Sapporo, Japan). Of these oligonucleotides, R2-D9* and R1-D9* are 5’-phosphorylated, while the others are not. The sequences of these oligonucleotides are 5’-uugcaugccTGCAGGTCG-3’ for R9-D9*, 5’-ccTGCAGGTCG-3’ for R2-D9*, 5’-cTGCAGGTCG-3’ for R1-D9*, 5’-uugcaug-3’ for R7, 5’-uugcaugc-3’ for R8, and 5’-AATAGAGAAAAAGAAaAAAGATGGCAAAG-3’ for *D15-R1-D13 and D15-R1-

D13*, where deoxyribonucleotides and ribonucleotides are shown by uppercase and lowercase letters respectively. The sequence of *D29 is identical to that of *D15-R1-D13. The sequences of D18 and D29 are complementary to those of R9-D9* and *D15-R1-D13 respectively. FAM represents 6-carboxyfluorescein.

5.2.3. ENZYMATIC ACTIVITY

The R9-D9*/D18, R2-D9*/D18, and R1-D9*/D18 duplexes were prepared by hybridizing R9-D9*, R2-D9*, and R1-D9* with a 2 molar equivalent of D18 respectively. The R7:R2-D9*/D18 and R8:R1-D9*/D18 duplexes were prepared by hybridizing R2-D9* and R1-D9* with a 2 molar equivalent of D18 in the presence of a 2 molar equivalent of R7 and R8 respectively. The *D15-R1-D13/D29, D15-R1-D13*/D29, and *D29/D29 duplexes were prepared by hybridizing *D15-R1-D13, D15-R1-D13*, and *D29 with a 2 molar equivalent of D29 respectively. These duplexes were used as substrates. Hydrolysis of the substrate at 30°C for 15 or 30 min and separation of the products on a 20% polyacrylamide gel containing 7 M urea were carried out as described previously [11]. The reaction buffer contained 10 mM Tris-HCl (pH 8.5), 1 mM 2-mercaptoethanol, 0.01% BSA, 10 mM NaCl, and $MnCl_2$ or $MgCl_2$ at the concentration indicated. The substrate concentration was 1 μM. The products were detected by Typhoon 9240 Imager (GE Healthcare, Tokyo, Japan).

5.3. RESULTS AND DISCUSSION

5.3.1. OLIGOMERIC SUBSTRATES

The oligomeric substrates used in this chapter are summarized in **Figure 5.2**. The asterisk indicates the fluorescein-labeled site. The R9-D9*/D18 substrate represents

an Okazaki fragment-like substrate labeled at the 3'-end. The R1-D9*/D18 and R2-D9*/D18 substrates represent Okazaki fragment-like substrates containing one and two ribonucleotides labeled at the 3'-ends. The R8:R1-D9*/D18 and R7:R2-D9*/D18 substrates represent the R9-D9*/D18 substrates with a nick at the P-O3' bond between the first and second and between the second and third ribonucleotides from the RNA-DNA junction respectively. The *D15-R1-D13/D29 and D15-R1-D13*/D29 substrates represent dsDNA containing a single ribonucleotide ($dsDNA^{R1}$) labeled at the 5'- and 3'-ends respectively. The *D29/D29 substrate represents dsDNA labeled at the 5'-end. For an Okazaki fragment-like substrate, the first and second ribonucleotides from the RNA-DNA junction are termed R(-1) and R(-2) respectively. Likewise, the first and second deoxyribonucleotides from the RNA-DNA junction are termed D(+1) and D(+2) respectively. The phosphodiester bonds between R(-2) and R(-1), between R(-1) and D(+1), and between D(+1) and D(+2) are designated as R(-2)-R(-1), RNA-DNA junction, and D(+1)-D(+2) respectively. For $dsDNA^{R1}$, the 5'- and 3'-sides of the ribonucleotide are designated as (5')DNA-RNA(3') and (5')RNA-DNA(3') junctions respectively.

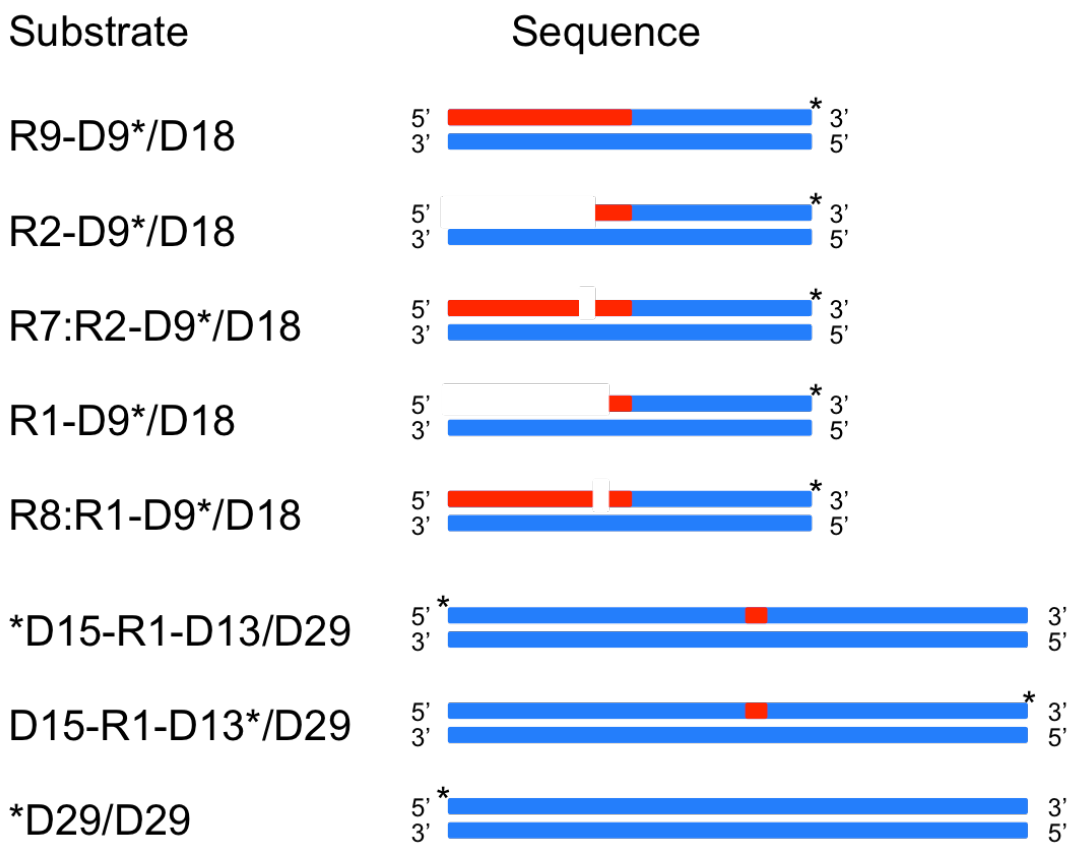

Figure 5.2. **The oligomeric substrates used in this study are schematically shown.** The RNA and DNA strands are shown by red and blue boxes respectively. The asterisk indicates the fluorescein-labeled site. The R2-D9* and R2-D9* strands in the R2-D9*/D18, R7:R2-D9*/D18, R1-D9*/D18, and R8:R1-D9*/D18 duplexes are 5'-phosphorylated.

5.3.2. CLEAVAGE OF R9-D9/D18 SUBSTRATE BY *E. COLI* RNASE H1

It has been reported that *E. coli* RNase H1 cleaves an Okazaki fragment-like substrate most effectively at R(-2)-R(-1) and less effectively at the RNA-DNA junction in the presence of 5 mM $MnCl_2$ [50], indicating that *E. coli* RNase H1 exhibits a weak 3'-JRNase activity for this substrate in the presence of manganese ions. However, two conflicting results that *E. coli* RNase H1 can [50,55] and cannot [59,60] cleave this substrate at the RNA-DNA junction in the presence of magnesium ions have been reported. Therefore, the R9-D9*/D18 substrate was first cleaved by *E. coli* RNase H1 either in the presence of 1 mM $MnCl_2$ or 10 mM $MgCl_2$, to examine whether *E. coli* RNase H1 exhibits 3'-JRNase activity for this substrate in the

presence of magnesium ions. These concentrations of the metal ions were chosen, because the 3'-JRNase activity of the enzyme determined in the presence of 1 mM $MnCl_2$ may not be significantly different from that previously determined in the presence of 5 mM $MnCl_2$ [50] and the optimum concentration of $MgCl_2$ for the RNase H activity of *E. coli* RNase H1 is 5-10 mM [101]. The results are shown in **Figure 5.3**. The D9* fragment is detected as one of the major products when the substrate is extensively cleaved by the enzyme. This band is produced more effectively in the presence of manganese ions than in the presence of magnesium ions. These results indicate that *E. coli* RNase H1 cleaves the R9-D9*/D18 substrate at the RNA-DNA junction either in the presence of manganese or magnesium ions, but more effectively in the presence of manganese ions than in the presence of magnesium ions. This result is consistent with that previously reported [50]. Thus, *E. coli* RNase H1 exhibits 3'-JRNase activity for an Okazaki fragment-like substrate either in the presence of manganese or magnesium ions, but more strongly in the presence of manganese ions. This metal ion preference is opposite to that for the RNase H activity of this enzyme determined using an RNA/DNA substrate [101].

E. coli RNase H1 cleaves the R9-D9*/D18 substrate almost exclusively at R(-2)-R(-1) and RNA-DNA junction in the presence of 1 mM $MnCl_2$, whereas it cleaves this substrate preferentially at R(-3)-R(-2) and R(-2)-R(-1) in the presence of 10 mM $MgCl_2$ (**Fig. 5.3**). It has been reported that hydrolysis of this substrate by *E. coli* RNase H1 is initiated by the cleavage at R(-5)-R(-4), R(-4)-R(-3), and R(-3)-R(-2) in the presence of 10 mM $MgCl_2$ [55]. These results suggest that the R9-D9*/D18 substrate is cleaved by *E. coli* RNase H1 preferentially at the upstream region of the RNA-DNA junction in the presence of magnesium ions due to its RNase H activity. This substrate is not cleaved by *E. coli* RNase H1 at the upstream region of the RNA-

DNA junction in the presence of 1 mM $MnCl_2$, except for R(-2)-R(-1), probably due to a very weak RNase H activity. It has been reported that the RNase H activity of *E. coli* RNase H1 determined using an RNA/DNA substrate in the presence of the optimum concentration of manganese ions (2-4 μM) is lower than that determined in the presence of the optimum concentration of magnesium ions (5-10 mM) by only 5 fold [101], whereas the RNase H activity of *E. coli* RNase H1 determined using a 12 base pair RNA/DNA substrate in the presence of 5 mM $MnCl_2$ is lower than that determined in the presence of 5 mM $MgCl_2$ by 1000 fold [50]. As a result, *E. coli* RNase H1 cleaves the R9-D9*/D18 substrate more effectively in the presence of 10 mM $MgCl_2$ than in the presence of 1 mM $MnCl_2$ (**Fig. 5.3.a**).

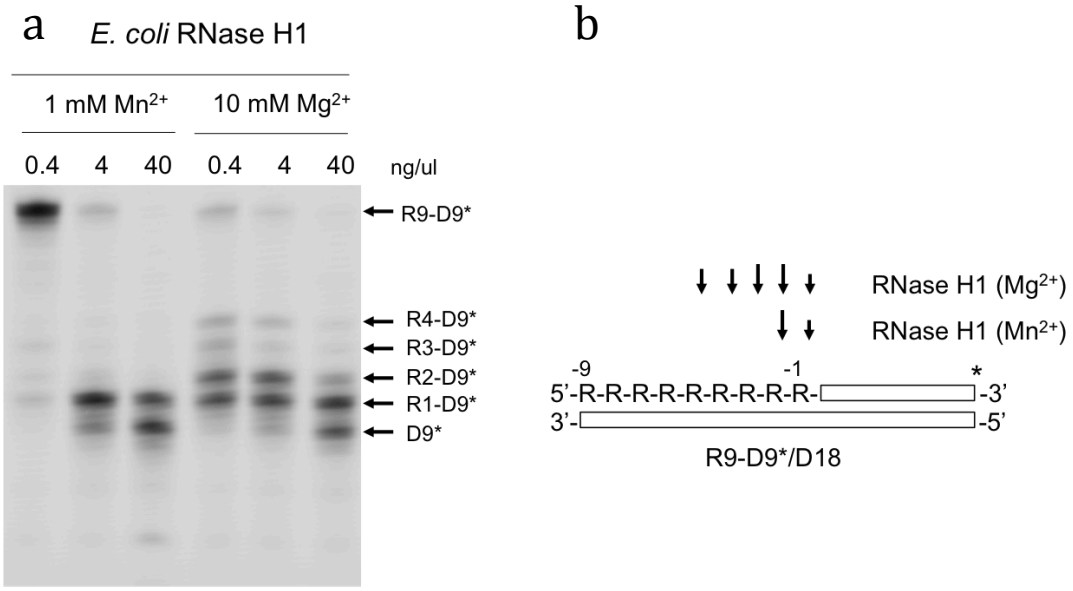

Figure 5.3. **Cleavage of R9-D9/D18 substrate.** (a) The R9-D9*/D18 substrate was hydrolyzed by the enzyme at 30°C for 15 min and the products were separated on a 20% polyacrylamide gel containing 7 M urea as described in Section 5.2.3. The concentration of the substrate was 1.0 μM. The enzyme used to cleave this substrate is shown above the gel. The concentration of the enzyme in the reaction mixture (10 μL) is indicated above each lane. The metal cofactors used to cleave this substrate are also shown above the gel together with their concentrations. (b) The cleavage sites are schematically shown. "R" represents the ribonuclotide, which is inversely numbered from -1 from the RNA-DNA junction to the 5' end. The open box represents the DNA strand (either D9 or D18). The differences in the lengths of the arrows reflect relative cleavage intensities at the position indicated.

It is noted that a short DNA fragment is detected as a minor product when the concentration of the enzyme is highly elevated (**Fig. 5.3.a**), suggesting that the R9-D9* strand is cleaved near the 3'-end. It remains to be determined whether this site is cleaved by *E. coli* RNase H1 or another enzyme contaminated.

5.3.3. CLEAVAGE OF R1-D9/D18 AND R8:R1-D9/D18 SUBSTRATES BY *E. COLI* RNASE H1

The R1-D9* fragment is detected as one of the major products when the R9-D9*/D18 substrate is extensively cleaved by *E. coli* RNase H1 (**Fig. 5.3.a**), suggesting that the R1-D9*/D18 substrate is not cleaved by *E. coli* RNase H1. To examine whether *E. coli* RNase H1 does not cleave this substrate, but cleaves it at the RNA-DNA junction when 8 b RNA (R8) complementary to the single stranded region of the R1-D9*/D18 substrate is supplied, the R1-D9*/D18 and R8:R1-D9*/D18 substrates were cleaved by *E. coli* RNase H1 either in the presence of 1 mM $MnCl_2$ or 10 mM $MgCl_2$. The results are shown in **Figure 5.4**. *E. coli* RNase H1 does not cleave the R1-D9*/D18 substrate regardless of the metal cofactors. In contrast, it cleaves the R8:R1-D9*/D18 substrate at the RNA-DNA junction, but only in the presence of manganese ions. This result suggests that *E. coli* RNase H1 cleaves an Okazaki fragment-like RNA-DNA/DNA substrate at the RNA-DNA junction regardless of whether this substrate contains a nick at R(-2)-R(-1). The RNA-DNA junction of the R8:R1-D9*/D18 substrate is not fully cleaved by *E. coli* RNase H1, probably because the upstream region of the RNA-DNA junction is cleaved before the RNA-DNA junction is completely cleaved. The RNA-DNA junction of the R9-D9*/D18 substrate is cleaved by the 3'-JRNase activity of *E. coli* RNase H1 less effectively in the presence of magnesium ions than in the presence of manganese ions, probably because the upstream region of the RNA-DNA junction is cleaved by the

RNase H activity of *E. coli* RNase H1 more effectively in the presence of magnesium ions than in the presence of manganese ions. The RNA-DNA junction of the R8:R1-D9*/D18 substrate is not cleaved by *E. coli* RNase H1 in the presence of magnesium ions, probably because the presence of a nick at R(-2)-R(-1) alter the interaction between the substrate and metal ion, in such a way that the scissile phosphate group of the substrate and magnesium ions are not arranged ideally.

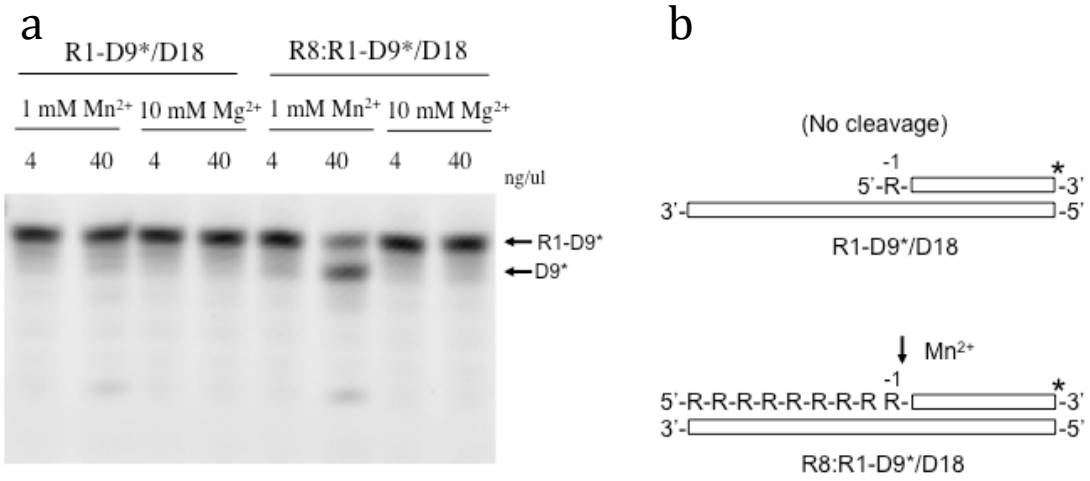

Figure 5.4. **Cleavage of R1-D9/D18 substrate.** (a) The R1-D9*/D18 and R8:R1-D9*/D18 substrates were hydrolyzed by the enzyme as described for Figure 5.3. (b) The cleavage site is schematically shown. "R" represents the ribonuclotide, which is inversely numbered from -1 from the RNA-DNA junction to the 5' end. The open box represents the DNA strand (either D9 or D18).

5.3.4. CLEAVAGE OF R2-D9/D18 AND R7:R2-D9/D18 SUBSTRATES BY *E. COLI* RNASE H1

Inability of *E. coli* RNase H1 to cleave the R1-D9*/D18 substrate at the RNA-DNA junction indicates that multiple upstream ribonucleotides are necessary for the cleavage of an Okazaki fragment-like substrate by the enzyme at the RNA-DNA junction. To examine whether two upstream ribonucleotides are sufficient for this

cleavage, the R2-D9*/D18 substrate was cleaved by *E. coli* RNase H1 either in the presence of 1 mM $MnCl_2$ or 10 mM $MgCl_2$. The results are shown in **Figure 5.5**.

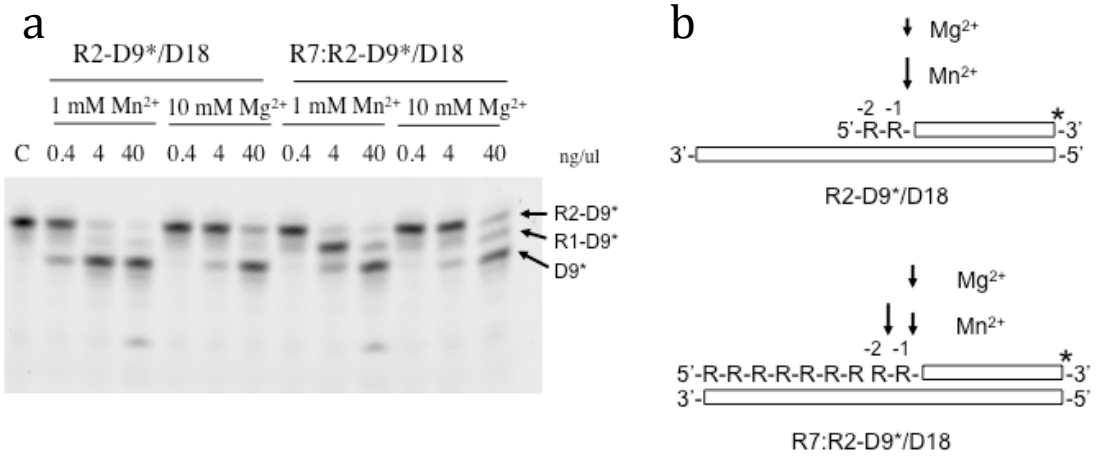

Figure 5.5. **Cleavage of R2-D9/D18 substrates.** (a) The R2-D9*/D18 and R7:R2-D9*/D18 substrates were hydrolyzed by the enzyme as described for Figure 5.3. (b) The cleavage sites are schematically shown. "R" represents the ribonuclotide, which is inversely numbered from -1 from the RNA-DNA junction to the 5' end. The open box represents the DNA strand (either D9 or D18). The differences in the lengths of the arrows reflect relative cleavage intensities at the position indicated.

E. coli RNase H1 cleaves the R2-D9*/D18 substrate at the RNA-DNA junction either in the presence of manganese or magnesium ions, but more effectively in the presence of manganese ions. This result indicates that the presence of two upstream ribonucleotides is sufficient for the cleavage of an Okazaki fragment-like substrate by *E. coli* RNase H1 at the RNA-DNA junction. To examine whether this cleavage site is shifted by supplying an RNA strand that facilitates the formation of an upstream duplex structure, the R7:R2-D9*/D18 substrate was also examined by *E. coli* RNase H1. The results are shown in **Figure 5.5**. *E. coli* RNase H1 most effectively cleaves this substrate at R(-2)-R(-1) in the presence of manganese ions. This site is also cleaved in the presence of magnesium ions, but much less effectively, probably because the RNA/DNA region of the R7:R2-D9*/D18 substrate is effectively cleaved by the RNase H activity of the enzyme in the presence of magnesium ions. Thus, the

primary products of the R7:R2-D9*/D18 substrate upon cleavage with *E. coli* RNase H1 in the presence of manganese and magnesium ions are probably the R7:R1-D9*/D18 and R2-D9*/D18 duplexes respectively. The RNA-DNA junctions of these primary products are cleaved only when the concentration of the enzyme is greatly elevated.

5.3.5. CLEAVAGE OF D15-R1-D13/D29 SUBSTRATE BY *E. COLI* RNASE H1

To examine whether *E. coli* RNase H1 exhibits 3'-JRNase activity for $dsDNA^{R1}$, the D15-R1-D13*/D29 and *D15-R1-D13/D29 substrates were subjected to cleavage by *E. coli* RNase H1 either in the presence of 1 mM $MnCl_2$ or 1 mM $MgCl_2$. The results are shown in **Figure 5.6**. The D13* and *D15-R1 fragments are detected as the major products only in the presence of manganese ions, indicating that *E. coli* RNase H1 cleaves these substrates mainly at the (5')RNA-DNA(3') junction only in the presence of manganese ions to produce the D15-R1-D13/D29 duplex containing a nick at the (5')RNA-DNA(3') junction. In addition to these fragments, the D12* and *D15 fragments are detected as minor products, indicating that *E. coli* RNase H1 can cleave these substrates at D(+1)-D(+2) and (5')DNA-RNA(3') junction, but much less effectively. *E. coli* RNase H1 does not cleave the *D29/D29 substrate at all neither in the presence of 1 mM $MnCl_2$ nor 1 mM $MgCl_2$, indicating that the presence of the ribonucleotide is required for the cleavage of the D15-R1-D13/D29 substrate by the 3'-JRNase activity of *E. coli* RNase H1. This result suggests that the substrate specificity of *E. coli* RNase H1 is less specific in the presence of manganese ions than in the presence of magnesium ions. Decreased substrate specificity and cleavage-site selectivity in the presence of manganese ions have also been reported for other RNases H [36,43,52,55,56].

Detection of the other minor cleavage sites than the (5')RNA-DNA(3') junction suggests that the specificity of *E. coli* RNase H1 to the (5')RNA-DNA(3') junction is not so strict. *E. coli* RNase H1 can weakly cleave the D15-R1-D13/D29 substrate at the (5')DNA-RNA(3') junction (**Fig. 5.6**), suggesting that it exhibits a 5'-JRNase-like activity as well. *E. coli* RNase H1 cleaves the R9-D9*/D18 substrate most effectively at R(-2)-R(-1) in the presence of manganese ions probably due to this 5'-JRNase-like activity (**Fig. 5.3**). It is unlikely that this cleavage is catalyzed by the RNase H activity of *E. coli* RNase H1, because *E. coli* RNase H1 exhibits very poor RNase H activity in the presence of 1 mM $MnCl_2$ [50], as mentioned above. Interestingly, *E. coli* RNase H1 can also weakly cleave the D15-R1-D13/D29 duplex at D(+1)-D(2+) (**Fig. 5.6**). This is the first time to show the cleavage of the phosphodiester bond between the deoxyribonucleotides by an RNase H enzyme. Because *E. coli* RNase H1 does not cleave the *D29/D29 substrate, recognition of the single ribonucleotide by the enzyme is absolutely necessary for the cleavage of the D15-R1-D13/D29 substrate by the enzyme at DNA(+1)-DNA(2+).

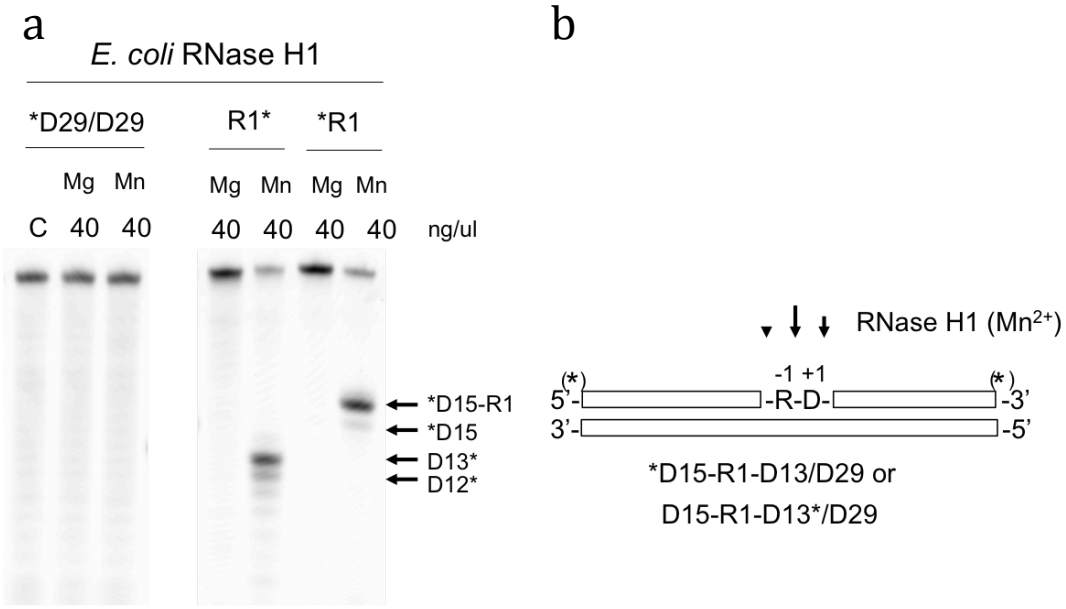

Figure 5.6. **Cleavage of D15-R1-D13/D29 substrate.** (a) The *D15-R1-D13/D29, D15-R1-D13*/D29, and *D29/D29 substrates (1.0 μM) were hydrolyzed by *E. coli* RNase H1 (40 ng μL^{-1}) at 30°C for 15 min either in the presence of 1 mM $MgCl_2$ or 1 mM $MnCl_2$ and the products were separated on a 20% polyacrylamide gel containing 7 M urea. The enzymes, metal cofactors, and substrates are shown above the gel. *R1 and R1* represent *D15-R1-D13/D29 and D15-R1-D13*/D29 respectively. (b) The cleavage sites are schematically shown. "R" and "D" represent the ribonuclotide and deoxyribonucleotide respectively. The open box represents the DNA strand. The differences in the lengths of the arrows reflect relative cleavage intensities at the position indicated.

5.3.6. CLEAVAGE OF R9-D9/D18 AND D15-R1-D13/D29 SUBSTRATES BY *E. COLI* RNASE H2

The finding that *E. coli* RNase H1 can cleave the D15-R1-D13/D29 substrate at the (5')RNA-DNA(3') junction promotes us to examine whether a single ribonucleotide of $dsDNA^{R1}$ can be removed by the combination of the 5'-JRNase activity of *E. coli* RNase H2 and the 3'-JRNase activity of *E. coli* RNase H1. *E. coli* RNase H2 has been shown to exhibit 5'-JRNase activity for an Okazaki fragment-like substrate [50]. A crude extract from *E. coli* cells exhibits 5'-JRNase activity for $dsDNA^{R1}$, whereas that from RNase H2-deficient *E. coli* cells does not exhibit this activity [22], suggesting that *E. coli* RNase H2 also exhibits 5'-JRNase activity for

dsDNA^{R1}. However, it remains to be determined whether the purified protein of *E. coli* RNase H2 exhibits this activity for dsDNA^{R1}. Therefore, the *D15-R1-D13/D29 and D15-R1-D13*/D29 substrates were subjected to cleavage by *E. coli* RNase H2 either in the presence of $MnCl_2$ or $MgCl_2$, to examine whether this enzyme exhibits 5'-JRNase activity for dsDNA^{R1}. The R9-D9*/D18 substrate was also cleaved by this enzyme for comparative purpose either in the presence of $MnCl_2$ or $MgCl_2$.

As shown in **Figure 5.7**, *E. coli* RNase H2 cleaved the R9-D9*/D18 substrate almost exclusively at R(-2)-R(-1) either in the presence of manganese or magnesium ions, but more effectively in the presence of magnesium ions.

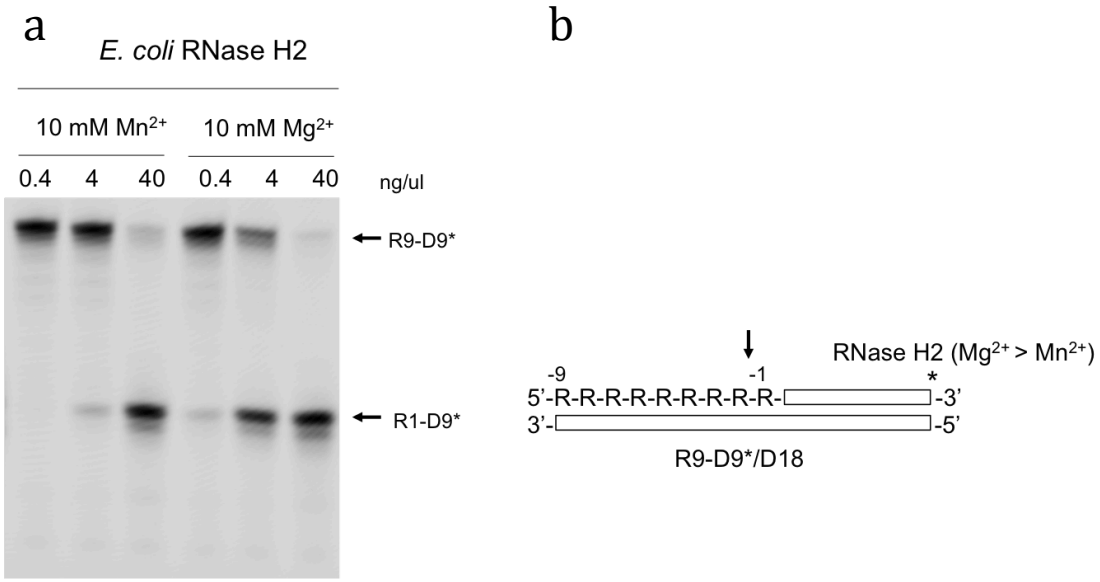

Figure 5.7. **Cleavage of R9-D9/D18 substrate.** (a) The R9-D9*/D18 substrate was hydrolyzed by the enzyme as described for Figure 5.3. (b) The cleavage site is schematically shown. "R" represents the ribonuclotide, which is inversely numbered from -1 from the RNA-DNA junction to the 5' end. The open box represents the DNA strand (either D9 or D18).

Likewise, as shown in **Figure 5.8**, *E. coli* RNase H2 cleaved the *D15-R1-D13/D29 and D15-R1-D13*/D29 substrates almost exclusively at the (5')DNA-RNA(3') junction to produce the D15-R1-D13/D29 duplex containing a nick at the (5')DNA-RNA(3') junction either in the presence of manganese or magnesium ions,

but more effectively in the presence of magnesium ions. Thus, *E. coli* RNase H2 exhibits 5'-JRNase activity for dsDNA^{R1} either in the presence of manganese or magnesium ions, but more strongly in the presence of magnesium ions. This metal ion preference is opposite to that for the RNase H activity of this enzyme determined using an RNA/DNA substrate possibly due to the different number of coordination bonds needed between the enzyme and the specific substrate [50,100].

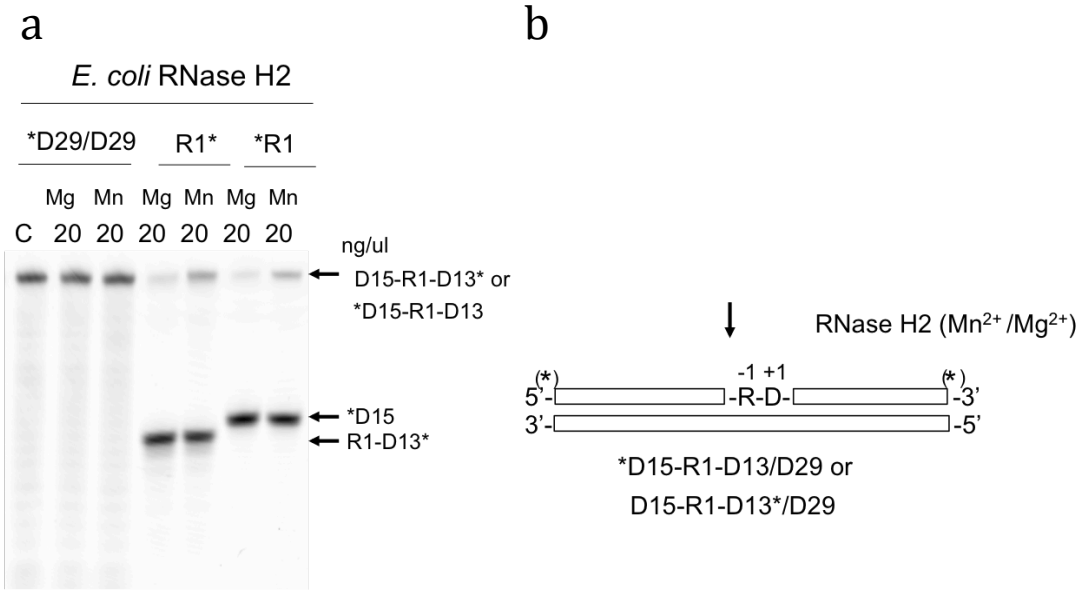

Figure 5.8. **Cleavage of D15-R1-D13/D29 substrate.** (a) The *D15-R1-D13/D29, D15-R1-D13*/D29, and *D29/D29 substrates (1.0 μM) were hydrolyzed by *E. coli* RNase H2 (20 ng μL^{-1}) at 30°C for 15 min either in the presence of 1 mM $MgCl_2$ or 1 mM $MnCl_2$ and the products were separated on a 20% polyacrylamide gel containing 7 M urea. The enzymes, metal cofactors, and substrates are shown above the gel. *R1 and R1* represent *D15-R1-D13/D29 and D15-R1-D13*/D29 respectively. (b) The cleavage site is schematically shown. "R" and "D" represent the ribonuclotide and deoxyribonucleotide respectively. The open box represents the DNA strand.

The RNase H activity of *E. coli* RNase H2 determined in the presence of 5 mM $MgCl_2$ is lower than that determined in the presence of 5 mM $MnCl_2$ by 10 fold. The RNA/DNA hybrid region of the R9-D9*/D18 substrate is not cleaved by *E. coli* RNase H2, probably because the RNase H activity of this enzyme is very low. It has been reported that the RNase H activity of *E. coli* RNase H2 determined in the

presence of 5 mM $MnCl_2$ using an oligomeric RNA/DNA substrate is lower than those of *E. coli* RNase H1 determined in the presence of 5 mM $MgCl_2$ and 5 mM $MnCl_2$ by $2x10^4$ and 20 fold respectively [50]. Determination of the 5'-JRNase activity of *E. coli* RNase H2 in the presence of various concentrations (0.1-100 mM) of manganese or magnesium ions using the D15-R1-D13*/D29 substrate indicates that the optimum concentrations of manganese and magnesium ions for this activity are both 10 mM and the activity determined in the presence of 10 mM $MgCl_2$ is higher than that determined in the presence of 10 mM $MnCl_2$ by 15 fold.

5.3.7. STEPWISE CLEAVAGE OF D15-R1-D13/D29 SUBSTRATE BY *E. COLI* RNASES H1 AND H2

To examine whether a single ribonucleotide embedded in dsDNA can be removed by the combination of the 5'-JRNase activity of *E. coli* RNase H2 and 3'-JRNase activity of *E. coli* RNase H1, the D15-R1-D13/D29 substrate was subjected to cleavage by these enzymes in a stepwise manner. The results are shown in **Figure 5.9**.

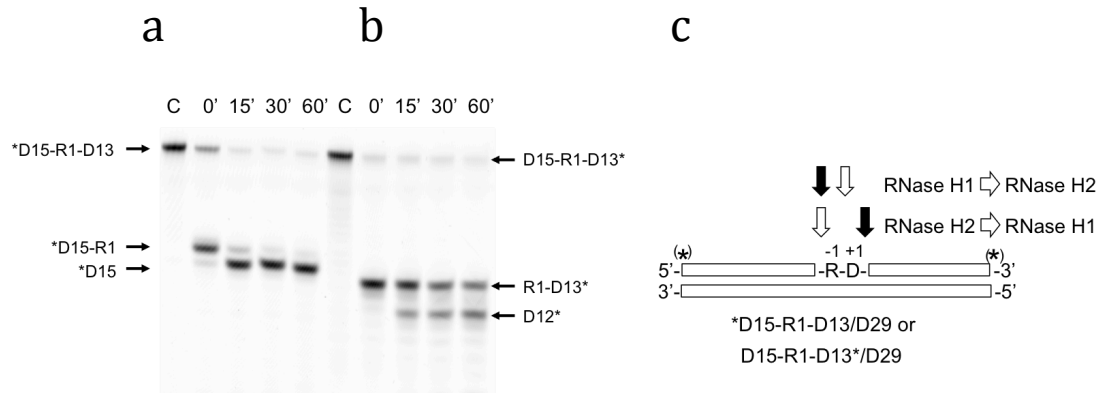

Figure 5.9. **Stepwise cleavage of D15-R1-D13/D29 substrate with *E. coli* RNases H1 and H2.** (a) The *D15-R1-D13/D29 substrate (1.0 μM) was hydrolyzed by *E. coli* RNase H1 (40 ng μL^{-1}) at 30°C for 30 min in the presence of 1 mM $MnCl_2$ at first. The resultant product, *D15-R1:D13/D29 duplex, was further hydrolyzed by *E. coli* RNase H2 (20 ng μL^{-1}) at 30°C for the period indicated above each lane in the presence of 1 mM $MgCl_2$ and the

products were separated on a 20% polyacrylamide gel containing 7 M urea. (b) The D15-R1-D13*/D29 substrate (1.0 μM) was hydrolyzed by *E. coli* RNase H2 (20 ng μL^{-1}) at 30°C for 30 min in the presence of 1 mM $MgCl_2$ at first. The resultant product, D15:R1-D13*/D29 duplex, was further hydrolyzed by *E. coli* RNase H1 (40 ng μL^{-1}) at 30°C for the period indicated above each lane in the presence of 1 mM $MnCl_2$ and the products were separated on a 20% polyacrylamide gel containing 7 M urea. (c) The cleavage sites are schematically shown. "R" and "D" represent the ribonuclotide and deoxyribonucleotide respectively. The open box represents the DNA strand. The open and solid arrows represent the first and second cleavage sites respectively.

When the *D15-R1-D13/D29 substrate was cleaved by *E. coli* RNase H1 in the presence of 1 mM $MnCl_2$ in the first step, and by *E. coli* RNases H1 and H2 in the presence of both 1 mM $MnCl_2$ and 1 mM $MgCl_2$ in the second step, the (5')RNA-DNA(3') and (5')DNA-RNA(3') junctions of the substrate were cleaved in the first and second steps respectively. As a result, the single ribonucleotide was removed from the substrate. Likewise, when the D15-R1-D13*/D29 substrate was incubated with *E. coli* RNase H2 in the presence of 1 mM $MgCl_2$ in the first step, and by *E. coli* RNases H1 and H2 in the presence of both 1 mM $MnCl_2$ and 1 mM $MgCl_2$ in the second step, the (5')DNA-RNA(3') junctions and the D(+1)-D(+2) bond were cleaved in the first and second steps respectively. As a result, the chimeric RNA-DNA dinucleotide was removed from the substrate. These results suggest that the presence of manganese and magnesium ions is not inhibitory for the 5'-JRNase activity of *E. coli* RNase H2 and 3'-JRNase activity of *E. coli* RNase H1 respectively. These results also suggest that *E. coli* RNases H1 and H2 exhibit 3'- and 5'-JRNase activities for $dsDNA^{R1}$ with a nick at the (5')DNA-RNA(3') and (5')RNA-DNA(3') junctions respectively, although the products released from this duplex vary for these enzymes (chimeric RNA-DNA dinulecotide for *E. coli* RNase H1 and single ribonucleotide for *E. coli* RNase H2). *E. coli* RNase H1 cleaves the D15-R1-D13/D29 substrate most effectively at the (5')RNA-DNA(3') junction and less effectively at D(+1)-D(2+)

(**Fig. 5.6**), whereas it almost exclusively cleaves this substrate at D(+1)-D(2+) when a nick is introduced at the (5')DNA-RNA(3') junction (**Fig. 5.9**), probably because introduction of this nick alters the interaction between the enzyme and substrate, in such a way that the D(+1)-D(2+) bond, instead of the (5')RNA-DNA(3') junction, contacts the active site of the enzyme. These results suggest that single ribonucleotides embedded in dsDNA can be removed as single ribonucleotides or chimeric RNA-DNA dinucleotides by a cooperative work of *E. coli* RNases H1 and H2.

5.4. CONCLUSION

In this chapter, I showed that the RNA-DNA junction of the RNA1-DNA9/DNA18 substrate is not cleaved by *E. coli* RNase H1 but is cleaved by the enzyme when a short RNA fragment is supplied to facilitate the formation of an upstream duplex structure.

I also showed and for the first time that *E. coli* RNase H1 exhibits 3'-JRNase activity for $dsDNA^{R1}$ in the presence of manganese ions, regardless of whether this substrate is cleaved by 5'-JRNase activity of *E. coli* RNase H2 in advance or not, and can excise the single ribonucleotide or the RNA-DNA dinucleotide from $dsDNA^{R1}$ in cooperation with *E. coli* RNase H2. These results suggest that not only RNase H2 but also RNase H1 is involved in the RER pathway and single ribonucleotides misincorporated into the genome of *E. coli* can be excised by a cooperative work of *E. coli* RNase H1 and H2.

CHAPTER 6

GENERAL DISCUSSION

6.1. GENERAL DISCUSSION

This study covers two aspects of proteomics: the structural and the functional. The structural aspect addresses type 1 ribonuclease H from *Halobacterium* sp. NRC-1 (Halo-RNase H1). Unlike all studied halophilic proteins which assume a partially folded state in a low salt condition thus rendering those of them classified as enzymes to be inactive, Halo-RNase H1 exhibits activity even in a low salt condition in the presence of moderate concentrations of divalent metal ions. Although divalent metal ions are absolute cofactors required for the activity of all the RNases H, I found out that in this case divalent metal ions play a dual role in inducing folding of Halo-RNase H1 by replacing salt in a low salt condition and suppressing the negative charge repulsion in a localized manner rather than increasing the ionic strength of the solution.

Using X-ray crystallography to determine the 3D-structure followed by structure-based site directed mutagenesis, I identified a quad-Asp site (two bi-aspartate sites located close to each other) on the surface of the protein which was mainly responsible for this unique behavior seen for Halo-RNase H1. Although the acidic active site, which indeed can bind at least one metal ion in its cavity, is important for stabilizing the folded state of this protein, it did not make a great effect in itself. That is why another type of RNase H, Halo-RNase H2, which shares a similar acidic active

site but lacks the quad-Asp site on its surface, did not exhibit a divalent metal ion-induced folding behavior.

In the model shown in **Figure 6.1**, I summarize the unique folding behavior of Halo-RNase H1 deduced from the secondary structure analysis conducted using CD spectroscopy. In a low salt condition, Halo-RNase H1 exists in a partially folded state (I-state). It changes to a denatured state (D-state) when it is subject to chemical denaturation with GdnHCl or heat denaturation. Upon the addition of NaCl, Halo-RNase H1 shifts to a native state (N-state). Furthermore, the addition of divalent metal ions (shown as purple spheres) can still bind to the protein in a high salt condition, at least one in the active site (shaded in red) and probably on the quad-Asp site (shaded in purple), and further increase its stability.

In an alternative pathway, Halo-RNase H1 in the I-state can shift to N-state upon the addition of divalent metal ions which bind first to the quad-Asp site present on the surface of the protein, initiate folding, and then bind to the acidic active site and stabilize the folded state.

The stability of Halo-RNase H1 in the presence of metal ions is lower than that in the presence of NaCl despite the fact that both are fully folded and exhibit comparable activity. This is due to the fact that NaCl not only suppress the negative charge repulsion at the surface of the protein, but also stabilizes the protein by increasing the hydrophobic interactions at its core.

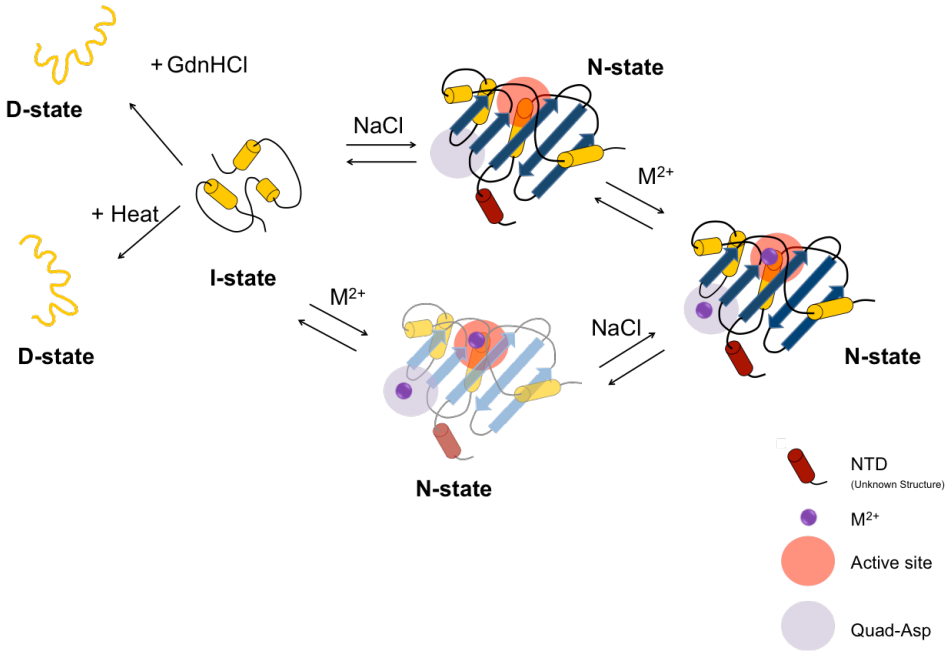

Figure 6.1. **Folding behavior of Halo-RNase H1**

Although the unique ability of Halo-RNase H1 to fold in the presence of moderate concentrations of divalent metal ions is interesting, its physiological significance is not yet clear. However, in an era where custom made proteins with specific functions and characteristics have started entering application areas, making use of a cluster of acidic residues arranged similarly to the ones found on the surface of Halo-RNase H1, might be a good ON/OFF switch for some enzymatic functions.

The functional aspect addresses the involvement of type 1 RNase H in a critical pathway responsible for repairing the genomic DNA from threat causing misincorporated ribonucleotides. As it is well known, DNA - the universal hereditary material that encodes genetic information and transfers them through self-replication - is essential for the existence of all cellular life and some viruses. However, its loyalty is often challenged with some externally induced modifications that render it unstable if left unrepaired. Of these modifications, the presence of single ribonucleotide monophosphates (rNMPs) misincorporated into the DNA backbone is one of the most

common risks that threaten the integrity of the genome and disturb the replication mechanism [13,23,102]. Recent studies indicate that RNase H2 saves the genome by removing these intruders and restoring the DNA back to its original form with the assistance of several other enzymes [13,24-26,53,103,104].

In this study, I showed that not only RNase H2, but probably RNase H1 is also involved in this pathway. In the experiments I did *in vitro* on dsDNA substrates containing a single ribonucleotide ($dsDNA^{R1}$), I showed that *E. coli* RNase H1 exhibits 3'-JRNase activity for $dsDNA^{R1}$ in the presence of manganese ions, regardless of whether this substrate is cleaved by 5'-JRNase activity of *E. coli* RNase H2 in advance or not, and can excise the single ribonucleotide or the RNA-DNA dinucleotide from $dsDNA^{R1}$ in cooperation with *E. coli* RNase H2.

The two possible RER pathways in which both enzymes are included are schematically shown in **Figure 6.2**. According to these pathways, removal of the single ribonucleotides (labeled as R in a red box)) misincorporated into DNA (blue box) is initiated by the 5'-JRNase activity of RNase H2 and completed by the 3'-JRNase activity of RNase H1, or vice versa.

However, human RNase H1 did not exhibit 3'-JRNase activity for $dsDNA^{R1}$ in the presence of magnesium or manganese ions (un-described observations), suggesting that RNase H1 is involved in the RER pathway only in the prokaryotic cells.

Another issue to address is the manganese dependency for the 3'-JRNase activity of *E. coli* RNase H1. It is known that the concentration of magnesium ions in *E. coli* cells is higher than that of manganese by several-fold. However, the fact that the presence of magnesium ions in my assays is not inhibitory for the 3'-JRNase activity of *E. coli* RNase H1 may suggest that *E. coli* RNase H1 exhibits this activity inside

the cells. The *in vivo* studies showing that *E. coli* RNase H1 helps in sanitizing the genome from errant rNMPs misincorporated in dsDNA when the *rnhB* gene encoding *E. coli* RNase H2 is inactivated, thus limiting the consequences of the excessive accumulation of ribonucleotides in the *E. coli* genome [53], supports my hypothesis.

Since maintaining the integrity of the transferred genetic material by repair mechanisms is an indispensable issue, the significance of my work is that it highlights a new possible role for bacterial type 1 RNases H in DNA repair pathway.

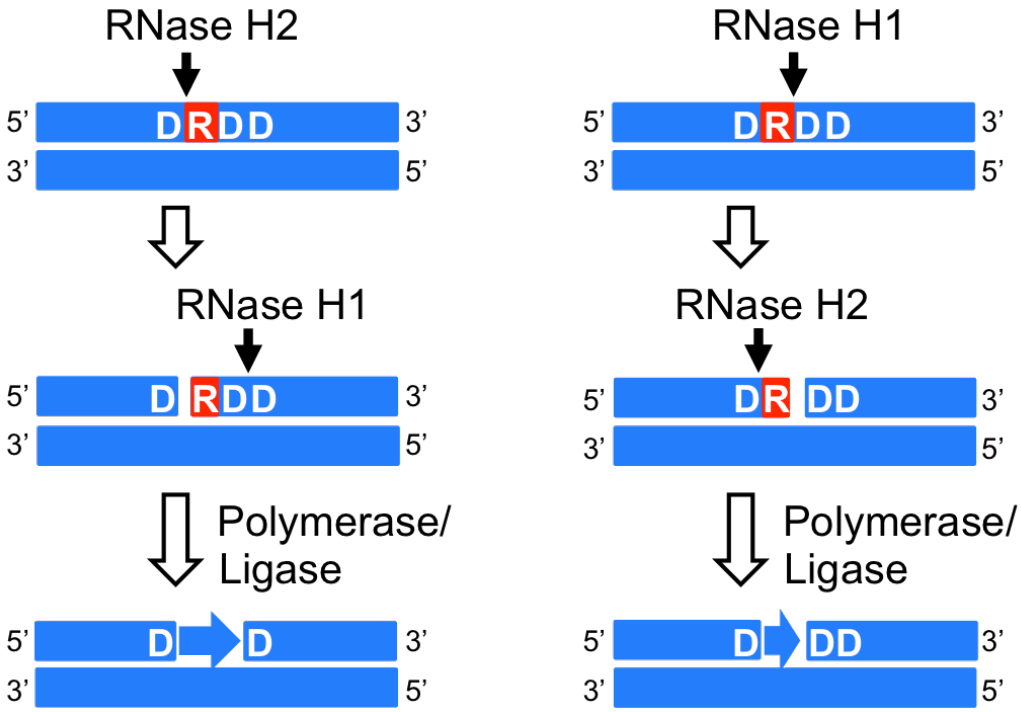

Figure 6.2. **Two possible RER pathways.**

6.2. FUTURE REMARKS

Although the structural determination and mutational studies identified the sites responsible for divalent metal-ion induced folding mechanism of Halo-RNase H1, the exact number and location of metal ions necessary for the folding are not certain. Further analysis using mass spectrometry may identify the number of metal ions bound to the protein in the apo- or substrate-bound form. Further structural analysis using 2A-RNase H1 (mutant without negative charge repulsion at the active site) and 6A-RNase H1 (mutant without negative charge repulsion at the bi/quad-Asp sites) folded in the presence of manganese ions may identify the location of metal ions bound to the protein in the apo-form.

As for the involvement of type 1 RNase H in DNA repair, my results show the ability of *E. coli* RNase H1 to act on the substrate *in vitro*. Additional investigations *in vivo*, as well as for RNases H from different organisms should be conducted to confirm my proposal and generalize or not this role for other organisms.

REFERENCES

1. Crouch RJ, Dirksen ML (1982) Ribonuclease H. Cold Spring Harbor Laboratory Press, Cold Spring Harbor, New York: In Nuclease (Linn SM and Roberts RJ eds). pp. 211-241.

2. Kanaya S, Crouch RJ (1983) DNA sequence of the gene coding for Escherichia coli ribonuclease H. J Biol Chem 258: 1276-1281.

3. Stein H, Hausen P (1969) Enzyme from calf thymus degrading the RNA moiety of DNA-RNA Hybrids: effect on DNA-dependent RNA polymerase. Science 166: 393-395.

4. Berkower I, Leis J, Hurwitz J (1973) Isolation and characterization of an endonuclease from Escherichia coli specific for ribonucleic acid in ribonucleic acid-deoxyribonucleic acid hybrid structures. J Biol Chem 248: 5914-5921.

5. Henry CM, Ferdinand FJ, Knippers R (1973) A hydridase from Escherichia coli. Biochem Biophys Res Commun 50: 603-611.

6. Miller HI, Riggs AD, Gill GN (1973) Ribonuclease H (hybrid) in Escherichia coli. Identification and characterization. J Biol Chem 248: 2621-2624.

7. Katayanagi K, Miyagawa M, Matsushima M, Ishikawa M, Kanaya S, et al. (1990) Three-dimensional structure of ribonuclease H from E. coli. Nature 347: 306-309.

8. Itaya M (1990) Isolation and characterization of a second RNase H (RNase HII) of Escherichia coli K-12 encoded by the rnhB gene. Proc Natl Acad Sci U S A 87: 8587-8591.

9. Ohtani N, Haruki M, Morikawa M, Kanaya S (1999) Molecular diversities of RNases H. J Biosci Bioeng 88: 12-19.

10. Tadokoro T, Kanaya S (2009) Ribonuclease H: molecular diversities, substrate binding domains, and catalytic mechanism of the prokaryotic enzymes. FEBS J 276: 1482-1493.

11. Ohtani N, Haruki M, Morikawa M, Crouch RJ, Itaya M, et al. (1999) Identification of the genes encoding Mn2+-dependent RNase HII and Mg2+-dependent RNase HIII from Bacillus subtilis: classification of RNases H into three families. Biochemistry 38: 605-618.

12. Tadokoro T, Chon H, Koga Y, Takano K, Kanaya S (2007) Identification of the gene encoding a type 1 RNase H with an N-terminal double-stranded RNA binding domain from a psychrotrophic bacterium. FEBS J 274: 3715-3727.

13. Lazzaro F, Novarina D, Amara F, Watt DL, Stone JE, et al. (2012) RNase H and postreplication repair protect cells from ribonucleotides incorporated in DNA. Mol Cell 45: 99-110.

14. Ogawa T, Okazaki T (1984) Function of RNase H in DNA replication revealed by RNase H defective mutants of Escherichia coli. Mol Gen Genet 193: 231-237.

15. Qiu J, Qian Y, Frank P, Wintersberger U, Shen B (1999) Saccharomyces cerevisiae RNase H(35) functions in RNA primer removal during lagging-strand DNA synthesis, most efficiently in cooperation with Rad27 nuclease. Mol Cell Biol 19: 8361-8371.

16. Sato A, Kanai A, Itaya M, Tomita M (2003) Cooperative regulation for Okazaki fragment processing by RNase HII and FEN-1 purified from a hyperthermophilic archaeon, Pyrococcus furiosus. Biochem Biophys Res Commun 309: 247-252.

17. Cerritelli SM, Frolova EG, Feng C, Grinberg A, Love PE, et al. (2003) Failure to produce mitochondrial DNA results in embryonic lethality in Rnaseh1 null mice. Mol Cell 11: 807-815.

18. Bubeck D, Reijns MA, Graham SC, Astell KR, Jones EY, et al. (2011) PCNA directs type 2 RNase H activity on DNA replication and repair substrates. Nucleic Acids Res 39: 3652-3666.

19. Broccoli S, Rallu F, Sanscartier P, Cerritelli SM, Crouch RJ, et al. (2004) Effects of RNA polymerase modifications on transcription-induced negative supercoiling and associated R-loop formation. Mol Microbiol 52: 1769-1779.

20. Cheng B, Rui S, Ji C, Gong VW, Van Dyk TK, et al. (2003) RNase H overproduction allows the expression of stress-induced genes in the absence of topoisomerase I. FEMS Microbiol Lett 221: 237-242.

21. Drolet M, Phoenix P, Menzel R, Massé E, Liu LF, et al. (1995) Overexpression of RNase H partially complements the growth defect of an Escherichia coli delta topA mutant: R-loop formation is a major problem in the absence of DNA topoisomerase I. Proc Natl Acad Sci U S A 92: 3526-3530.

22. Rydberg B, Game J (2002) Excision of misincorporated ribonucleotides in DNA by RNase H (type 2) and FEN-1 in cell-free extracts. Proc Natl Acad Sci U S A 99: 16654-16659.

23. Nick McElhinny SA, Kumar D, Clark AB, Watt DL, Watts BE, et al. (2010) Genome instability due to ribonucleotide incorporation into DNA. Nat Chem Biol 6: 774-781.

24. Sparks JL, Chon H, Cerritelli SM, Kunkel TA, Johansson E, et al. (2012) RNase H2-initiated ribonucleotide excision repair. Mol Cell 47: 980-986.

25. Hiller B, Achleitner M, Glage S, Naumann R, Behrendt R, et al. (2012) Mammalian RNase H2 removes ribonucleotides from DNA to maintain genome integrity. J Exp Med 209: 1419-1426.

26. Reijns MA, Rabe B, Rigby RE, Mill P, Astell KR, et al. (2012) Enzymatic removal of ribonucleotides from DNA is essential for mammalian genome integrity and development. Cell 149: 1008-1022.

27. Beilhartz GL, Götte M (2010) HIV-1 Ribonuclease H: Structure, Catalytic Mechanism and Inhibitors. Viruses 2: 900-926.

28. Itaya M, Omori A, Kanaya S, Crouch RJ, Tanaka T, et al. (1999) Isolation of RNase H genes that are essential for growth of Bacillus subtilis 168. J Bacteriol 181: 2118-2123.

29. Kogoma T, Foster PL (1998) Physiological functions of *E.coli* RNase H1. INSERM; Paris: In Ribonuclease H. (Crouch RJ and Toulme JJ eds). pp. 39-66.

30. Arudchandran A, Cerritelli S, Narimatsu S, Itaya M, Shin DY, et al. (2000) The absence of ribonuclease H1 or H2 alters the sensitivity of Saccharomyces cerevisiae to hydroxyurea, caffeine and ethyl methanesulphonate: implications for roles of RNases H in DNA replication and repair. Genes Cells 5: 789-802.

31. Crow YJ, Leitch A, Hayward BE, Garner A, Parmar R, et al. (2006) Mutations in genes encoding ribonuclease H2 subunits cause Aicardi-Goutières syndrome and mimic congenital viral brain infection. Nat Genet 38: 910-916.

32. Repaske R, Hartley JW, Kavlick MF, O'Neill RR, Austin JB (1989) Inhibition of RNase H activity and viral replication by single mutations in the 3' region of Moloney murine leukemia virus reverse transcriptase. J Virol 63: 1460-1464.

33. Tisdale M, Schulze T, Larder BA, Moelling K (1991) Mutations within the RNase H domain of human immunodeficiency virus type 1 reverse transcriptase abolish virus infectivity. J Gen Virol 72 (Pt 1): 59-66.

34. Tramontano E, Di Santo R (2010) HIV-1 RT-associated RNase H function inhibitors: Recent advances in drug development. Curr Med Chem 17: 2837-2853.

35. Esposito F, Corona A, Tramontano E (2012) HIV-1 Reverse Transcriptase Still Remains a New Drug Target: Structure, Function, Classical Inhibitors, and New Inhibitors with Innovative Mechanisms of Actions. Mol Biol Int 2012: 586401.

36. Nowotny M, Gaidamakov SA, Ghirlando R, Cerritelli SM, Crouch RJ, et al. (2007) Structure of human RNase H1 complexed with an RNA/DNA hybrid: insight into HIV reverse transcription. Mol Cell 28: 264-276.

37. Nowotny M, Gaidamakov SA, Crouch RJ, Yang W (2005) Crystal structures of RNase H bound to an RNA/DNA hybrid: substrate specificity and metal-dependent catalysis. Cell 121: 1005-1016.

38. Nguyen TN, You DJ, Matsumoto H, Kanaya E, Koga Y, et al. (2013) Crystal structure of metagenome-derived LC11-RNase H1 in complex with RNA/DNA hybrid. J Struct Biol 182: 144-154.

39. Haruki M, Noguchi E, Kanaya S, Crouch RJ (1997) Kinetic and stoichiometric analysis for the binding of Escherichia coli ribonuclease HI to RNA-DNA hybrids using surface plasmon resonance. J Biol Chem 272: 22015-22022.

40. Cerritelli SM, Crouch RJ (1998) Cloning, expression, and mapping of ribonucleases H of human and mouse related to bacterial RNase HI. Genomics 53: 300-307.

41. Itaya M, McKelvin D, Chatterjie SK, Crouch RJ (1991) Selective cloning of genes encoding RNase H from Salmonella typhimurium, Saccharomyces cerevisiae and Escherichia coli rnh mutant. Mol Gen Genet 227: 438-445.

42. Haruki M, Hayashi K, Kochi T, Muroya A, Koga Y, et al. (1998) Gene cloning and characterization of recombinant RNase HII from a hyperthermophilic archaeon. J Bacteriol 180: 6207-6214.

43. Permanasari ED, Angkawidjaja C, Koga Y, Kanaya S (2013) Role of N-terminal extension of Bacillus stearothermophilus RNase H2 and C-terminal extension of Thermotoga maritima RNase H2. FEBS J 280: 5065-5079.

44. Chon H, Matsumura H, Koga Y, Takano K, Kanaya S (2006) Crystal structure and structure-based mutational analyses of RNase HIII from Bacillus stearothermophilus: a new type 2 RNase H with TBP-like substrate-binding domain at the N terminus. J Mol Biol 356: 165-178.

45. Jongruja N, You DJ, Angkawidjaja C, Kanaya E, Koga Y, et al. (2012) Structure and characterization of RNase H3 from Aquifex aeolicus. FEBS J 279: 2737-2753.

46. Nguyen TN, You DJ, Kanaya E, Koga Y, Kanaya S (2013) Crystal structure of metagenome-derived LC9-RNase H1 with atypical DEDN active site motif. FEBS Lett 587: 1418-1423.

47. Yang W, Lee JY, Nowotny M (2006) Making and breaking nucleic acids: two-Mg2+-ion catalysis and substrate specificity. Mol Cell 22: 5-13.

48. Nowotny M, Yang W (2006) Stepwise analyses of metal ions in RNase H catalysis from substrate destabilization to product release. EMBO J 25: 1924-1933.

49. Eder PS, Walder RY, Walder JA (1993) Substrate specificity of human RNase H1 and its role in excision repair of ribose residues misincorporated in DNA. Biochimie 75: 123-126.

50. Ohtani N, Tomita M, Itaya M (2008) Junction ribonuclease activity specified in RNases HII/2. FEBS J 275: 5444-5455.

51. Haruki M, Tsunaka Y, Morikawa M, Kanaya S (2002) Cleavage of a DNA-RNA-DNA/DNA chimeric substrate containing a single ribonucleotide at the DNA-RNA junction with prokaryotic RNases HII. FEBS Lett 531: 204-208.

52. Rychlik MP, Chon H, Cerritelli SM, Klimek P, Crouch RJ, et al. (2010) Crystal structures of RNase H2 in complex with nucleic acid reveal the mechanism of RNA-DNA junction recognition and cleavage. Mol Cell 40: 658-670.

53. McDonald JP, Vaisman A, Kuban W, Goodman MF, Woodgate R (2012) Mechanisms employed by Escherichia coli to prevent ribonucleotide incorporation into genomic DNA by Pol V. PLoS Genet 8: e1003030.

54. Nick McElhinny SA, Watts BE, Kumar D, Watt DL, Lundström EB, et al. (2010) Abundant ribonucleotide incorporation into DNA by yeast replicative polymerases. Proc Natl Acad Sci U S A 107: 4949-4954.

55. Jongruja N, You DJ, Kanaya E, Koga Y, Takano K, et al. (2010) The N-terminal hybrid binding domain of RNase HI from Thermotoga maritima is important for substrate binding and Mg2+-dependent activity. FEBS J 277: 4474-4489.

56. Nguyen TN, Angkawidjaja C, Kanaya E, Koga Y, Takano K, et al. (2012) Activity, stability, and structure of metagenome-derived LC11-RNase H1, a homolog of Sulfolobus tokodaii RNase H1. Protein Sci 21: 553-561.

57. Lu Z, Liang R, Liu X, Hou J, Liu J (2012) RNase HIII from Chlamydophila pneumoniae can efficiently cleave double-stranded DNA carrying a chimeric ribonucleotide in the presence of manganese. Mol Microbiol 83: 1080-1093.

58. Lu Z, Hou J, Wang Y, Liu J (2012) Involvement of Ser94 in RNase HIII from Chlamydophila pneumoniae in the recognition of a single ribonucleotide misincorporated into double-stranded DNA. Biochim Biophys Acta 1824: 859-865.

59. Ohtani N, Yanagawa H, Tomita M, Itaya M (2004) Identification of the first archaeal Type 1 RNase H gene from Halobacterium sp. NRC-1: archaeal RNase HI can cleave an RNA-DNA junction. Biochem J 381: 795-802.

60. Ohtani N, Yanagawa H, Tomita M, Itaya M (2004) Cleavage of double-stranded RNA by RNase HI from a thermoacidophilic archaeon, Sulfolobus tokodaii 7. Nucleic Acids Res 32: 5809-5819.

61. Ng WV, Kennedy SP, Mahairas GG, Berquist B, Pan M, et al. (2000) Genome sequence of Halobacterium species NRC-1. Proc Natl Acad Sci U S A 97: 12176-12181.

62. Eisenberg H (1995) Life in unusual environments: progress in understanding the structure and function of enzymes from extreme halophilic bacteria. Arch Biochem Biophys 318: 1-5.

63. Paul S, Bag SK, Das S, Harvill ET, Dutta C (2008) Molecular signature of hypersaline adaptation: insights from genome and proteome composition of halophilic prokaryotes. Genome Biol 9: R70.

64. Elcock AH, McCammon JA (1998) Electrostatic contributions to the stability of halophilic proteins. J Mol Biol 280: 731-748.

65. Madern D, Ebel C, Zaccai G (2000) Halophilic adaptation of enzymes. Extremophiles 4: 91-98.

66. Tadeo X, López-Méndez B, Trigueros T, Laín A, Castaño D, et al. (2009) Structural basis for the aminoacid composition of proteins from halophilic archea. PLoS Biol 7: e1000257.

67. Frolow F, Harel M, Sussman JL, Mevarech M, Shoham M (1996) Insights into protein adaptation to a saturated salt environment from the crystal structure of a halophilic 2Fe-2S ferredoxin. Nat Struct Biol 3: 452-458.

68. Mevarech M, Frolow F, Gloss LM (2000) Halophilic enzymes: proteins with a grain of salt. Biophys Chem 86: 155-164.

69. Zaccai G, Cendrin F, Haik Y, Borochov N, Eisenberg H (1989) Stabilization of halophilic malate dehydrogenase. J Mol Biol 208: 491-500.

70. Kanaya S, Oobatake M, Nakamura H, Ikehara M (1993) pH-dependent thermostabilization of Escherichia coli ribonuclease HI by histidine to alanine substitutions. J Biotechnol 28: 117-136.

71. Schägger H (2006) Tricine-SDS-PAGE. Nat Protoc 1: 16-22.

72. Kanaya S, Kimura S, Katsuda C, Ikehara M (1990) Role of cysteine residues in ribonuclease H from Escherichia coli. Site-directed mutagenesis and chemical modification. Biochem J 271: 59-66.

73. Goodwin TW, Morton RA (1946) The spectrophotometric determination of tyrosine and tryptophan in proteins. Biochem J 40: 628-632.

74. Schwede T, Kopp J, Guex N, Peitsch MC (2003) SWISS-MODEL: An automated protein homology-modeling server. Nucleic Acids Res 31: 3381-3385.

75. Watkins HA, Baker EN (2010) Structural and functional characterization of an RNase HI domain from the bifunctional protein Rv2228c from Mycobacterium tuberculosis. J Bacteriol 192: 2878-2886.

76. Baker NA, Sept D, Joseph S, Holst MJ, McCammon JA (2001) Electrostatics of nanosystems: application to microtubules and the ribosome. Proc Natl Acad Sci U S A 98: 10037-10041.

77. Katayanagi K, Okumura M, Morikawa K (1993) Crystal structure of Escherichia coli RNase HI in complex with Mg2+ at 2.8 A resolution: proof for a single Mg(2+)-binding site. Proteins 17: 337-346.

78. Goedken ER, Marqusee S (2001) Co-crystal of Escherichia coli RNase HI with Mn2+ ions reveals two divalent metals bound in the active site. J Biol Chem 276: 7266-7271.

79. Tsunaka Y, Takano K, Matsumura H, Yamagata Y, Kanaya S (2005) Identification of single Mn(2+) binding sites required for activation of the mutant proteins of E.coli RNase HI at Glu48 and/or Asp134 by X-ray crystallography. J Mol Biol 345: 1171-1183.

80. Kanaya S (1998) Enzymatic activity and protein stability of *E. coli* ribonuclease HI.: In *Ribonucleases H* (Crouch, R.J., and Toulmé, J.J., Eds.) pp. 1-38. INSERM, Paris.

81. Kanaya S, Oobatake M, Liu Y (1996) Thermal stability of Escherichia coli ribonuclease HI and its active site mutants in the presence and absence of the Mg2+ ion. Proposal of a novel catalytic role for Glu48. J Biol Chem 271: 32729-32736.

82. Kuwajima K (1989) The molten globule state as a clue for understanding the folding and cooperativity of globular-protein structure. Proteins 6: 87-103.

83. Kanaya S, Katsuda-Nakai C, Ikehara M (1991) Importance of the positive charge cluster in Escherichia coli ribonuclease HI for the effective binding of the substrate. J Biol Chem 266: 11621-11627.

84. Bergqvist S, Williams MA, O'Brien R, Ladbury JE (2003) Halophilic adaptation of protein-DNA interactions. Biochem Soc Trans 31: 677-680.

85. O'Brien R, DeDecker B, Fleming KG, Sigler PB, Ladbury JE (1998) The effects of salt on the TATA binding protein-DNA interaction from a hyperthermophilic archaeon. J Mol Biol 279: 117-125.

86. Vagin A, Teplyakov A (2010) Molecular replacement with MOLREP. Acta Crystallogr D Biol Crystallogr 66: 22-25.

87. Langer G, Cohen SX, Lamzin VS, Perrakis A (2008) Automated macromolecular model building for X-ray crystallography using ARP/wARP version 7. Nat Protoc 3: 1171-1179.

88. Emsley P, Cowtan K (2004) Coot: model-building tools for molecular graphics. Acta Crystallogr D Biol Crystallogr 60: 2126-2132.

89. You DJ, Chon H, Koga Y, Takano K, Kanaya S (2007) Crystal structure of type 1 ribonuclease H from hyperthermophilic archaeon Sulfolobus tokodaii: role of arginine 118 and C-terminal anchoring. Biochemistry 46: 11494-11503.

90. Arakawa T, Tokunaga M (2004) Electrostatic and hydrophobic interactions play a major role in the stability and refolding of halophilic proteins. Protein Pept Lett 11: 125-132.

91. Besir H, Zeth K, Bracher A, Heider U, Ishibashi M, et al. (2005) Structure of a halophilic nucleoside diphosphate kinase from Halobacterium salinarum. FEBS Lett 579: 6595-6600.

92. Premkumar L, Greenblatt HM, Bageshwar UK, Savchenko T, Gokhman I, et al. (2005) Three-dimensional structure of a halotolerant algal carbonic anhydrase predicts halotolerance of a mammalian homolog. Proc Natl Acad Sci U S A 102: 7493-7498.

93. Winter JA, Christofi P, Morroll S, Bunting KA (2009) The crystal structure of Haloferax volcanii proliferating cell nuclear antigen reveals unique surface charge characteristics due to halophilic adaptation. BMC Struct Biol 9: 55.

94. Coquelle N, Talon R, Juers DH, Girard E, Kahn R, et al. (2010) Gradual adaptive changes of a protein facing high salt concentrations. J Mol Biol 404: 493-505.

95. Tokunaga H, Arakawa T, Tokunaga M (2008) Engineering of halophilic enzymes: two acidic amino acid residues at the carboxy-terminal region confer halophilic characteristics to Halomonas and Pseudomonas nucleoside diphosphate kinases. Protein Sci 17: 1603-1610.

96. Laemmli UK (1970) Cleavage of structural proteins during the assembly of the head of bacteriophage T4. Nature 227: 680-685.

97. Bradford MM (1976) A rapid and sensitive method for the quantitation of microgram quantities of protein utilizing the principle of protein-dye binding. Anal Biochem 72: 248-254.

98. Keck JL, Goedken ER, Marqusee S (1998) Activation/attenuation model for RNase H. A one-metal mechanism with second-metal inhibition. J Biol Chem 273: 34128-34133.

99. Davies JF, Hostomska Z, Hostomsky Z, Jordan SR, Matthews DA (1991) Crystal structure of the ribonuclease H domain of HIV-1 reverse transcriptase. Science 252: 88-95.

100. Ohtani N, Haruki M, Muroya A, Morikawa M, Kanaya S (2000) Characterization of ribonuclease HII from Escherichia coli overproduced in a soluble form. J Biochem 127: 895-899.

101. Keck JL, Marqusee S (1996) The putative substrate recognition loop of Escherichia coli ribonuclease H is not essential for activity. J Biol Chem 271: 19883-19887.

102. Kim N, Huang SN, Williams JS, Li YC, Clark AB, et al. (2011) Mutagenic processing of ribonucleotides in DNA by yeast topoisomerase I. Science 332: 1561-1564.

103. Lujan SA, Williams JS, Clausen AR, Clark AB, Kunkel TA (2013) Ribonucleotides are signals for mismatch repair of leading-strand replication errors. Mol Cell 50: 437-443.

104. Ghodgaonkar MM, Lazzaro F, Olivera-Pimentel M, Artola-Borán M, Cejka P, et al. (2013) Ribonucleotides misincorporated into DNA act as strand-discrimination signals in eukaryotic mismatch repair. Mol Cell 50: 323-332.

LIST OF PUBLICATIONS

1. Tannous E, Yokoyama K, You DJ, Koga Y, Kanaya S (2012) A dual role of divalent metal ions in catalysis and folding of RNase H1 from extreme halophilic archaeon *Halobacterium* sp. NRC-1. FEBS Open Bio 2: 345-352.

2. You DJ, Jongruja N, Tannous E, Angkawidjaja C, Koga Y, Kanaya S (2014) Structural basis for salt-dependent folding of ribonucelase H1 from halophilic archaeon *Halobacterium* sp. NRC-1. J Struct Biol 187: 119-128.

3. Tannous E, Kanaya S (2014) Divalent metal ion-induced folding mechanism of RNase H1 from extreme halophilic archaeon *Halobacterium* sp. NRC-1. PLoS ONE 9(9): e109016.

4. Tannous E, Kanaya E, Kanaya S (2014) Role of RNase H1 in DNA repair: removal of single ribonucleotide misincorporated into DNA in cooperation with RNase H2. (manuscript in preparation)

ACKNOWLEDGEMENTS

I would like to express my deepest gratitude to my supervisor Professor Shigenori Kanaya for his continuous and valuable support throughout my study and research. I specifically appreciate his patience, encouragement, inspiration, and sharing his immense knowledge. His guidance on a daily basis and long hours of discussion made it possible for me to handle the research work and write this dissertation.

Thanks are also due to Assistant Professor Clement Angkawidjaja who introduced the research life to me and spent generous time teaching me how to conduct experiments.

I am grateful to Professor Satoshi Harashima and Professor Hajime Watanabe for carefully revising this dissertation and giving constructive comments.

I would also like to thank Professor Kazufumi Takano, Associate Professor Yuichi Koga, Dr. Eiko Kanaya and all Kanaya lab members for all their help and support.

Special thanks go to my senior colleagues Dr. Cahyo Budiman, Dr. Tri Nhan Nguyen and Dr. Ryo Uehara for sharing their experience and for the valuable discussions and advices throughout my experimental work.

Thanks also go to Mrs. Reiko Matsumoto for her administrative assistance and for her continuous support to make my stay in Japan smooth.

I owe thanks to my cousin Dr. May Shikhani for her exceptional support both within her field of expertise and as a special member of the family. Her continuous and unlimited love keeps me focused on making my family proud.

My utmost thanks to both my mother Odette and my sister Rania, whose unconditional love and lifetime support cannot be acknowledged with words. I owe them my present accomplishment and all my future success. Their prayers and wishes, along with the prayers of my aunt and my late grandma, protected me and gave me abundant blessings.

Many thanks to my friends in Japan who share similar challenges and with whom I overcame many obstacles and enjoyed my journey in Japan. Ahmed who was always there to support, Tatyana who gave true-heart emotions and immense care and support, and all my friends, without missing anyone, contributed greatly to this work.

More thanks go to my high school teacher Mr. Raif Mufarrij and my undergraduate advisor and teacher Professor Jihad Attieh. Besides inspiring me to love Biology, their encouragement and belief in me greatly contributed to all the stages of my studies.

At last, I would like to thank the Ministry of Education, Culture, Sports, Science, and Technology of Japan for their financial support.

This work is only the beginning of my research career to explore the magnificent wonders of The Divine Creator.